AN ABSTRACT OF THE THESIS OF

N. Mike Jackson for the degree of Doctor of Philosophy in Civil Engineering

presented on June 17, 1992.

Title: Analysis of Thermal Fatigue Distress of Asphalt Concrete Pavements

Abstract approved: *Redacted for Privacy*

Ted S. Vinson

Thermal cracking of asphalt concrete pavements is responsible for millions

of dollars in annual maintenance and rehabilitation costs in the United States and

Canada. Thermal cracking is typically associated with low temperatures in

northern climates and at high elevations. However, another form of thermal

cracking, known as thermal fatigue cracking, has been proposed by several

researchers as a potential mode of distress in regions with relatively moderate

climates but significant differences in high and low daily temperatures.

The primary purpose of the research reported herein was to evaluate the

possibility of occurrence of the thermal fatigue cracking mode of distress. A

secondary objective was to identify a suitable laboratory test procedure to facilitate

a mechanistic analysis of the thermal fatigue mode of distress. In light of these

objectives, several laboratory test procedures were evaluated in the bituminous

materials laboratory at Oregon State University (OSU). The test procedures

evaluated included the phenomenological Thermal Stress Restrained Specimen Test

(TSRST), the Energy Rate Integral Test (ERIT), the Direct Tension Test under constant rate of extension (DTT), and the Direct Tensile Creep Test (DTCT). The TSRST results were used to evaluate the possibility of occurrence of the thermal fatigue mode of distress. The ERIT, DTT, and DTCT procedures were evaluated with respect to the identification of a suitable laboratory test procedure to facilitate a mechanistic analysis of thermal fatigue.

The results from the laboratory test program indicate that thermal fatigue distress in asphalt concrete mixtures is not a viable mode of distress in the absence of environmental aging. Based on the data presented herein and the results of previous researchers, it is evident that distress often attributed to thermal fatigue cracking is more likely the result of low temperature cracking of environmentally aged mixtures, and/or subgrade-related distress; fatigue distress due to thermal loading of semi-restrained pavements does not occur.

ANALYSIS OF THERMAL FATIGUE DISTRESS
OF ASPHALT CONCRETE PAVEMENTS

by

N. Mike Jackson

A THESIS

submitted to

Oregon State University

in partial fulfillment of
the requirements for the
degree of

Doctor of Philosophy

Completed June 17, 1992

Commencement June, 1993

APPROVED:

_____*Redacted for Privacy*_____

Professor of Civil Engineering in charge of major

Redacted for Privacy

Head of department of Civil Engineering

Redacted for Privacy

Dean of Graduate School

Date thesis is presented_____June 17, 1992_____

Typed by_____N. Mike Jackson_____

ACKNOWLEDGEMENT

TABLE OF CONTENTS

LIST OF FIGURES

LIST OF TABLES

ANALYSIS OF THERMAL FATIGUE DISTRESS
OF ASPHALT CONCRETE PAVEMENTS

1.0 INTRODUCTION

1.1 Problem Definition

Asphalt concrete pavements are known to be susceptible to thermal distress when subjected to changes in ambient temperatures. Several researchers have proposed that thermal cracking can be divided into two different modes of distress: (1) low temperature cracking and (2) thermal fatigue cracking (Lytton, et. al., 1983, Carpenter, 1983, Sugawara and Moriyoshi, 1984, Gerritsen, et. al., 1988, and Vinson, et. al., 1989).

Low temperature cracking occurs when pavement temperatures drop below the critical restrained fracture temperature of the mixture. This form of distress is common in cold regions such as Alaska, Canada, and the northern tier states of the United States. Low temperature cracking has been well documented and most existing analytical models pertaining to thermal cracking are devoted entirely to this mode of distress.

In moderate climates, thermal stresses are typically not great enough to cause immediate fracture, but it is conceivable that cyclic thermal variations above the fracture temperature may induce fatigue in the pavement and make it more susceptible to cracking under subsequent thermal and/or traffic induced stresses

(Gerritsen, et. al., 1988). Severe transverse cracking observed in west Texas has been attributed to thermal fatigue of the asphalt concrete surface layer (Carpenter, et. al., 1974). However, the results of subsequent research suggest that other causes may play a primary role in the distress observed in this region (Carpenter and Lytton, 1977, and Anderson and Epps, 1983). Regardless of whether distress results from low temperature or thermal fatigue cracking, such distress will ultimately lead to a reduced service life for asphalt concrete pavements and costly maintenance requirements.

Conventional laboratory mixture design procedures such as the Marshall and Hveem methods do not address thermal distress of asphalt-aggregate mixtures. Thus, in regions susceptible to extremely cold temperatures or broad daily fluctuations in ambient temperature, it is desirable to incorporate in the mix design a laboratory test program which will facilitate analysis of the resistance of the mixture to thermal distress.

Several laboratory test methods which may be suitable for the analysis of thermal fatigue distress of asphalt concrete pavements have been identified through a national survey questionnaire conducted by the U.S. Army Cold Regions Research and Engineering Laboratory (USA CRREL) and an exhaustive literature review (Vinson, et al., 1989). The most promising test procedures identified by this survey have been further evaluated through a contract with the Strategic Highway Research Program (SHRP), the University of California at Berkeley, and Oregon State University (OSU). The test procedures identified in the above-

referenced study and evaluated herein include the Energy Rate Integral Test

(ERIT), the Direct Tension Test under constant rate of extension (DTT), the Direct

Tensile Creep Test (DTCT), and the Thermal Stress Restrained Specimen Test

(TSRST).

1.2   Statement of Purpose

This research effort is part of the Strategic Highway Research Program

(SHRP) Project A-003A "Performance-Related Testing and Measuring of Asphalt-

Aggregate Interactions and Mixtures." The primary objective of the A-003A

contract is to validate the relationships between asphalt binder properties and

pavement performance. A secondary objective is to develop accelerated mixture

performance test procedures to be incorporated into standard design specifications.

The purposes of the research program reported herein were: (1) to evaluate

the possibility of occurrence of the thermal fatigue mode of distress; and (2)

identify a suitable laboratory test procedure to facilitate a mechanistic analysis of

the thermal fatigue mode of distress. In order to achieve these goals, an extensive

laboratory test program and review of documented thermal fatigue cracking studies

were conducted. The specific tasks performed for this study are outlined below:

- Review of existing literature relating to thermal fatigue cracking in

  asphalt concrete mixtures. The results of this literature review are

summarized in Chapters 2 and 3.

- Performance of an extensive test program to evaluate potential laboratory test methods with respect to the development of accelerated mixture performance test procedures. This task is summarized in Chapters 4 and 5.

- A phenomenological evaluation of thermal fatigue distress in asphalt concrete mixtures, utilizing the TSRST device developed at OSU. The results of this evaluation are also included in Chapters 4 and 5.

- Review of an existing thermal fatigue cracking model with respect to the use of laboratory generated material properties for input parameters. The results of this study are presented in Chapter 6.

- Analysis of the results obtained in this study and development of summary conclusions and recommendations based on the results presented herein. The conclusions and recommendations developed based on this study are presented in Chapters 7 and 8.

2.0 BACKGROUND

2.1 Thermal Fatigue Cracking

Transverse cracking that is believed to result from thermal cycling above

the critical fracture temperature of the pavement binder has been categorized as

thermal fatigue cracking. Thermal cycling at relatively low temperatures produces

cyclic tensile stresses within restrained pavement sections due to volumetric

contraction of the asphalt concrete mixture. A simple free-body-diagram

displaying the forces acting on a fully restrained pavement section under thermal

loading is presented in Figure 2.1. The approximate temperature range within

which thermal fatigue is believed to occur is estimated to be between about -7°C

(20°F) and 21°C (70°F) (Carpenter, 1983). Above this range, thermal stresses

cannot be sustained in the pavement due to stress relaxation. Below this range,

low temperature cracking is considered to be the dominant mode of distress. The

approximate temperature ranges of interest in thermal cracking analyses are

reproduced in Figure 2.2 (Carpenter, 1983).

Load cycle fatigue tests performed in the laboratory have demonstrated that

fatigue phenomena occurs in asphalt-aggregate mixtures under low loading

frequencies such as those induced by thermal cycling (Gerritsen, et al., 1988).

Thermal cyclic fatigue tests performed on asphalt-aggregate mixtures indicate

binder properties tend to control thermal induced stress response in
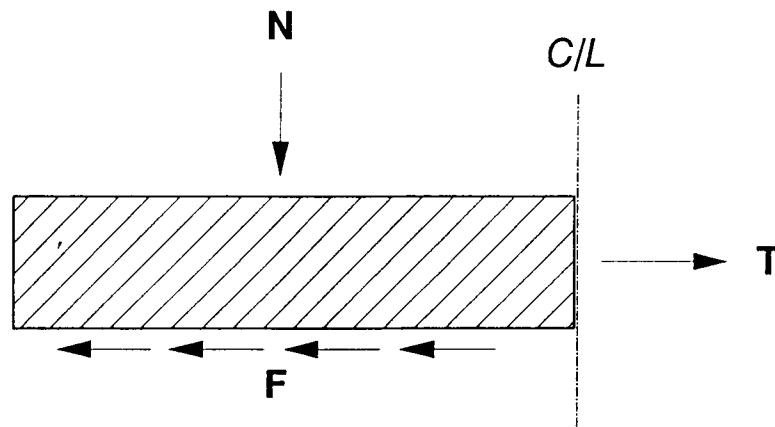
N = Normal Force Including Mass of Pavement Section.
T = Tensile Force Resulting From Thermal Contraction.
F = Friction Force Mobilized Between Pavement and Base Course.

Figure 2.1   **Free-Body-Diagram of a Typical Restrained Pavement Section Under Thermal Loading.**

Note: 1 psi = 6.9 kPa
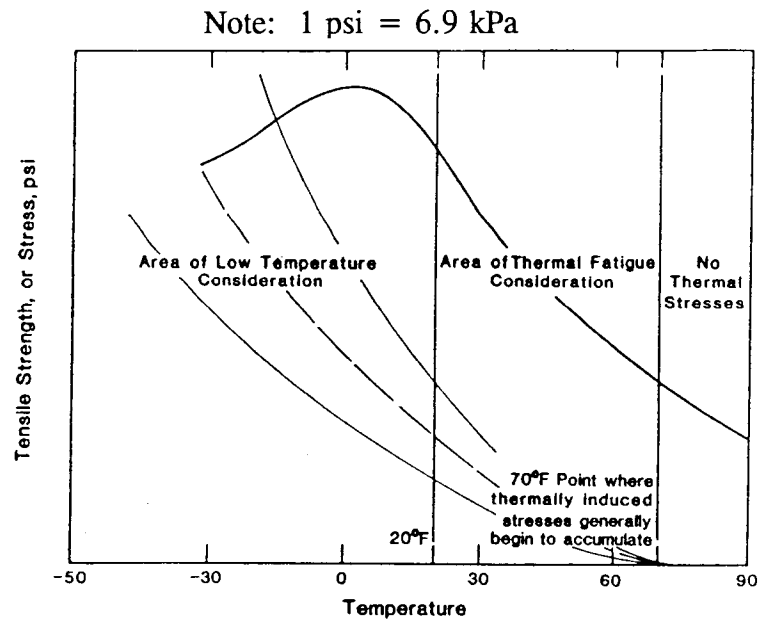
Figure 2.2   **Approximate Temperature Ranges of Interest in Thermal Cracking Analyses (Carpenter, 1983).**

mixtures. In addition, soft grade asphalt tends to resist thermal distress to a greater degree than harder grade asphalt (Sugawara and Moriyoshi, 1984). In general, the failure mechanism associated with thermal cracking is predominantly tension related as shown in Figure 2.1. It has been shown that typical aggregates utilized in asphalt concrete pavements have minimal influence in tensile failure at low temperatures as long as the aggregate is sound and does not alter the properties of the asphalt cement through selective or excessive absorption (Carpenter, 1983).

West Texas, and the southwest U.S. in general, experience a great deal of transverse cracking which has been attributed to thermal fatigue distress. The climatic conditions in this region are generally sufficient to promote fatigue damage (Carpenter, et. al., 1977). However, it has been suggested that the distress observed in west Texas may be the result of problems related to base and subgrade materials (Carpenter and Lytton, 1977). In addition, Anderson and Epps (1983), demonstrated that the cracking observed in west Texas could be the result of low temperature cracking of environmentally aged asphalt concrete mixtures. Based on this existing data, it is not clear whether or not thermal fatigue cracking is actually responsible for the transverse cracking observed in west Texas.

2.2 Visco-Elastic Material Response

Asphalt concrete mixtures can be idealized as visco-elastic materials since the stress and strain response is known to be dependent on time and temperature. Visco-elastic materials, like ideal elastic solids, possess a definite shape in the

natural, unstressed state and deform instantaneously under applied loading.

However, unlike ideal elastic solids, a flow process follows this instantaneous

deformation. Immediately upon removal of the applied load, a portion of the

deformation is recovered. Additional recovery occurs in a time dependent manner.

Complete recovery of the initial unstressed state may or may not be achieved

depending on the magnitude of permanent strain imparted during loading.

Characteristic visco-elastic material response is shown in Figure 2.3.

A visco-elastic material is said to be linear visco-elastic if (1) the stress and

strain are proportional at a given time, and (2) the principle of linear superposition

is valid (Findley, et. al., 1989). Asphalt concrete is generally assumed to be a

linear visco-elastic material within typical working stress levels and at low

temperatures. The basic criteria for linear visco-elasticity is shown in Figure 2.4.

A common material property used to characterize visco-elastic response is

the relaxation modulus. The relaxation modulus is considered to be unique at a

given temperature and time of loading. It provides a relationship between stress

and strain at a given time and temperature. It is common to transform such

modulus results to a standard temperature. The results may then be presented in

the form of a transformed stiffness curve at the standard temperature. The

transformed stiffness curve represents the stress, strain, time, and temperature

relationship for a given mixture. The general procedure for transforming modulus

data at several temperatures to a standard temperature is outlined in Figure 2.5

(Stephanos, 1990). The procedure results in the construction of the "transformed"

or "master" stiffness curve.
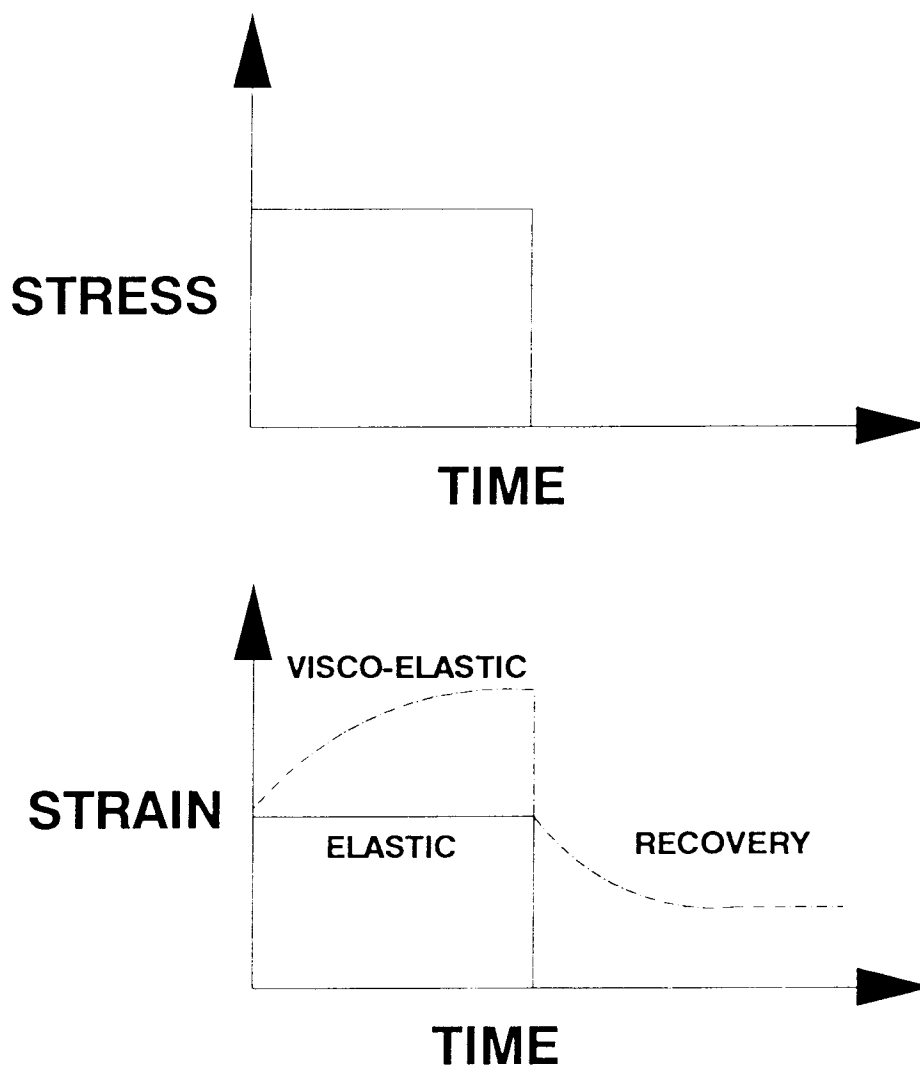
Figure 2.3   Characteristic Visco-Elastic Material Response.
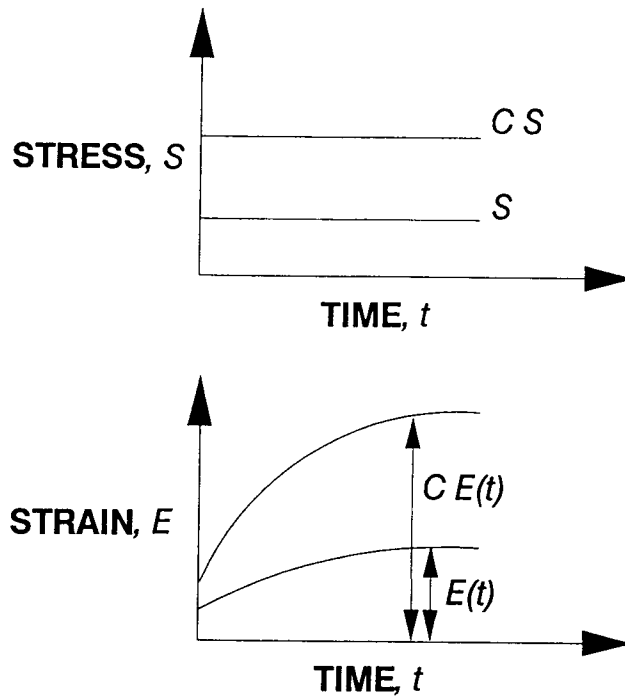
Figure 2.4 (a)   Stress and Strain are Proportional.
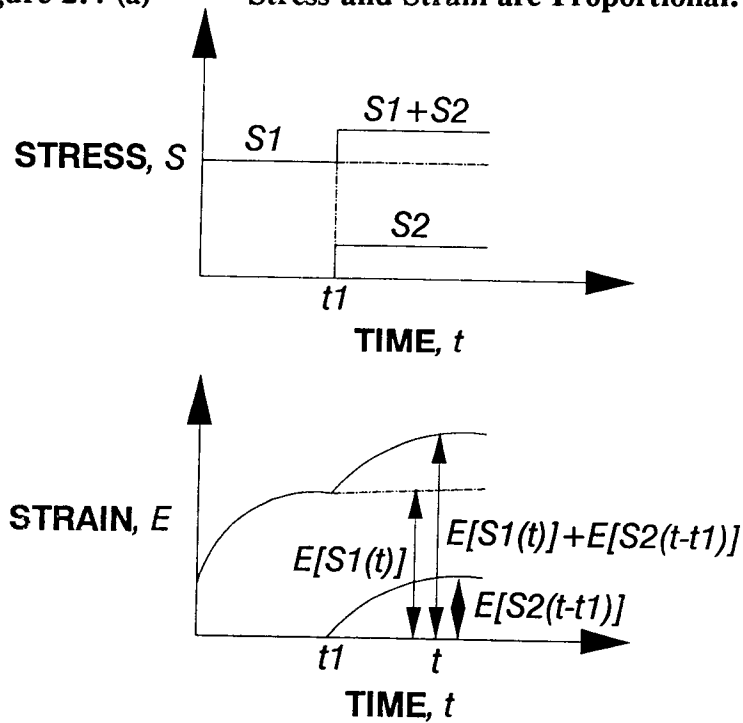
Figure 2.4 (b)   Principle of Linear Superposition is Valid.

Figure 2.4   Basic Criteria for Linear Visco-Elasticity (Findley, et. al., 1989).
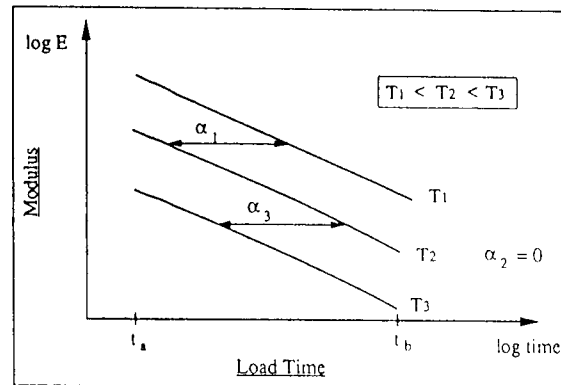
Figure 2.5 (a)   **Modulus vs. Time in Log₁₀-Log₁₀ Space.**
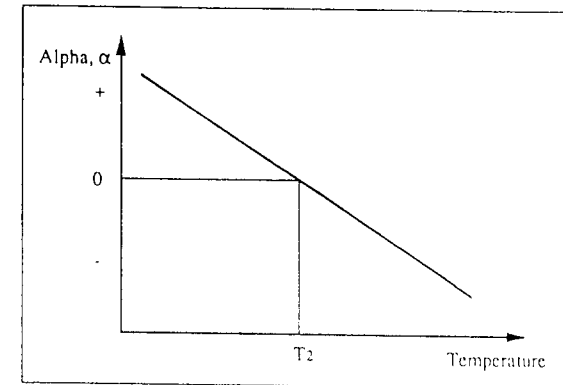
Figure 2.5 (b)   **Alpha vs. Temperature.**
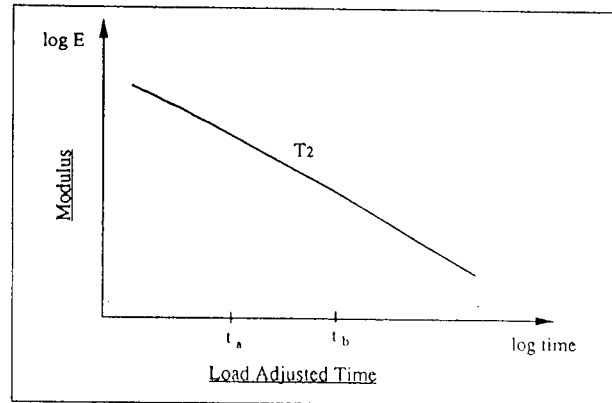
Figure 2.5 (c)   **Transformed Curve in Log₁₀-Log₁₀ Space.**
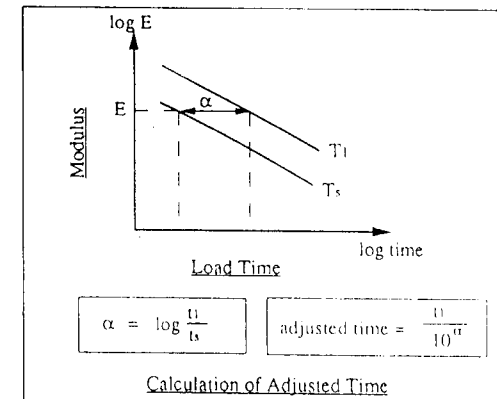
Figure 2.5 (d)   **Transformed Time.**

Figure 2.5   **Procedure For Transforming Creep Modulus Data to Transformed Curve at a Standard Temperature (Stephanos, 1990).**

2.3 Analytical Methods

Thermal distress has typically been evaluated from either a phenomenological or mechanistic approach (Vinson, et al., 1989). These two general analytical methods are addressed in the following paragraphs.

2.3.1 Phenomenological Approach

Phenomenological analysis approaches generally attempt to model actual field performance as closely as possible with suitable laboratory test procedures. Such approaches typically consist of correlations between laboratory test results and documented field distress. Miner's hypothesis (1945) is commonly applied in phenomenological fatigue analyses. In general, Miner's hypothesis suggests that fatigue damage is cumulative and failure occurs when the sum of the ratios of fatigue life expended at incremental stress or strain levels is equal to or greater than unity. Miner's theory may be expressed as follows:

$$\sum_{i} \frac{n_i}{N_i} = 1 \qquad (2.1)$$

where

n_i =   number of load applications at level i

N_i =   number of load applications to failure at level i

As previously noted, this relationship has historically been applied to relate distress measured in the laboratory to field performance. Due to the high frequencies associated with most laboratory fatigue test methods, empirical "shift" factors may be required to correlate field performance with laboratory test results. In addition, results obtained from phenomenological test methods are typically unique for the specific boundary conditions tested in the laboratory. These limitations to phenomenological approaches have prompted a great deal of research toward the development of mechanistic based design procedures.

2.3.2 Mechanistic Approach

Mechanistic models generally correlate pavement distress to fundamental material properties such as relationships between stress, strain, time, and temperature. Most existing mechanistic thermal cracking models are based, at least in part, on fracture mechanics. These models generally relate pavement cracking to fracture mechanics parameters such as the Stress Intensity Factor (K), the J-Integral (J), or more recently, the Energy Release Rate Integral or C*-Line Integral (C*). Several fracture mechanics based models are discussed in the following section.

2.4 Fracture Mechanics Based Fatigue Models

Majidzadeh (1970) and Salam (1971) applied a quantitative relationship for

crack growth in asphalt concrete with respect to the number of load applications in the following form:

$$\frac{da}{dN} = AK_I^n \qquad \qquad \textbf{(2.2)}$$

where

a	=	crack length
N	=	fatigue load cycles
A, n	=	material constants
K_I	=	Stress Intensity Factor (mode 1 case only)

The constants in this relationship were estimated from regression analysis based on limited laboratory test data. Salam notes that the merits of this approach include the ability to obtain a quantitative measure of the fatigue process and it is flexible enough to be adopted on a rigorous microscopic level or a phenomenological basis of design. However, this approach requires a considerable amount of experimental data which is not available at present.

A similar relationship, utilizing the J-Integral and elastic strain energy, was employed by Abdulshafi and Majidzadeh (1985). The form of this relationship is as follows:

$$\frac{da}{dN} = A \left(\frac{J_I}{2U_e} \right) \qquad \qquad \textbf{(2.3)}$$

where

a	=	crack length
N	=	fatigue load cycles
A	=	material constant
U_c	=	elastic strain energy
J_I	=	J-Integral (mode 1 case only)

Experimental results indicate this relationship may provide similar predictions for fatigue life as the Stress Intensity Factor approach, however, additional laboratory testing is necessary to establish a relationship between the two approaches.

The Stress Intensity Factor and J-Integral are typically associated with elastic or elasto-plastic material behavior. Another fracture mechanics parameter, the C*-Line Integral has been related to fatigue fracture of asphalt concrete mixtures by Abdulshafi (1983). The relationship applied by Abdulshafi to correlate fatigue crack growth to the C*-Integral is as follows:

$$\ln\frac{da}{dN} = \ln R + q \ln C^*$$ (2.4)

where

a	=	crack length
N	=	fatigue load cycles
R,q	=	material constants
C^*	=	C^*-Line Integral

As with the previously mentioned fracture mechanics parameters, laboratory test data pertaining to the C*-Line Integral is limited at this time. However, the data presented by Abdulshafi suggests the C* parameter may be appropriate for evaluation of fatigue crack resistance of asphalt concrete mixtures.

Majidzadeh (1977) has noted that a weakness of the phenomenological approach is that it does not specifically account for crack initiation, propagation, and subsequent redistribution of stresses within a pavement system. In an attempt to account for propagation and ultimate fracture, Majidzadeh, et al. (1976) developed a mechanistic model based on linear elastic fracture mechanics. The Majidzadeh model was evaluated with respect to Equations 2.2 and 2.3 and the J-Integral, J_I, was identified as the most appropriate parameter for characterization of elastic and elasto-plastic fracture (Abdulshafi and Majidzadeh, 1985). Crack initiation was not accounted for in these analyses but it was noted that crack initiation could be evaluated based on the number of cycles required to develop the initial crack independently of crack propagation.

In a more recent study, the Energy Rate Integral associated with creep crack growth, the C*-Line Integral, was successfully applied to differentiate the performance of modified asphalt concrete mixtures with respect to load fatigue cracking distress at moderate temperatures (Abdulshafi and Kaloush, 1988). Abdulshafi and Kaloush have suggested that the C*-Line Integral may also be successfully applied to the study of thermal fatigue cracking.

The development of a mechanistic model to evaluate thermal fatigue

cracking is beyond the scope of this study. A mechanistic thermal cracking model
is currently being developed under the SHRP A-005 contract. However, this
model is not currently available. Thus, the existing thermal cracking model,
developed by Lytton, Shanmugham, and Garrett (1983) is utilized for analysis
purposes herein. Based on an extensive literature review, this model appears to be
the most comprehensive existing mechanistic model capable of handling thermal
fatigue cracking. The Lytton, Shanmugham, and Garrett model is described
further in the following section.

2.5 Lytton, Shanmugham, and Garrett Thermal Fatigue Model

The Lytton, Shanmugham, and Garrett model consists of the computer
programs VISCO and THERM, developed at the Texas Transportation Institute.
The model is based on fracture mechanics with thermal stresses calculated from
visco-elastic theory. The basic fracture mechanics equation employed in this
model was originally derived from fatigue testing of metals by Paris and Erdogan
(1963). The general form of this equation is as follows:

$$\frac{dc}{dN} = A \, (\Delta K)^n \qquad\qquad (2.5)$$

where,

$$\frac{dc}{dN}$$ = rate of growth of crack length (depth) with respect to the number of thermal cycles, N,

A, n = time and temperature dependent material constants,

ΔK = change in stress intensity factor at the crack tip from the time of maximum temperature to minimum temperature.

As noted by Lytton, et. al. (1983), in order to successfully apply equation 2.5 for predicting cracking in asphalt concrete pavements, a methodology had to be developed for estimating the Stress Intensity Factor, K, and the visco-elastic fracture parameters, A and n.

Lytton, et. al. (1983) presented computational methods for determining the Stress Intensity Factor using a finite element computer program developed by Chang, Lytton, and Carpenter (1976). Computational methods were also presented for the calculation of the parameters, A and n. These are basically regression equations developed from test results obtained at the Texas Transportation Institute.

As part of the Lytton, Shanmugham, and Garrett model, the program VISCO utilizes Van der Poel's nomograph, as computerized by de Bats, to develop the transformed stiffness curve for the mixture. The program THERM makes use of an expression developed by Schapery which relates the slope, m_1, of the transformed curve at 25°C (77°F) to the material constant, n. This expression is as follows:

$$n=2\left(1+\frac{1}{m_1}\right) \qquad (2.6)$$

Based on laboratory results obtained by Germann and Lytton (1979), the material

constant n must be divided by a scaling factor of 2.5 in order for the calculated

values to agree with laboratory observations. Another relationship developed

through crack propagation testing at the Texas Transportation Institute is used to

estimate the fracture parameter, A, as follows:

$$n=-0.69-0.511\log_{10}A \qquad (2.7)$$

The THERM program calculates the stress intensity factor based on environmental

data and visco-elastic material properties and estimates the cumulative crack

growth for each consecutive thermal cycle. If unstable crack growth occurs, low

temperature cracking is predicted.

2.6   Modifications to the Lytton, Shanmugham, and Garrett Model

The visco-elastic fracture parameters, A and n, can also be estimated from

laboratory test data, bypassing the use of the VISCO program and providing a

more direct and mechanistic means of predicting thermal distress. The results of

relaxation or creep tests performed at three or more temperatures can be used to

develop a transformed stiffness curve at a standard temperature. Subsequently,

Equations 2.6 and 2.7 can be used to obtain the fracture parameters, A and n. The

calculation of the parameters A and n, based on the laboratory test data can be

performed within the THERM program with only minor modifications to the

existing program source code. A listing of the fortran source code for the program

THERM, including the necessary changes to enable utilization of laboratory test

data, is reproduced in Appendix D.

In this study, transformed stiffness curves were estimated with laboratory

test data. The DTCT results, at three different temperatures, were transformed to

a standard temperature of -10°C (14°F) as outlined in Figure 2.5. A typical

Transformed Creep Modulus Curve and associated Time-Temperature Shift Factor

Curve are presented in Figure 2.6. The standard temperature (T_m), the slope (m_1)

and intercept(E_0) of the transformed curve, and the slope (m_2) and the power law

constant (T_a) of the time-temperature shift factor curve make up the visco-elastic

mixture properties required as input to the THERM program. Direct input of these

laboratory generated parameters enables a more fundamental, mechanistic approach

to the analysis of thermal distress.
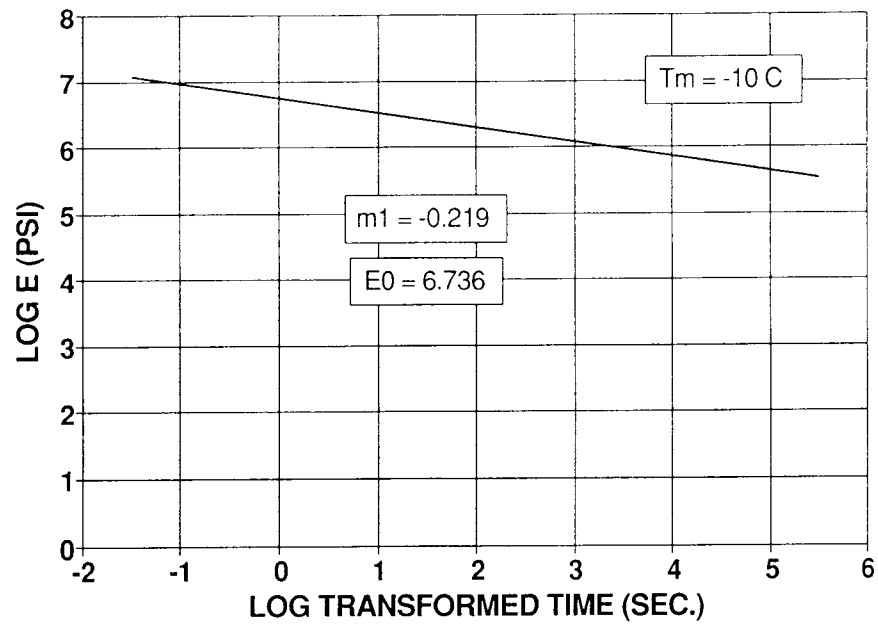
Figure 2.6 (a)   Typical Transformed Stiffness Curve.

Note: 1 psi = 6.9 kPa
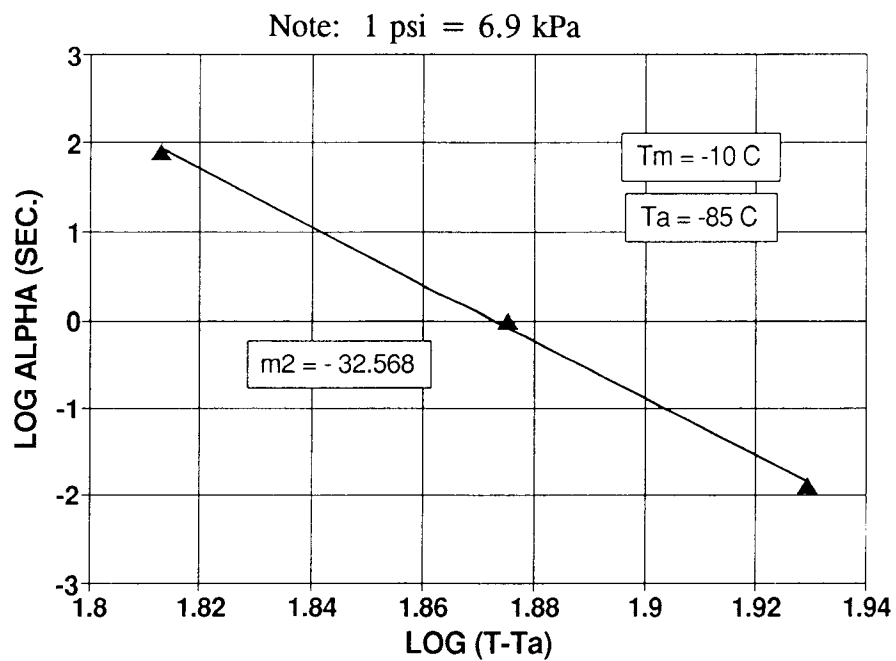
Figure 2.6 (b)   Time-Temperature Shift Factor Curve.

Figure 2.6   Typical Transformed Stiffness and Shift Factor Curves.

3.0 FACTORS INFLUENCING THERMAL FATIGUE DISTRESS

The primary factors which influence thermal distress may be divided into three basic categories consisting of (1) material factors, (2) environmental factors, and (3) geometric factors (Vinson, et al., 1989). The material factors addressed herein include asphalt concrete mixture properties including (1) asphalt cement properties, and (2) voids content. The primary environmental factor of interest is temperature. All other variables including geometry, environmental aging, and variability in base and subgrade conditions are beyond the scope of this study. It is important to note that these additional factors may significantly impact thermal distress in the field. Results of field studies in west Texas suggest that base and subgrade conditions and environmental aging may contribute significantly to transverse cracking. However, the objective of this study is to evaluate thermal fatigue distress under carefully controlled conditions in the laboratory.

3.1 Asphalt Cement Properties

The asphalt cement is believed to be the most critical factor affecting thermal distress. A lower viscosity grade of asphalt cement will produce a lower rate of increase in stiffness with decreasing temperature and consequently reduce the potential for thermal cracking. In other words, soft grade asphalt cement tends to resist thermal cracking to a greater degree than harder grade asphalt cement

(Sugawara and Moriyoshi, 1984). The temperature susceptibility of the asphalt cement is also critical when evaluating the stress/strain response of mixtures over a range of temperatures. The relative ranking of the stiffness properties of asphalt cement will often change with temperature. Thus, it is important to possess rheological data over the range of temperatures of interest. Knowledge of the coefficient of thermal contraction of the binder is also important. Asphalt cement with relatively large coefficients will exhibit greater potential strains and thus, greater internal stresses than cement with lower thermal coefficients.

3.2 Voids Content

The voids content of an asphaltic concrete pavement provides an indicator of the degree of compaction imparted to the pavement. The voids content, within a reasonable range, is not believed to be a primary factor which affects thermal distress in asphalt concrete pavements. However, high void contents may increase pavement susceptibility to environmental degradation due to moisture and atmospheric aging. In general, fracture stresses and fracture temperatures tend to increase slightly with decreasing void contents (Jung, 1990).

3.3 Ambient Temperature

As the surface temperature decreases, the resulting stresses within a

restrained asphalt concrete pavement section tend to increase. Below the glass transition temperature, asphalt concrete mixtures generally respond as brittle materials. It is important to note that the temperature range of interest in thermal cracking may straddle the glass transition temperature of the binder. The temperature range in which thermal fatigue has been proposed to be critical is estimated to be between about -7°C (20°F) and 21°C (70°F) (Carpenter, 1983). Below this range, low temperature cracking is of primary concern. Above this range, significant thermal stresses are not developed within typical asphalt concrete pavements.

4.0 LABORATORY TEST PROGRAM

The test procedures evaluated in this study include the Energy Rate Integral

Test (ERIT), the Direct Tension Test under constant rate of extension (DTT), the

Direct Tensile Creep Test (DTCT), and the Thermal Stress Restrained Specimen

Test (TSRST). As previously noted, all of these test procedures were identified

through a national survey questionnaire conducted by the USA CRREL and an

exhaustive literature review (Vinson, et. al, 1989). The selected test methods were

evaluated in the bituminous materials research laboratory at OSU. Tests were

performed on asphalt concrete mixtures fabricated from SHRP MRL materials.

The materials utilized in this study, experiment designs, and respective test

procedures are described below. Detailed protocols for the respective test methods

are contained in Appendix B. Test specimen preparation protocols are contained in

Appendix C. The laboratory test data collected in this study is contained in

Appendix E.

4.1   Materials Utilized

4.1.1   Mineral Aggregate

Mineral aggregate from a single source was included in this test program.

The aggregate utilized here is identified by the SHRP MRL as RB. The RB

aggregate is described as a relatively non-stripping aggregate and predominantly

consists of mechanically crushed granite. The physical properties of the RB

aggregate, as provided by MRL, are summarized in Table 4.1.

The RB aggregate was handled and processed in general accordance with

ASTM procedures and SHRP MRL protocols. The general procedures followed in

this study for handling and processing the RB aggregate are summarized in

Appendix C.

4.1.2 Asphalt Cement

Four asphalt cements were utilized in this study. The variable binders were

included here to evaluate the suitability of the respective test procedures. The

asphalt cements included in this study are identified by the SHRP MRL as AAG-1,

AAG-2, AAK-1, and AAK-2. The AAG and AAK designations represent different

crude sources with differing temperature susceptibility characteristics. The

numeric suffix designations represent different asphalt grades from the respective

sources. The pertinent binder properties, as provided by the SHRP MRL are

summarized in Table 4.2. Additional chemical, rheometric, and visco-elastic

properties of these binders are available from the SHRP MRL. The asphalt

cements evaluated in this study were handled and processed in general accordance

with ASTM procedures and SHRP MRL protocols, as documented in Appendix C.

Table 4.1   **Physical Properties of the RB Aggregate (from SHRP MRL).**

L.A. Abrasion	30.0
H_2O Absorption	1.03

Specific Gravity:
      Bulk
      Apparent
	
	2.742
	2.656

Flakiness Index	9.6

Table 4.2   **Summary of Asphalt Cement Properties (from SHRP MRL).**

SHRP MRL Code	AAG1	AAG2	AAK1	AAK2
Asphalt Grade	AR-4000	AR-2000	AC-30	AC-10
Original Asphalt Properties:				
Viscosity (140°F, Poises)	1862	1056	3256	996
Penetration (25°C, 100 gm, 5 sec)	53	76	70	154
Ring & Ball Softening Point, °F	120	111	121	108
Residual Properties:				
Mass Change, %	-0.18	-0.19	-0.55	-1.23
Viscosity (140°F, Poises)	3253	1781	9708	3098
Viscosity (275°F, Cst)	304	216	930	533
Viscosity Ratio (140°F)	1.75	1.69	2.89	3.11
Component Analysis:				
Asphaltenes, %	5.8	5.1	21.1	20.5
Polar Aromatics, %	51.2	51.0	41.8	39.4
Naph. Aromatics, %	32.5	35.3	30.0	30.6
Saturates, %	8.5	6.6	5.1	7.5

4.2 Experiment Design Matrices

Experiment designs were developed for each of the test methods evaluated in this study. The respective experiment designs were based on the above-referenced SHRP MRL materials. Test samples consisting of mixtures of the SHRP MRL materials were compacted to the prescribed void contents and tested under prescribed thermal conditions. Experiment designs for this study were developed with assistance from Louis J. Painter, statistical consultant to the SHRP A-003A contract. The respective experiment design matrices are summarized in Tables 4.3 through 4.6.

4.3 Test Variable Identification System

In order to account for the different variables included in this test program, an abbreviated test identification system was developed. Materials were identified based on the last letter of the SHRP MRL material code designations. Void levels were identified as either high (H) or low (L). Test temperature was noted in degrees Celsius, where applicable. The basic test variable identification system utilized throughout this study is summarized in Table 4.7.

Table 4.3   Energy Rate Integral Test Experiment Design Matrix.

AGG. TYPE	BINDER TYPE	VOIDS (%)	TEMP. (°C)	DISP. RATE (in/min)	REPS.
RB	AAG1	4	10	0.012	1
	AAG2			0.030	
	AAK1	8	20	0.048	2
	AAK2				

Note: 1 in/min = 0.042 cm/sec

Table 4.4 Direct Tension Test Experiment Design Matrix.

Table 4.4 (a) Oregon State University DTT Study.

AGG. TYPE	BINDER TYPE	VOIDS (%)	TEMP (°C)	REPS.
RB	AAG1	4	-17.8	1
	AAG2			
	AAK1	8	-34.4	2
	AAK2			

Table 4.4 (b) University of Waterloo DTT Study.

AGG. TYPE	BINDER TYPE	VOIDS (%)	TEMP. (°C)	REPS.
RB	AAG1	4	0.0	1
	AAG2		-17.8	2
	AAK1	8		
	AAK2		-34.4	3

Table 4.5   **Direct Tensile Creep Test Experiment Design Matrix.**

AGG. TYPE	BINDER TYPE	VOIDS (%)	TEMP. (°C)	REPS.
RB	AAG1	4	0.0	1
			-10.0	
	AAK2	8	-20.0	2

Table 4.6   **Thermal Stress Restrained Specimen Test Experiment Design Matrix.**

AGG. TYPE	BINDER TYPE	VOIDS (%)	REPS.
RB	AAG1	4	1
	AAK2	8	2

Table 4.7   Test Variable Identification System

Example Test Specimen Designation: BG1L-10 1

B	-	SHRP MRL Designation RB Aggregate (Crushed Granite)
G1	-	SHRP MRL Designation AAG1 Asphalt Cement (AR-4000)
L	-	Low Void Content (4 +/- 1% Voids)
-10	-	Test Temperature (-10°C)
1	-	Replicate Test Number (2 Replicates)

4.4   Energy Rate Integral Test Program (ERIT)

The Energy Rate Integral associated with creep crack growth, the C*-Line

Integral, has been successfully related to load fatigue fracture of asphalt concrete

mixtures by Abdulshafi (1983). The C*-Line Integral has also recently been

utilized to differentiate the performance of modified asphalt concrete mixtures with

respect to fatigue cracking at moderate temperatures (Abdulshafi and Kaloush,

1988). Abdulshafi has suggested that this fracture parameter may also be

applicable to the study of thermal fatigue cracking (1990). Based on the recent

successes with the C*-Line Integral, as applied to load-related fatigue cracking, the

ERIT was included in this thermal fatigue cracking study.

4.4.1 General Test Procedure

The ERIT was evaluated in the bituminous materials research laboratory at

OSU. Notched, cylindrical specimens of dimensions 10 cm (4 in.) diameter by 10

cm (4 in.) thick were utilized in this study. The notched, cylindrical samples were

tested under indirect loading conditions as illustrated in Figure 4.1. A modular,

electro-hydraulic, closed loop testing system was utilized to apply a constant rate

of actuator displacement to the notched cylindrical specimens. The rate of

extension of the actuator was controlled with an internal Linear Variable

Displacement Transducer (LVDT). The resulting load applied to the test specimen

was monitored with a load cell mounted in line with the test specimen and the

LOAD

TOP LOAD PLATEN

LOAD PLATEN WEDGES
WITH TEFLON STRIPS

1.9 cm (.75 in)

INITIAL FATIGUE CRACK
< .05 cm (.02 in)

RADIUS = 5.08 cm (2 in)

BOTTOM LOAD PLATEN
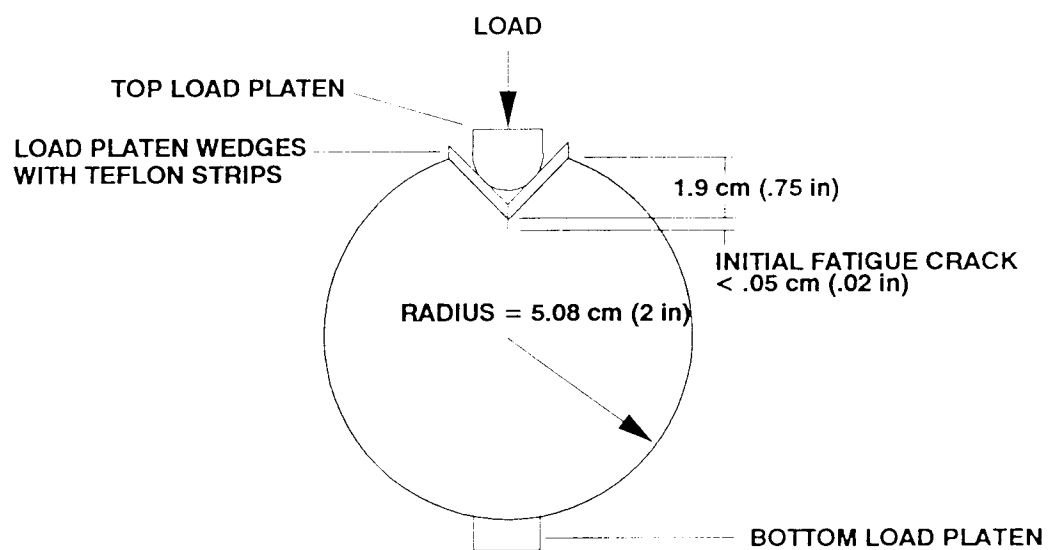
Figure 4.1   Sketch of Notched Cylindrical Energy Rate Integral
                    Test Specimen.

hydraulic actuator. The crack length observed at the surface of the specimen was monitored visually and recorded with electric switches connected to the data acquisition system. Simple on/off switching was used to monitor the crack advancement at equal spaced intervals of .635 cm (.25 in.). The modular test system utilized in this study is described in detail in Appendix A. A conceptual sketch of the modular OSU test system is presented in Figure 4.2.

Tests were conducted at two different temperatures, 10°C (50°F) and 20°C (68°F). Attempts to conduct the ERIT at temperatures lower than about 10°C (50°F) were not successful due to predominantly brittle behavior of the mixtures tested in this study. A cryogenic environmental chamber with closed loop temperature control was utilized to control the test specimen temperature during testing. The chamber was equipped with an internal RTD temperature sensor capable of measuring to +/- 0.1°C (.18°F). A typical notched cylindrical specimen mounted in the OSU test system is presented in Figure 4.3.

4.4.2 Interpretation of Test Results

The Energy Rate Integral or C*-Line Integral is conventionally interpreted as the energy release rate for steady-state, time dependant crack growth. Due to the complex nature of the data acquisition and reduction technique followed herein, a schematic representation of the multiple specimen test method is outlined in Figures 4.4 and 4.5. The analytical procedure presented here was originally introduced by Landes and Begley (1976) and was first applied to asphalt-aggregate

SERVO-HYDRAULIC
SYSTEM

LVDT

LOAD
CELL

ENVIRONMENTAL
CABINET
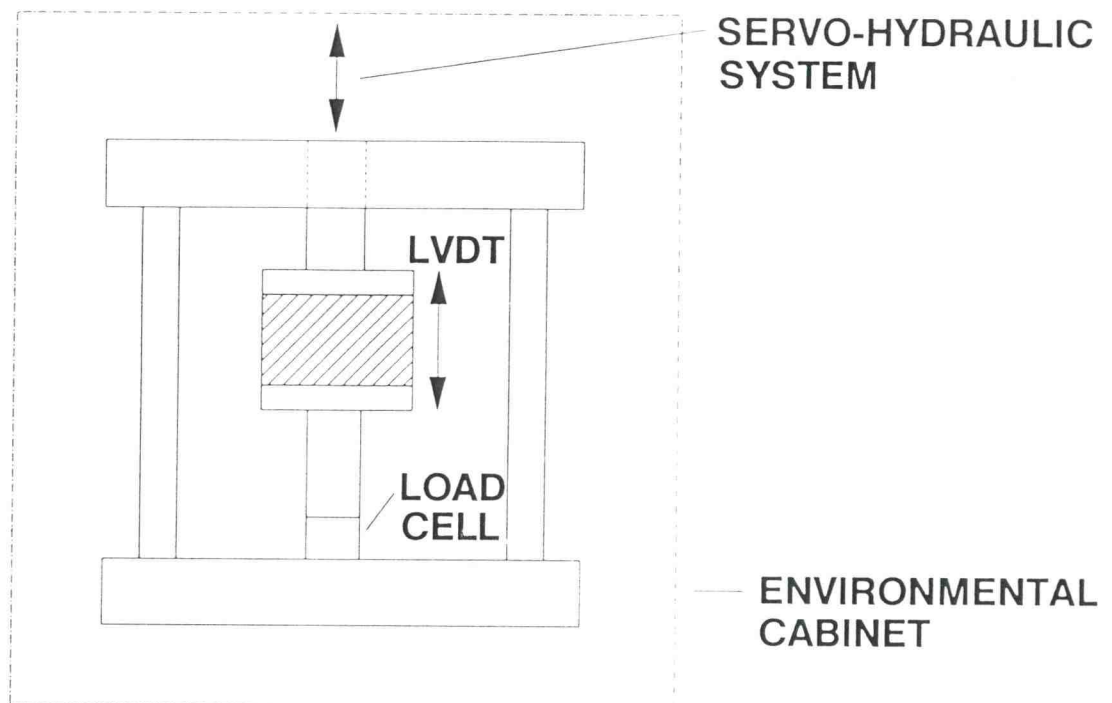
Figure 4.2   Conceptual Sketch of the Modular Test System
Used in this Study.
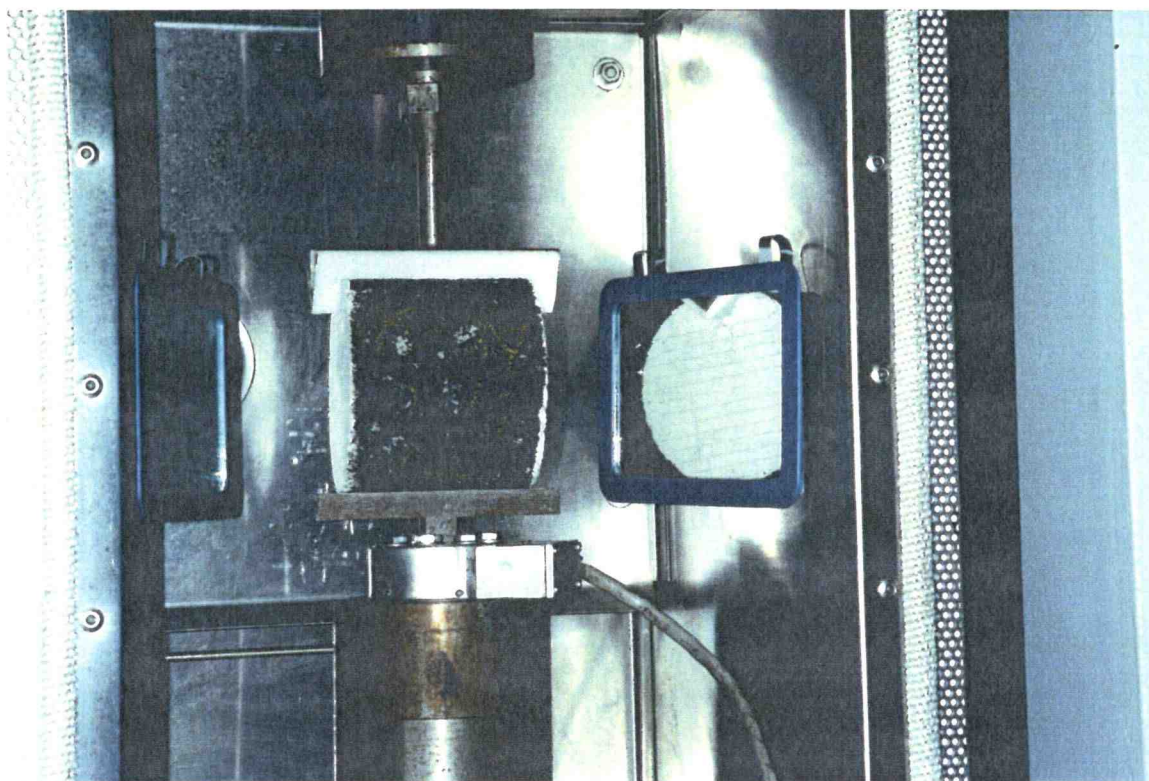
Figure 4.3   Typical Notched Cylindrical Test Specimen Mounted
in the Modular OSU Test System.
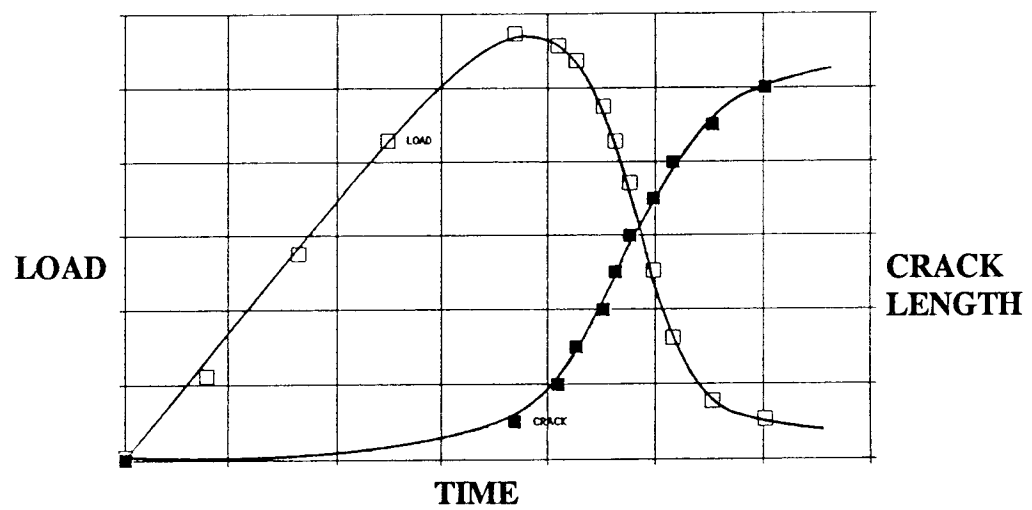
Figure 4.4   Load and Crack Length Versus Time for the Energy Rate
Integral Test.
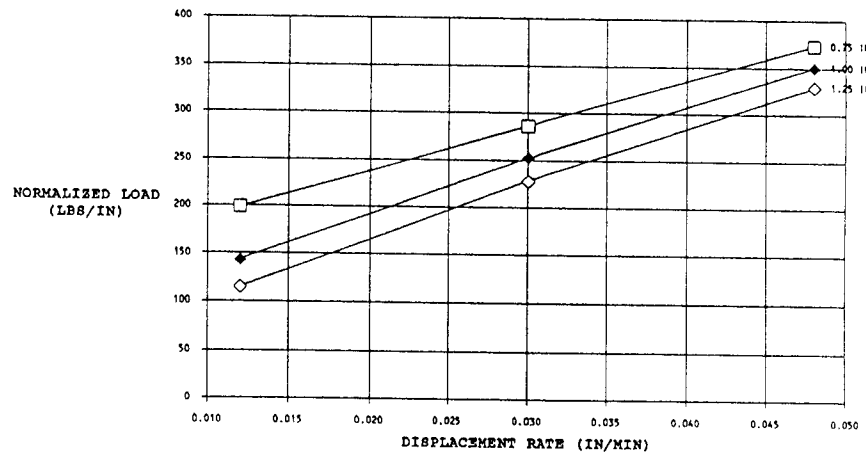
Figure 4.5 (a)   Load vs. Displacement Rate.
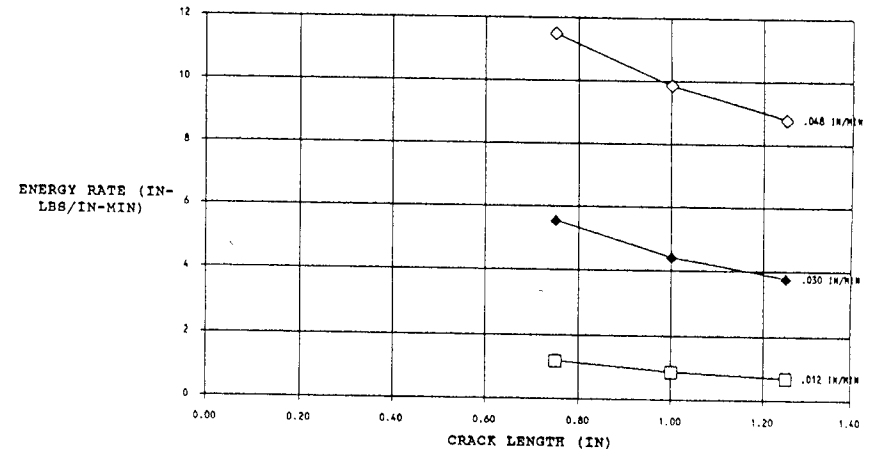
Figure 4.5 (b)   Energy Rate vs. Crack Length.
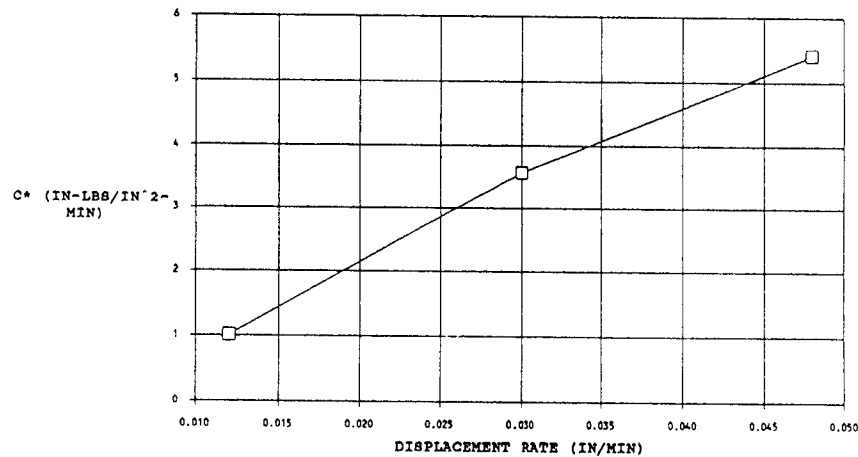
Figure 4.5 (c)   C*-Integral vs. Displacement Rate.
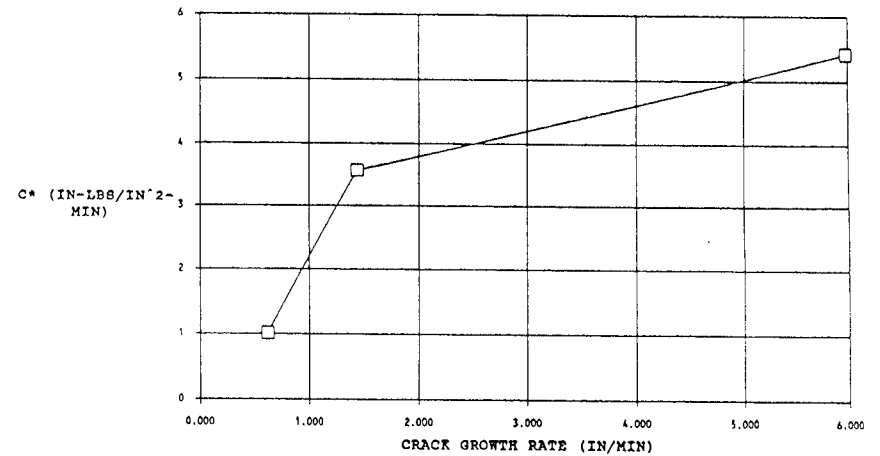
Figure 4.5 (d)   C*-Integral vs. Crack Rate.

Figure 4.5   Multiple Specimen Test Procedure for the Energy Rate Integral Test.

mixtures by Abdulshafi (1983). In general, multiple specimens are subjected to different constant displacement rates. The load and crack length are monitored as a function of time as shown in Figure 4.4. This plot represents the actual data collection phase of the test. The data are then cross plotted to yield the load per unit crack plane thickness as a function of the displacement rate for fixed crack lengths. This step is shown in Figure 4.5(a). The area under the load versus displacement rate curve is interpreted as the rate of energy dissipated per unit crack plane thickness and is plotted against the crack length as shown in Figure 4.5(b). The slope of the curve in the previous step is the Energy Rate Integral, C*-Line Integral, as shown plotted versus displacement rate in Figure 4.5(c). Finally, the C*-Line Integral is plotted versus the crack growth rate as shown in Figure 4.5(d).

In this study, crack growth was generally observed just prior to the point of maximum load. Shortly thereafter, the curve of crack length versus time exhibited nearly constant rate of crack growth. This constant crack growth rate was typically accompanied by a nearly constant rate of decrease in load. Landes and Begley (1976) noted that these nearly constant rates can be interpreted as a steady state region of crack growth. In interpreting ERIT data, Landes and Begley only worked with data recorded after the maximum load was achieved, thus eliminating all transient effects. This general approach was also followed in this study.

4.5   Direct Tension Test Program (DTT)

The DTT method has been utilized for over 20 years to study low temperature cracking in Canada at the University of Waterloo. The constant rate of extension method has been shown to provide relevant information for the analysis of thermal distress of asphalt concrete pavements (Haas, 1973). The successful application of the DTT method to low temperature cracking suggests that this procedure may provide relevant information for the analysis of thermal fatigue cracking.

4.5.1   General Test Procedure

The DTT was evaluated in the bituminous materials research laboratory at OSU. An expanded, parallel test program was also conducted under the supervision of professor Ralph Haas at the University of Waterloo in Ontario, Canada. The test was evaluated in both studies with rectangular asphalt concrete beam specimens fabricated at OSU. Testing was conducted in general accordance with the constant rate of extension procedure developed by Haas (1973).

In general, rectangular beam specimens were subjected to constant rates of extension on the order of 2.0X10-4 in./min (8.5X10-6 cm/sec). Loading rates were chosen to provide a reasonable testing time to fracture (i.e. between about one half to two hours). The corresponding stress, strain, and elapsed time were recorded during testing.

The modular test system depicted in Figure 4.2 and described in Appendix A was utilized at OSU to apply a constant rate of extension to the beam specimens. A similar electro-mechanical test system was utilized for the University of Waterloo study. The load applied to the test specimen was monitored with a load cell in line with the actuator. The constant rate of extension of the specimen was controlled in the OSU study with a spring loaded, gage head LVDT mounted to one side of the specimen with an "anti-tilt" device. The "anti-tilt" device is described in detail in Appendix A. The purpose of the "anti-tilt" device is to minimize the effects of slight tilting in the end platens on the displacement reading in the LVDT. Proximeter gages, mounted on opposite faces of the test specimen, were used to control the constant rate of displacement in the University of Waterloo study.

Tests were conducted at OSU at two different temperatures, - 17.8°C (0°F) and -34.4°C (-30°F). The expanded study at the University of Waterloo included three different test temperatures, 0°C (32°F), -17.8°C (0°F) and -34.4°C (-30°F). A cryogenic environmental chamber was used to control the temperature of the specimens during testing. Thermistors were also attached to the specimens on opposite faces to monitor any thermal gradient effects. A typical DTT specimen mounted in the modular OSU test system is pictured in Figure 4.6.

4.5.2 Interpretation of Test Results

The DTT results were evaluated based on tensile strength, peak strain,
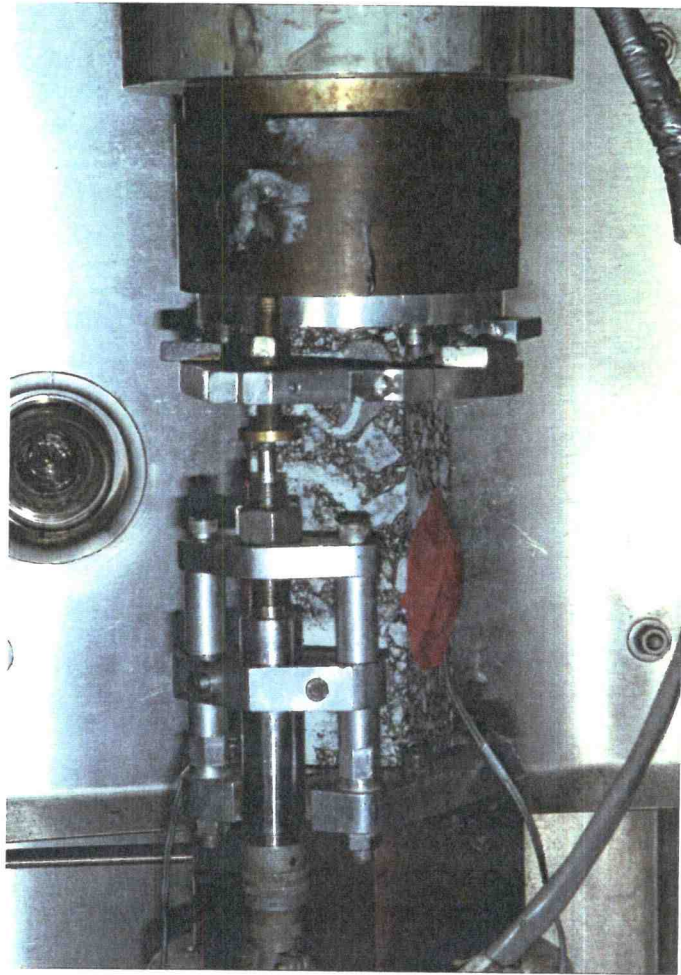
Figure 4.6   **Typical Direct Tension Test Specimen Mounted in the Modular OSU Test System.**

secant modulus, strain energy, and stiffness modulus versus time. The relative ranking of the mixtures based on the above parameters was compared to the ranking of the binders according to critical fracture temperature. The critical fracture temperatures of the asphalt cements were determined from the nomograph by Hills (1974) which correlates penetration at 25°C (77°F) and Penetration Index (PI) values with the critical fracture temperature of the binder. The nomograph developed by Hills and utilized here is reproduced in Figure 4.7. The relative ranking of the mixtures based on critical fracture temperature of the asphalt cement, after Hills, is as follows:

AAK2	(Highest Relative Crack Resistance)
AAK1	
AAG1	
AAG2	(Least Relative Crack Resistance)

4.6 Direct Tensile Creep Test Program (DTCT)

The DTCT provides a relatively direct means of characterizing the time-temperature dependent behavior of asphalt concrete mixtures. This method has been shown to provide reasonable estimates of stiffness modulus when compared with analytical approaches (Haas, 1973). Figure 4.8 presents a comparison of the stiffness modulus versus time relationships based on different methods. The DTCT

| Penetration at 25°C, 0.1mm | | Penetration at 0°C, 0.1mm | Penetration at 25°C, 0.1mm | | Critical temperature °C |
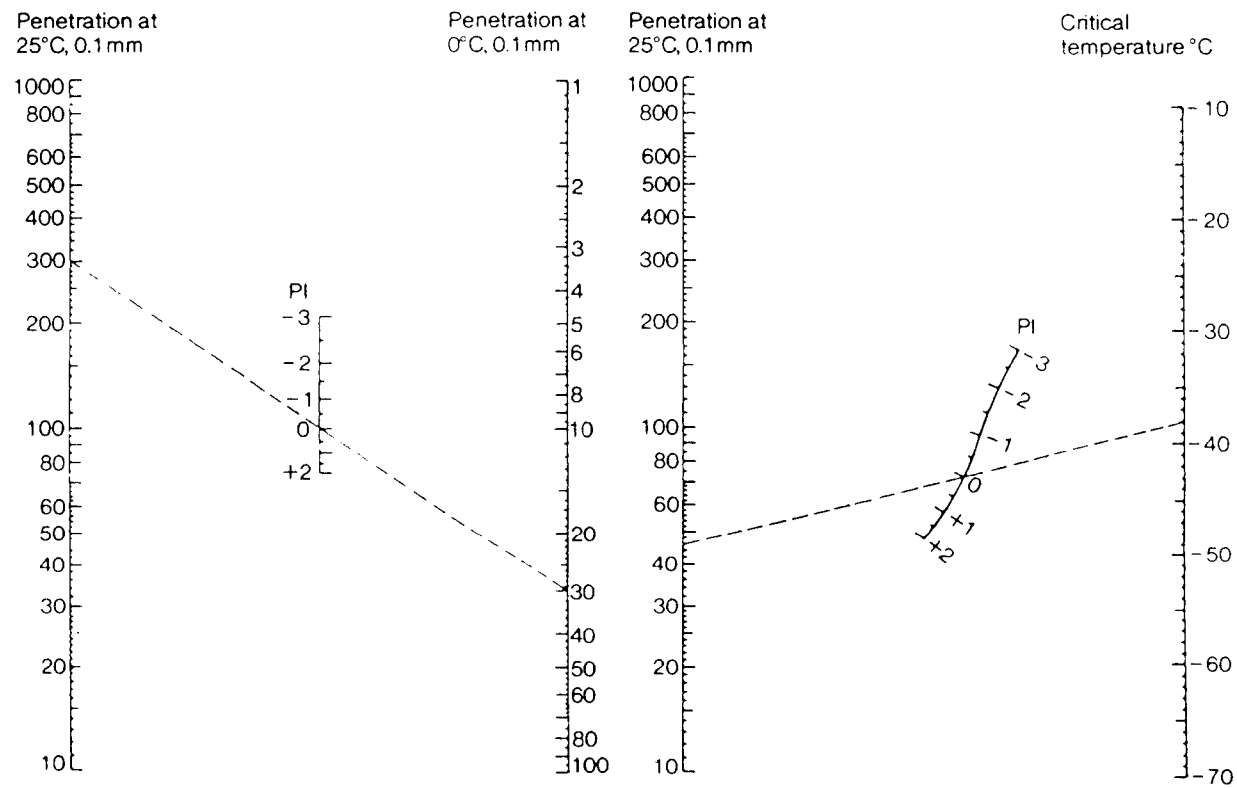
Figure 4.7 **Nomographs Used to Estimate Critical Fracture Temperature (Hills, 1974).**
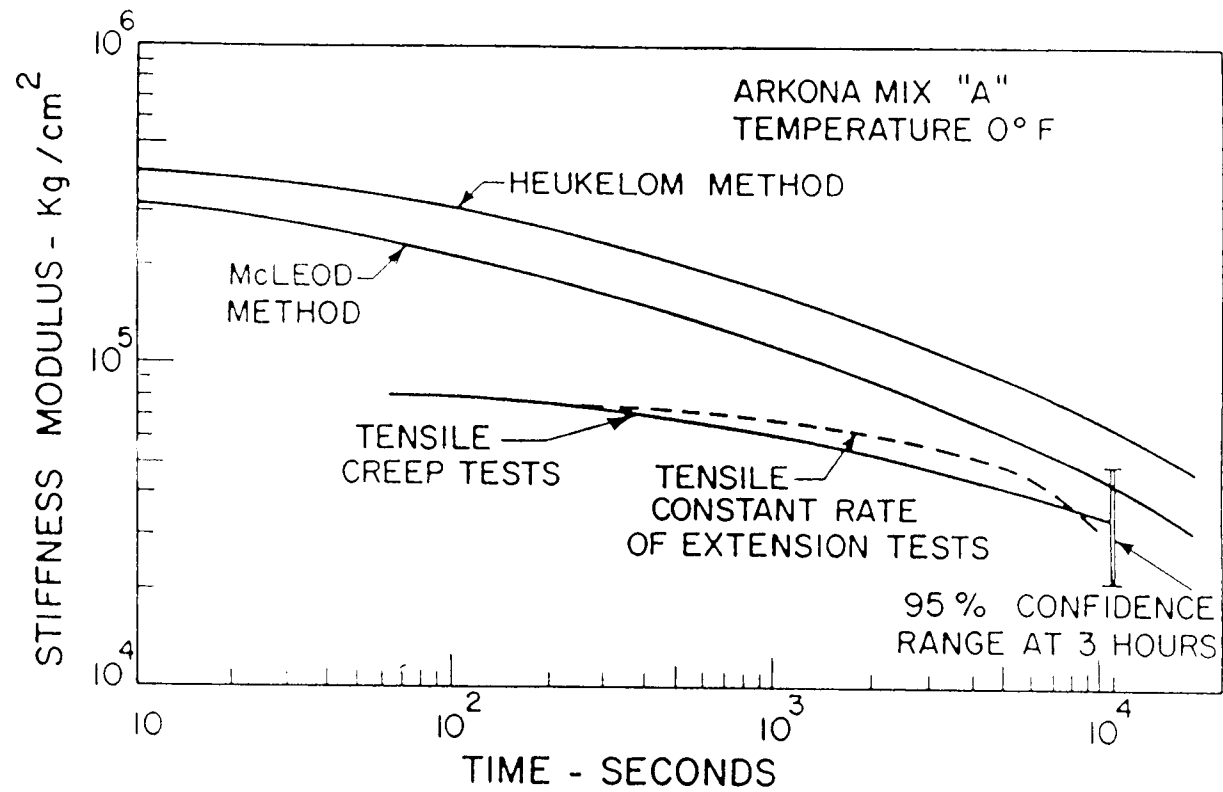
Figure 4.8   Comparison of Stiffness Modulus Versus Time Based on Analytical and Laboratory Methods (Haas, 1973).

was evaluated in this study with respect to the development of fundamental material properties to be implemented in a mechanistic analysis of thermal fatigue cracking of asphalt concrete mixtures.

4.6.1 General Test Procedure

The DTCT was conducted in the bituminous materials research laboratory at OSU. Tests were performed on selected asphalt concrete mixtures obtained from the SHRP MRL. The DTCT was conducted with the modular test system presented in Figure 4.2 and described in Appendix A.

In general, a constant load was applied to the cylindrical test specimens of dimensions 25.4 cm (10 in.) long by 5.72 cm (2.25 in.) diameter. The resulting strain was recorded with respect to the elapsed test time. Tests were conducted at three different test temperatures, 0°C (32°F), -10°C (14°F), and -20°C (-4°F). A typical cylindrical test specimen, mounted in the modular OSU test system, is pictured in Figure 4.9.

.The DTCT program was conducted at stress levels which were determined to be sufficiently low enough to satisfy the conditions of linear visco-elasticity as illustrated in Figure 2.4. A limited study was conducted prior to initiating the test program to establish suitable stress levels for the different mixtures and temperatures included in this study. In general, It was found that stress levels up to about 20 percent of the ultimate tensile strength were within the range of linear visco-elasticity at a temperature of 0°C (32°F). Higher stress levels were found to
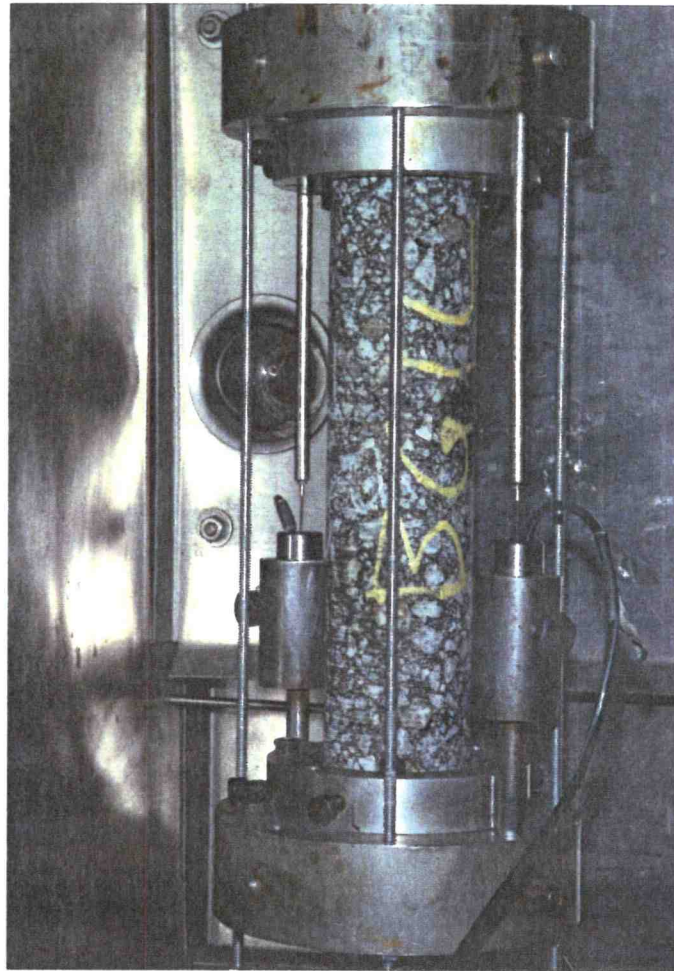
Figure 4.9   **Typical Cylindrical Direct Tensile Creep Test
Specimen Mounted in the Modular OSU Test System.**
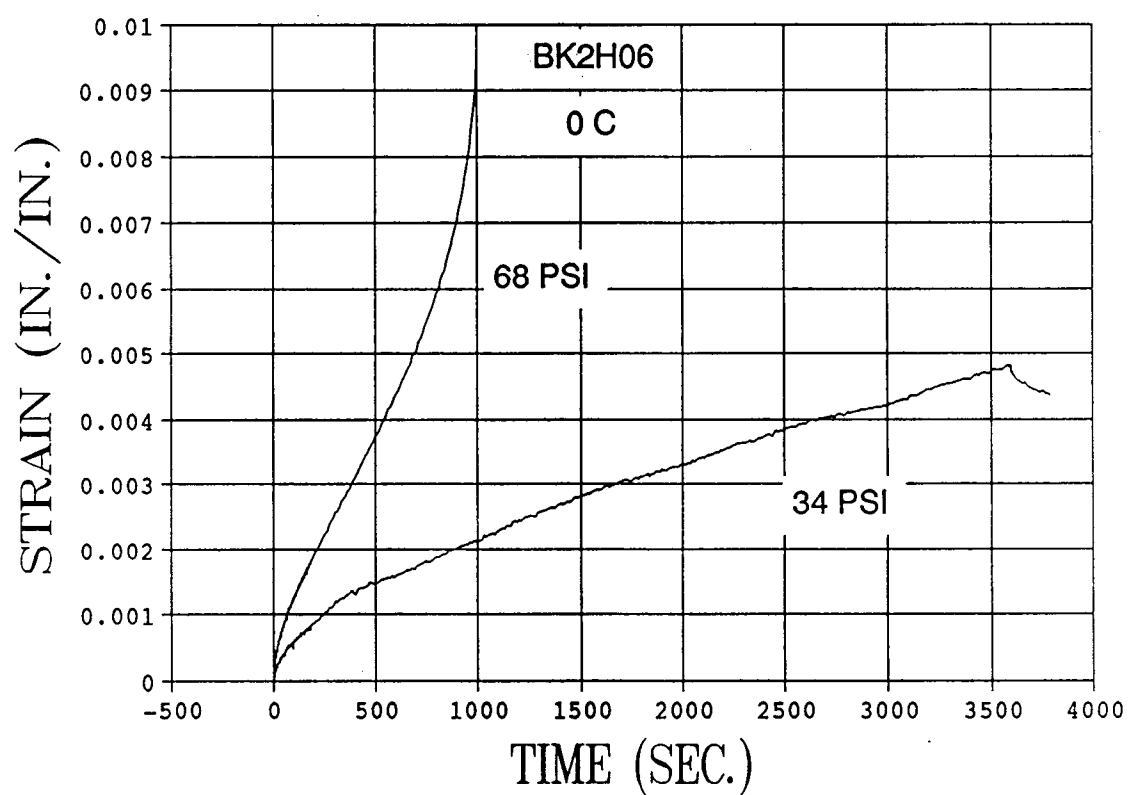
Figure 4.10   **Strain Versus Time For Asphalt Concrete Mixture Containing AAK-2 Binder with RB Aggregate and 8 +/- 1% Voids at 0°C.**

Note: 1 psi = 6.9 kPa
       1 in = 2.54 cm
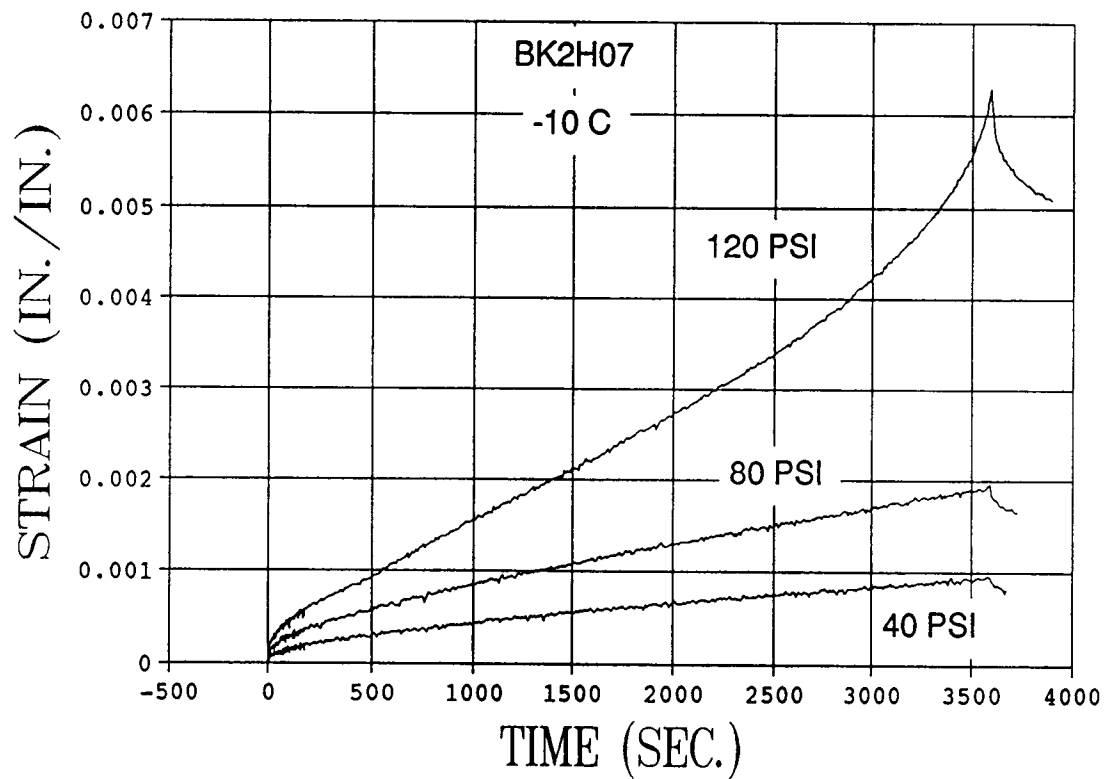
Figure 4.11   Strain Versus Time For Asphalt Concrete Mixture Containing AAK-2 Binder with RB Aggregate and 8 +/- 1% Voids at -10°C.

Note: 1 psi = 6.9 kPa
1 in = 2.54 cm
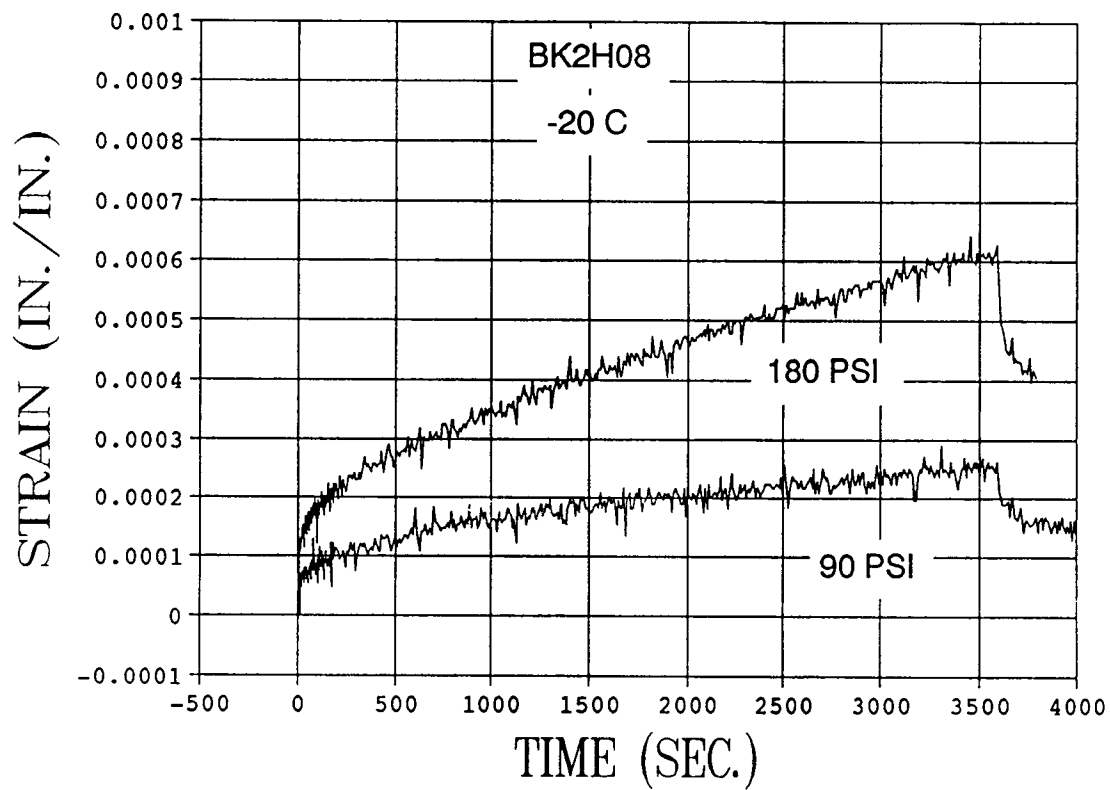
Figure 4.12   Strain Versus Time For Asphalt Concrete Mixture Containing AAK-2 Binder with RB Aggregate and 8 +/- 1% Voids at -20°C.

Note: 1 psi = 6.9 kPa

1 in = 2.54 cm

be acceptable at the lower temperatures of -10 and -20°C (14 and -4°F). Figures

4.10 through 4.12 display plots of strain versus time for different stress levels and

temperatures.

4.6.2   Interpretation of Test Results

DTCT results are typically plotted in the form of creep modulus versus

elapsed test time as presented in Figure 4.13. These curves, at three or more

temperatures, are then transformed to a standard temperature as previously outlined

in Figures 2.5 and 2.6. The standard temperature (T_M), the slope (m_1) and

intercept(E_0) of the transformed stiffness curve, and the slope (m_2) and the power

law constant (T_A) of the time-temperature shift factor curve are the characteristic

visco-elastic material properties which can be utilized in a mechanistic analysis of

thermal distress. A detailed discussion of the utilization of the visco-elastic

material properties developed from the DTCT is presented in Chapter 2, Sections

2.5 and 2.6.

4.7   Thermal Stress Restrained Specimen Test Program (TSRST)

Variations of the TSRST have been utilized by numerous researchers to

investigate thermal distress in asphalt concrete mixtures (Monismith, et. al., 1965,

Fabb, 1974, Sugawara and Moriyoshi, 1984, and Arand, 1987). This test method

enables a phenomenological evaluation of thermal distress in the controlled
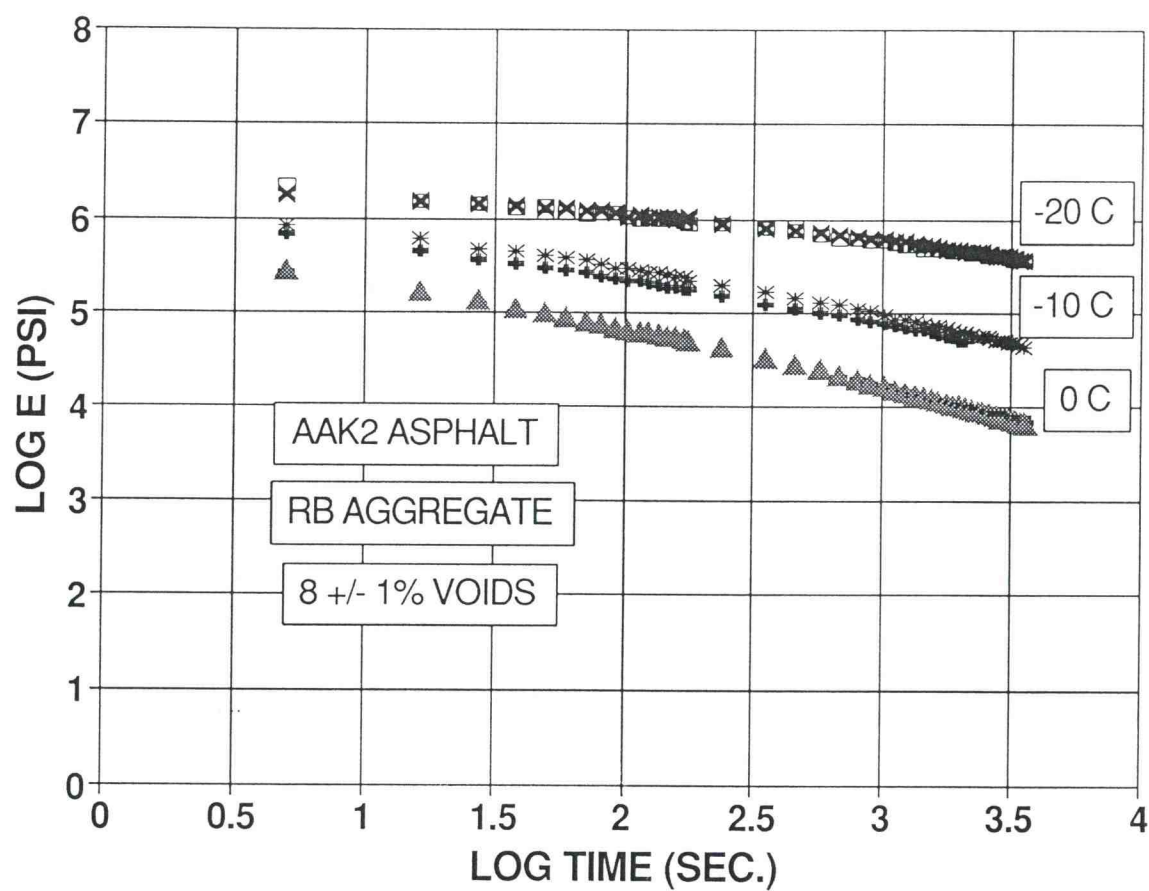
Figure 4.13 **Typical Direct Tensile Creep Test Results Plotted as Creep Modulus Versus Elapsed Test Time.**

Note: 1 psi = 6.9 kPa

environment of the laboratory. The Cyclic TSRST was included in this study to enable a phenomenological evaluation of the feasibility of the thermal fatigue mode of distress. Monotonic cooling tests were conducted to evaluate the overall repeatability of the test and establish appropriate limits for the cyclic cooling test program.

4.7.1 General Test Procedure

Phenomenological thermal fatigue tests and low temperature cracking tests were performed on selected asphalt concrete mixtures obtained from the SHRP MRL. This test program was conducted with the TSRST device developed at OSU under the SHRP A-003A contract. A schematic diagram displaying the major components of the OSU TSRST device is provided in Figure 4.14. In general, as pictured in Figure 4.14, the asphalt concrete test specimen is restrained at constant length by the electro-mechanical step motor as the temperature in the surrounding cryogenic environmental chamber is changed. The resulting thermally induced stress in the specimen is recorded with respect to the changing temperature at prescribed intervals during testing. A typical cylindrical test specimen mounted in the TSRST device is presented in Figure 4.15.

4.7.2 Interpretation of Test Results

Based on an extensive literature review and subsequent laboratory test program at OSU, the phenomenological TSRST has been identified as the most

Step Motor

Loading Rod

Supporting Rod

Swivel Jig

Clamp

Environmental
Chamber

LN2

Solenoid Valve

Invar Rod

AC Specimen

LVDT

End Platen

Circulating Fan

Micarta Block

Load Cell
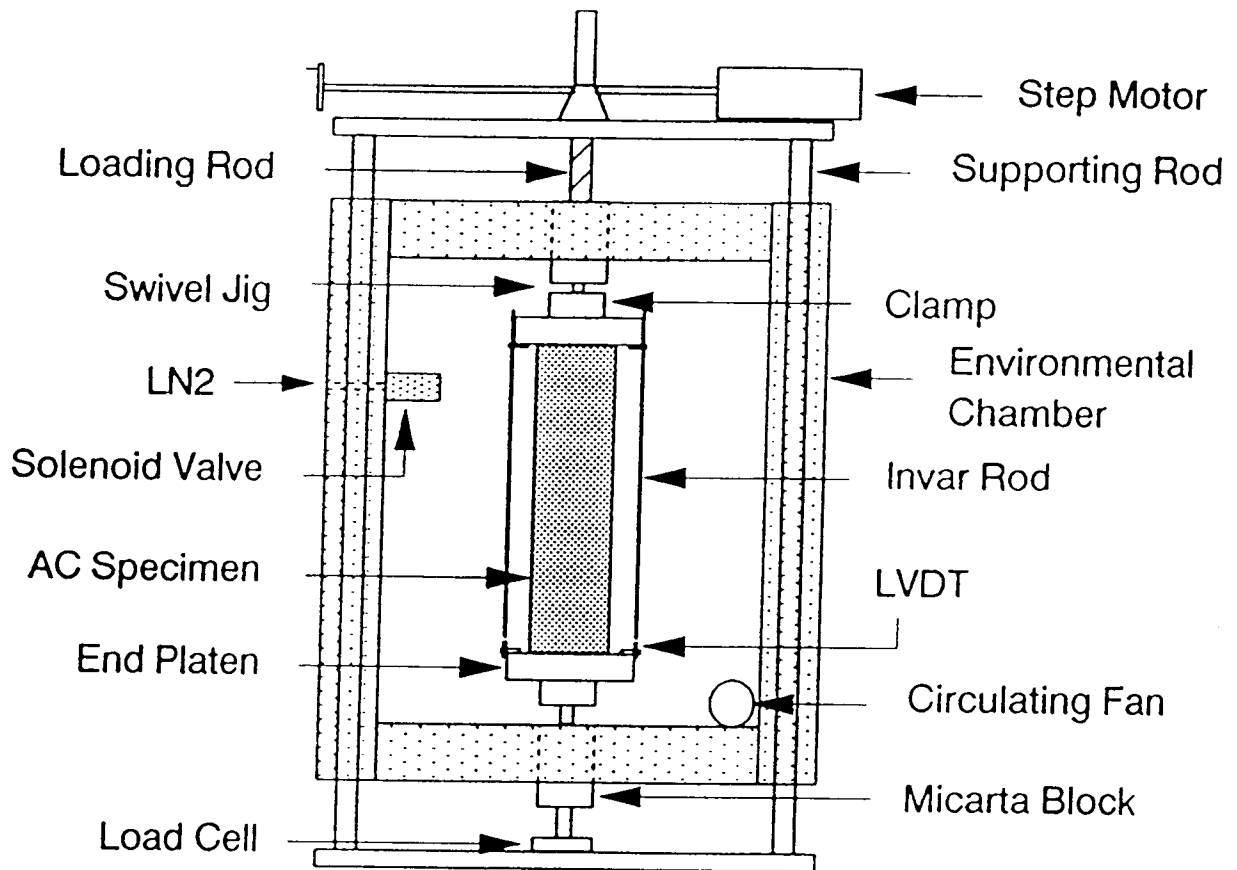
Figure 4.14   Schematic Diagram of the OSU TSRST Device
(Jung, 1990).
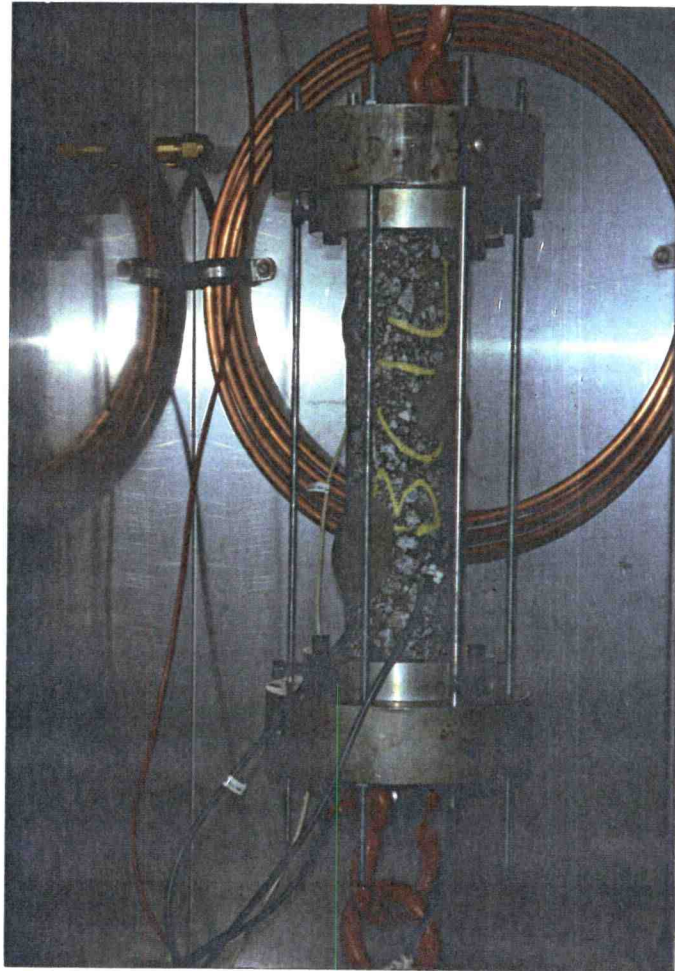
Figure 4.15   **Typical Cylindrical Test Specimen Mounted in the OSU TSRST Device.**

promising laboratory test method for validation of the relationship between asphalt mixture properties and pavement performance with respect to thermal effects. Correlations between laboratory TSRST results and actual field observations are currently being evaluated in a separate study under the SHRP A-003A contract. It is intended that these correlations will support the development of a probabilistic thermal cracking model at some future date. In the absence of such a model, the TSRST results obtained in this study are evaluated solely for validation purposes.

The TSRST is a phenomenological test procedure. Fundamental material properties are not currently attainable from this test method. However, the TSRST does enable direct analysis of thermal induced stresses under both monotonic and cyclic cooling. Typical TSRST results for both monotonic and cyclic cooling conditions are presented in Figures 4.16 and 4.17, respectively. Monotonic cooling tests are generally conducted to evaluate the temperature and stress at which low temperature cracking will occur. Cyclic cooling tests are performed to evaluate the potential for thermal fatigue cracking. Due to the extensive time periods required to perform cyclic cooling tests, the TSRST with cyclic cooling is not considered a realistic procedure for routine design. However, this procedure is valid for research purposes. The TSRST with monotonic cooling is considered to be a suitable candidate for routine design with respect to low temperature cracking.

The cyclic and monotonic TSRST results were utilized in this study for validation purposes only. As described in Chapter 2, Section 2.6, a modified
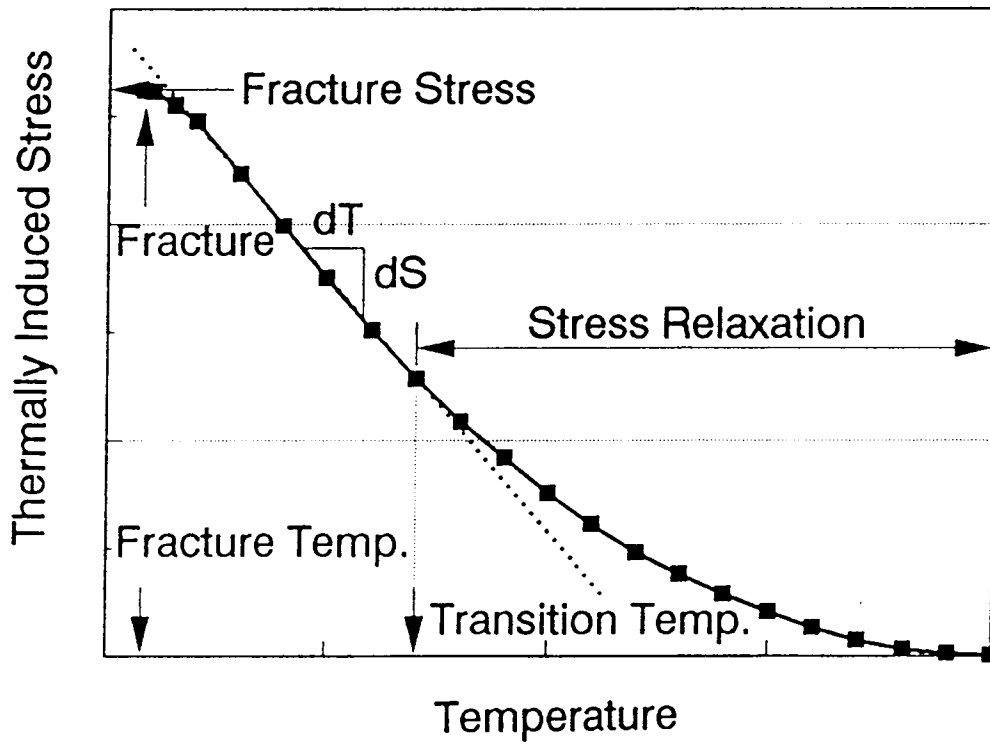
Figure 4.16   **Typical Monotonic Cooling TSRST Results.**
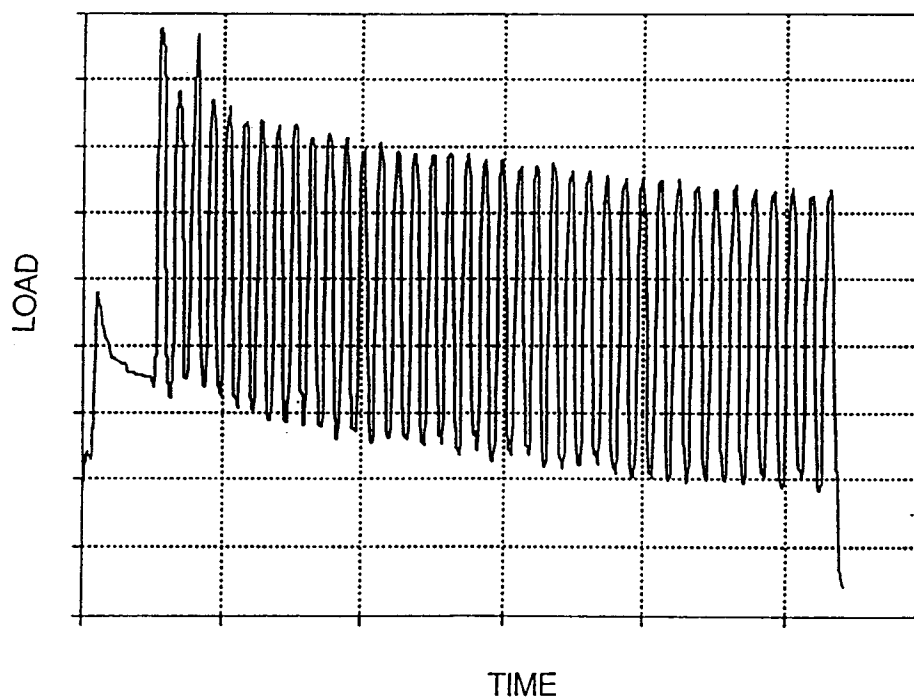
Figure 4.17   **Typical Cyclic Cooling TSRST Results.**

version of the Lytton, Shanmugham, and Garrett model was used to attempt to predict the response observed in the TSRST program. The results of the DTCT program were used to develop the visco-elastic input parameters for the Lytton, Shanmugham, and Garrett model. The results of this prediction analysis are documented in Chapter 6.

5.0 LABORATORY TEST RESULTS

5.1   Energy Rate Integral Test Results (ERIT)

The ERIT was evaluated with a full-factorial test program consisting of two

asphalt sources with two asphalt grades from each source, two levels of

compaction based on air voids, two test temperatures, three displacement rates, and

one aggregate type. In addition, all tests were replicated to evaluate the

repeatability of the test procedure. The test program consisted of a total of 96

tests.

The results of the test program are presented in Appendix E-1. The results

are summarized in Figures 5.1 and 5.2. Figures 5.1 and 5.2 present a graphical

comparison of the relative resistance to crack growth observed in the different

mixtures tested. The least squares best fit curves presented represent relative

resistance to crack growth for the respective mixtures. In general, mixtures

corresponding to steep slopes should possess greater resistance to crack growth

than those corresponding to flat slopes. This interpretation is based on the relative

energy required to develop a given crack speed.

The ERIT procedure appears to result in a relative ordering of the mixtures

with respect to resistance to fracture which is inconsistent with results obtained in

previous studies. In addition, as is noted in Appendix E-1, several mixtures

responded in brittle fracture at the test temperature and stroke rate applied. This is
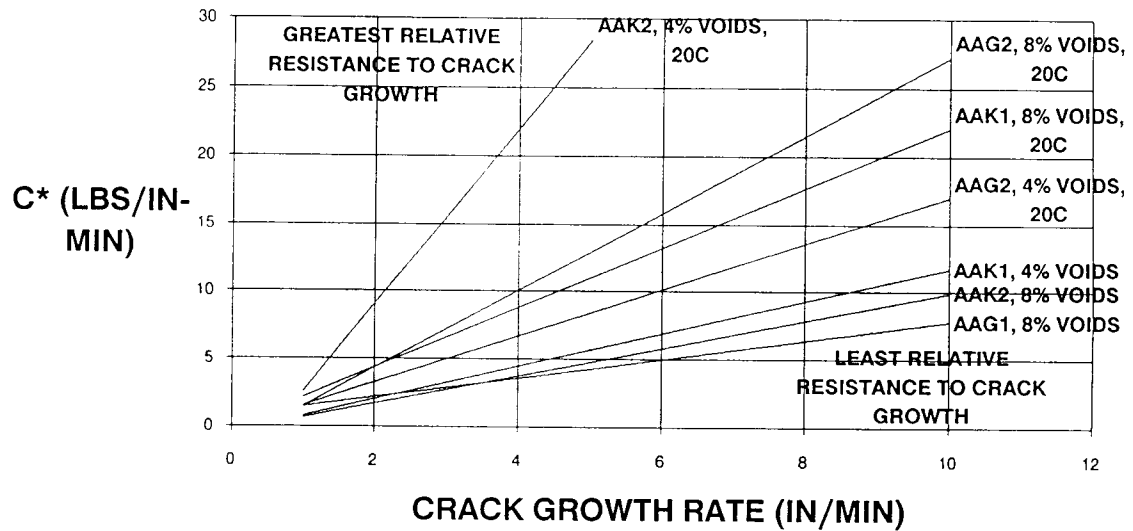
Figure 5.1   C*-Line Integral Versus Crack Growth Rate for
Different Asphalt Concrete Mixtures at 20 C.

Note: 1 lb/in-min = 0.029 N/cm-sec
1 in/min = 0.042 cm/sec
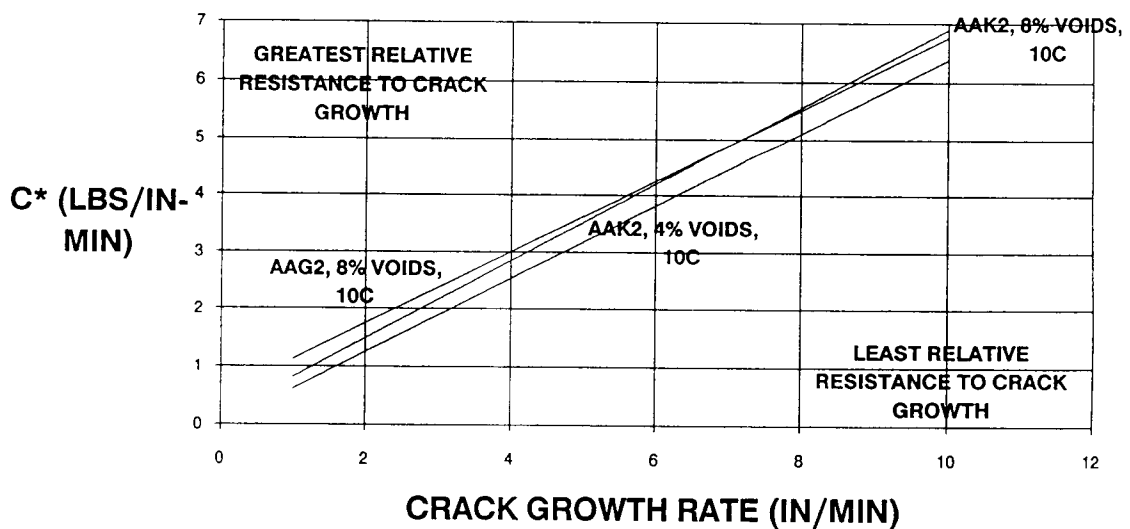
Figure 5.2   C*-Line Integral Versus Crack Growth Rate for
Different Asphalt Concrete Mixtures at 10 C.

an indicator that the ERIT, as performed here, may not be appropriate for the evaluation of crack growth at low temperatures.

Based on statistical analysis of the data, the Log_{10} of the least squares slope passing through the origin provides the most appropriate relationship for correlation between crack growth rate and the C*-Line Integral (Painter, 1990). However, the only statistically significant effect observed for the C*-Line Integral versus crack growth was temperature. No significant effects were found for either asphalt source or voids content. In addition, several mixtures could not be evaluated due to extremely rapid crack propagation.

As noted in Appendix E-1, only three of the mixtures tested at 10°C (50°F) could be evaluated. At relatively low temperatures, generally in the temperature range of interest for thermal fatigue cracking, the controlling fracture parameter is most likely the J-Integral, J_{IC} or more likely the Stress Intensity Factor, K_{IC}. The ERIT procedure does not readily provide sufficient small scale crack opening data for the determination of these parameters.

The ERIT does appear to be an appropriate test for investigating crack growth in asphalt concrete mixtures at moderate temperatures (Abdulshafi, et. al., 1990). However, at temperatures below about 20°C (68°F), the results appear to be inconsistent with established patterns. Significantly decreasing the test displacement rates may improve test performance at lower temperatures. However, test procedures would still have to be refined to account for the extremely rapid crack growth rates which occur at lower temperatures (Abdulshafi, et. al., 1990).

5.2 Direct Tension Test Results (DTT)

The DTT program at OSU was evaluated with a full-factorial test matrix. The test matrix consisted of two asphalt sources with two asphalt grades from each source, two levels of compaction based on air voids, two test temperatures, a single displacement rate, and one aggregate type. A similar, but expanded test program was also conducted at the University of Waterloo with the same material variables, three test temperatures, and three replicate tests.

The results of both the OSU test program and the University of Waterloo study are tabulated in Appendix E-2. In general, the results of the University of Waterloo study are consistent with those of the OSU study. The mean tensile strengths for the 16 combinations tested in the OSU study are summarized in graphical form in Figure 5.3. The mean strain energies for the same 16 combinations are presented in Figure 5.4.

Based on the relative ranking of the data with respect to the parameters measured herein, the DTT appears to provide a reasonable indication of the thermal response of asphalt concrete mixtures. As shown in Figure 5.3, ranking of the mixtures based on tensile strength is generally not consistent with the ranking of critical fracture temperature noted in the preceding section. This is also true for the samples tested in the University of Waterloo study. This observation is not surprising, however, based on previous research efforts. Test data presented by Mahboub (1985), Little and Mahboub (1985), and Abdulshafi and Kaloush (1988)
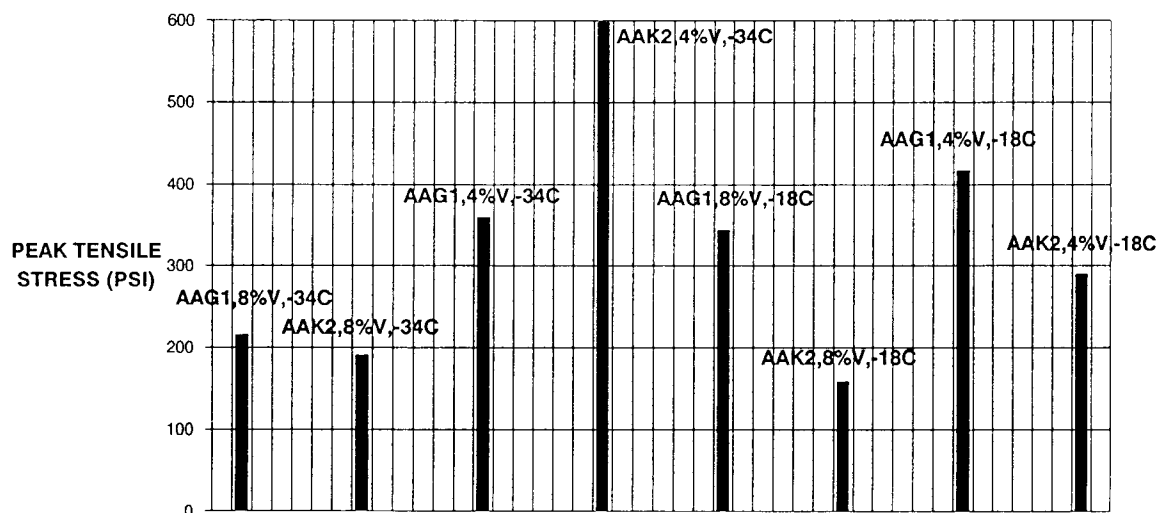
Figure 5.3   **Mean Tensile Strength for Different Asphalt Concrete Mixtures (OSU Study).**

Note: 1 psi = 6.9 kPa
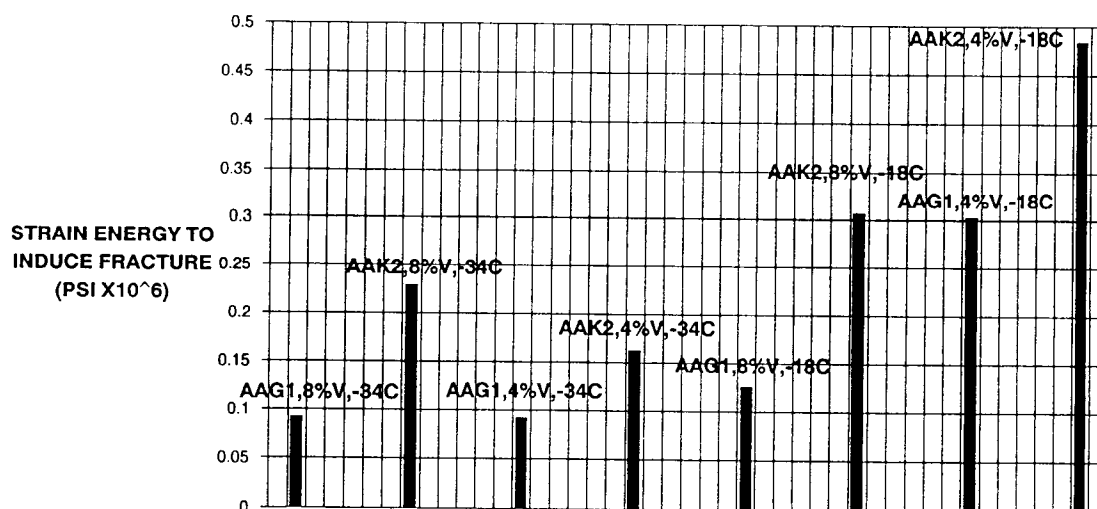
Figure 5.4   **Strain Energy at Fracture for Different Asphalt Concrete Mixtures (OSU Study).**

indicate that tensile strength, as determined from indirect tension testing, does not clearly differentiate between mixtures. Thus, attempts to rank the mixtures based solely on tensile strength will most likely yield misleading results.

The strain energy required to induce fracture appears to be a relatively reliable parameter for correlation with low temperature performance of the mixtures tested. Ranking of the mixtures based on strain energy, as shown in Figure 5.4, tends to be generally consistent with the low temperature properties of the binder (critical fracture temperature). In other words, the soft grade asphalt tends to require greater strain energy to produce fracture than the harder grade asphalt (AAK2 fails at a greater energy than AAG1). The test results from OSU and the University of Waterloo indicate, at constant voids, the energy required to fracture the specimens decreases with decreasing temperature. The test results also indicate, at constant temperature, the energy required to fracture the specimens decreases to some extent with increasing voids. However, the effect of voids is not as significant as that of temperature.

5.3   Direct Tensile Creep Test Results (DTCT)

The DTCT results obtained in this study are presented in the form of creep modulus versus elapsed test time in Appendix E-3. A typical plot of creep modulus versus elapsed test time is presented in Figure 4.11. The results are presented in Log_{10}-Log_{10} space to produce a relatively straight line which can be

readily characterized and evaluated with slope and intercept values. Replicate test results are plotted collectively on the same graph to illustrate the repeatability of the DTCT method. In general, the repeatability of the DTCT appears to be excellent. Coefficient of determination values for the replicate tests range from 0.813 to 0.994. The AAG-1 mixture tested with low voids and at -20°C (-4°F) is the only exception, with a relatively low coefficient of determination of 0.31.

The DTCT results were transformed to a standard temperature of -10°C (14°F). The transformed creep modulus curves and accompanying time-temperature shift factor curves are also presented in Appendix E-3. As noted above, these curves represent visco-elastic mixture properties which can be utilized in a mechanistic analysis of thermal distress. The standard temperature (T_m), the slope (m_1) and intercept(E_0) of the transformed curve, and the slope (m_2) and the power law constant (T_a) of the time-temperature shift factor curve make up the visco-elastic mixture properties required as input to the modified THERM program. The visco-elastic properties obtained from the DTCT program are summarized in Table 5.4.

5.4   Thermal Stress Restrained Specimen Test Results (TSRST)

The TSRST with monotonic cooling was evaluated with a full-factorial test program consisting of two asphalt sources, two levels of compaction based on air voids, and one aggregate type. Replicate tests were conducted for each test

68

Table 5.1   Summary of Visco-Elastic Material Properties Obtained From the DTCT Program and Utilized as Input to the Program THERM.

MIXTURE VARIABLE I.D.	T_m	m_1	E_0	T_a	m_2
BK2H	-10.0	-0.473	6.273	-35.0	-8.150
BK2L	-10.0	-0.461	6.452	-95.0	-33.957
BG1H	-10.0	-0.278	6.703	-85.0	-31.711
BG1L	-10.0	-0.219	6.736	-85.0	-32.568

T_m = Standard Temperature of Transformed Creep Modulus Curve.

m_1 = Slope of the Transformed Creep Modulus Curve.

E_0 = Intercept of the Transformed Creep Modulus Curve.

T_a = Power Law Constant for the Time-Temperature Shift Factor Curve.

m_2 = Slope of the Time-Temperature Shift Factor Curve.

combination. Cylindrical test specimens of dimensions 10 in. (25.4 cm) long by 2.25 in. (5.72 cm) diameter were utilized. The test program consisted of a total of 8 tests. The results of the monotonic cooling test program are summarized in Table 5.5. The monotonic cooling test results are also plotted in Appendix E-4. Replicate test results are presented together on the same figure to display test variability.

In general, the observed fracture temperature (T_f) for the mixture tested exhibits relatively minor variability between replicate test specimens. A maximum standard deviation of .4°C (.72°F) in T_f was observed for the mixtures containing AAK2 asphalt. A maximum standard deviation of 1.6°C (2.88°F) in T_f was observed for the mixtures containing AAG1 asphalt. A maximum standard deviation of 98 psi (676 kPa) in fracture stress (S_f) was observed between replicate specimens for all combinations tested in this study. In general, the results observed in this study are consistent with data obtained from extensive monotonic cooling testing of beam specimens with the TSRST device at OSU (Jung, 1990). It is worth noting that the relative ranking of the mixtures based on fracture stress does not coincide with the relative ranking based on fracture temperature. This observation coincides with the results obtained from the DTT program. That is, the fracture stress is not a reliable parameter with respect to evaluating thermal distress. The fracture temperatures noted in Table 5.2 were used in this study to establish thermal limits for the cyclic cooling TSRST study described in the following paragraphs.

Table 5.2   **Summary Table of Monotonic Cooling TSRST Results.**

MIXTURE VARIABLE I.D.	MEAN FRACT. TEMP. (°C)	STAND. DEVIAT. (°C)	MEAN FRACT. STRESS (PSI)	STAND. DEVIAT. (PSI)
BK2H	-31.8	0.1	458	15
BK2L	-30.3	0.4	431	98
BG1H	-18.6	1.6	388	77
BG1L	-15.4	1.1	496	10

Note: 1 psi = 6.9 kPa

As noted, the TSRST was also conducted under conditions of cyclic cooling. Cyclic cooling tests were conducted at OSU and at the USA CRREL in Hanover, New Hampshire to evaluate the proposed thermal fatigue mode of distress. The OSU TSRST device was utilized in both studies. The objective of this test program was to evaluate the feasibility of the proposed thermal fatigue distress mechanism in typical asphalt concrete mixtures. Due to the anticipated lengthy duration of the cyclic cooling tests (up to several months per test), it was not possible to develop a comprehensive experiment design in the time allowed for this study. However, several tests were conducted at both OSU and at the USA CRREL facilities. The results of several of the successful cyclic cooling tests performed at OSU and at the USA CRREL facilities are plotted in terms of thermal induced load or stress versus time in Appendix E-4. These cyclic cooling test results are summarized in Table 5.3. Many more tests were initiated and subsequently aborted due to mechanical difficulties with the testing equipment. Tests were conducted at cooling rates ranging from 10°C (18°F) per hour to 20°C (36°F) per hour with soak periods of approximately one hour in all cases. Fatigue cracking was not observed in any of the cyclic fatigue tests conducted in this study. A significant decrease in thermal stress with increasing number of thermal cycles was observed in most of the samples tested, however. Two tests conducted at the USA CRREL facilities endured for over 400 cycles before being terminated due to a power outage.

A plot of the peak thermal stress versus the number of thermal cycles for a

Table 5.3   **Summary Table of Cyclic Cooling TSRST Results.**

MIX. VAR. I.D.	THERM. RAMP (°C) FROM/TO	COOLING/ HEATING RATE (°C/HR.)	PEAK THERM. STRESS (PSI)	DECREASE IN THERMAL STRESS (PSI)	NUMBER OF CYCLES TESTED (N)
BK1H 1	-10/-20	10	171	63	40
BK1L 3	-10/-20	10	--	--	> 400
BK2L 2	0/-20	20	275	100	240
BG2L 6	-10/-20	10	305	105	87
BG2L 7	-10/-20	10	232	--	> 400
BG1H 1	0/-10	10	198	63	125

Note: 1 psi = 6.9 kPa

BG1L
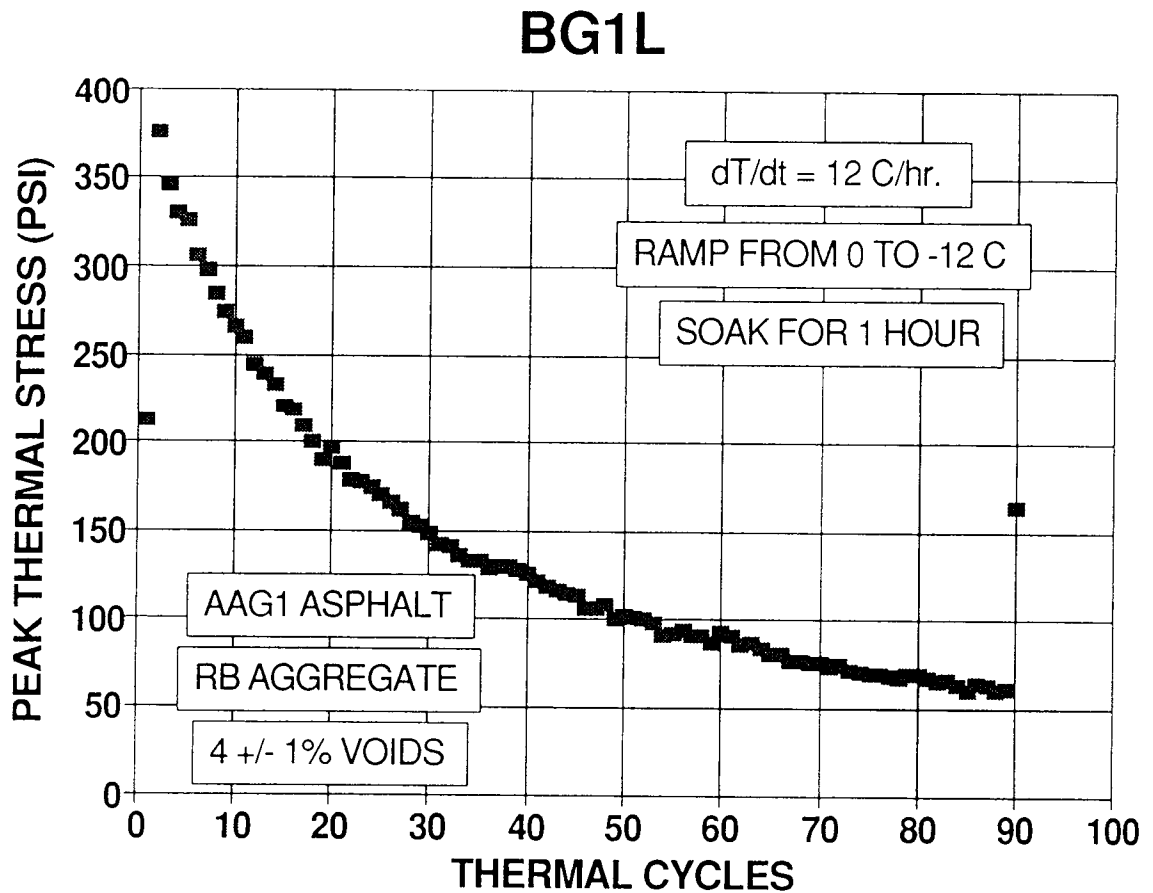
Figure 5.5   Peak Thermal Induced Stress vs. Thermal Cycles For an Asphalt Concrete Mixture Containing AAG-1 Binder with RB Aggregate and 4 +/- 1% Voids.

Note: 1 psi = 6.9 kPa

representative sample containing AAG1 asphalt and 4 +/- 1% voids is presented in Figure 5.5. This specific test was conducted with a cyclic thermal regime consisting of a one hour ramp from 0 to -10°C (32 to 14°F) and a one hour soak period at the respective thermal limits. The response depicted in Figure 5.5 is characteristic of the results obtained in this study. Similar laboratory results have also been documented by previous researchers (Sugawara and Moriyoshi, 1984).

In general, the peak stress resulting from thermal loading depicted in Figure 5.5 tends to decrease with increasing load applications. This response is similar to the characteristic visco-elastic behavior presented in Figure 2.3 for a controlled stress test. The TSRST is actually a controlled strain test. Thus, the response observed in Figure 5.5 is partially the result of stress relaxation. This stress relaxation results from permanent strain occurring in the restrained specimen during thermal contraction. Relaxation continues with subsequent thermal cycling until stresses eventually decrease to the range of elastic response. At this reduced stress level, thermal cycling can continue indefinitely without mechanically damaging the specimen.

The response depicted in Figure 5.5 has also been attributed to micro-cracking by several researchers (Sugawara and Moriyoshi, 1984, and Gerritsen and Jongeneel, 1988). In general, micro-cracking is believed to develop within asphalt concrete pavements subjected to thermal cycling and subsequently results in an overall reduction in thermal induced stresses. Regardless of whether stress relaxation results from visco-elastic response or micro-cracking, there is no known

mechanism available in the field to introduce additional stresses to the pavement once permanent strains have developed.

As shown in Table 5.3, a decrease in thermal induced stress of almost 50 percent was observed in all of the samples tested. However, close inspection of the samples tested in this study revealed no visible evidence of cracking. In addition, as shown in Figure 5.5, upon re-loading of the test specimens after terminating the cyclic testing, additional stresses could be maintained (note the final point shown on the curve presented in Figure 5.5).

It is important to remember that no significant environmental aging was imparted to the specimens tested in this study. These results suggest that thermal fatigue cracking may not be a significant mode of distress in the absence of environmental aging. The environmental aging component is likely a prerequisite to thermal fatigue distress. The conditions tested in the TSRST device represent the worst case scenario with the specimen being fully restrained. In the field, with only partial restraint provided by the pavement base course, cracking due to this mode of distress is even less likely than demonstrated in the laboratory.

Based on the results of this study, it is hypothesized that distress typically attributed to thermal fatigue is actually the result of a special case of low temperature cracking. TSRST results for environmentally aged specimens have demonstrated that fracture temperature tends to increase with increased aging (Vinson, et. al., 1992). This age hardening effect is presented in Figure 5.6 based on test data developed at OSU. At the point when the critical fracture temperature
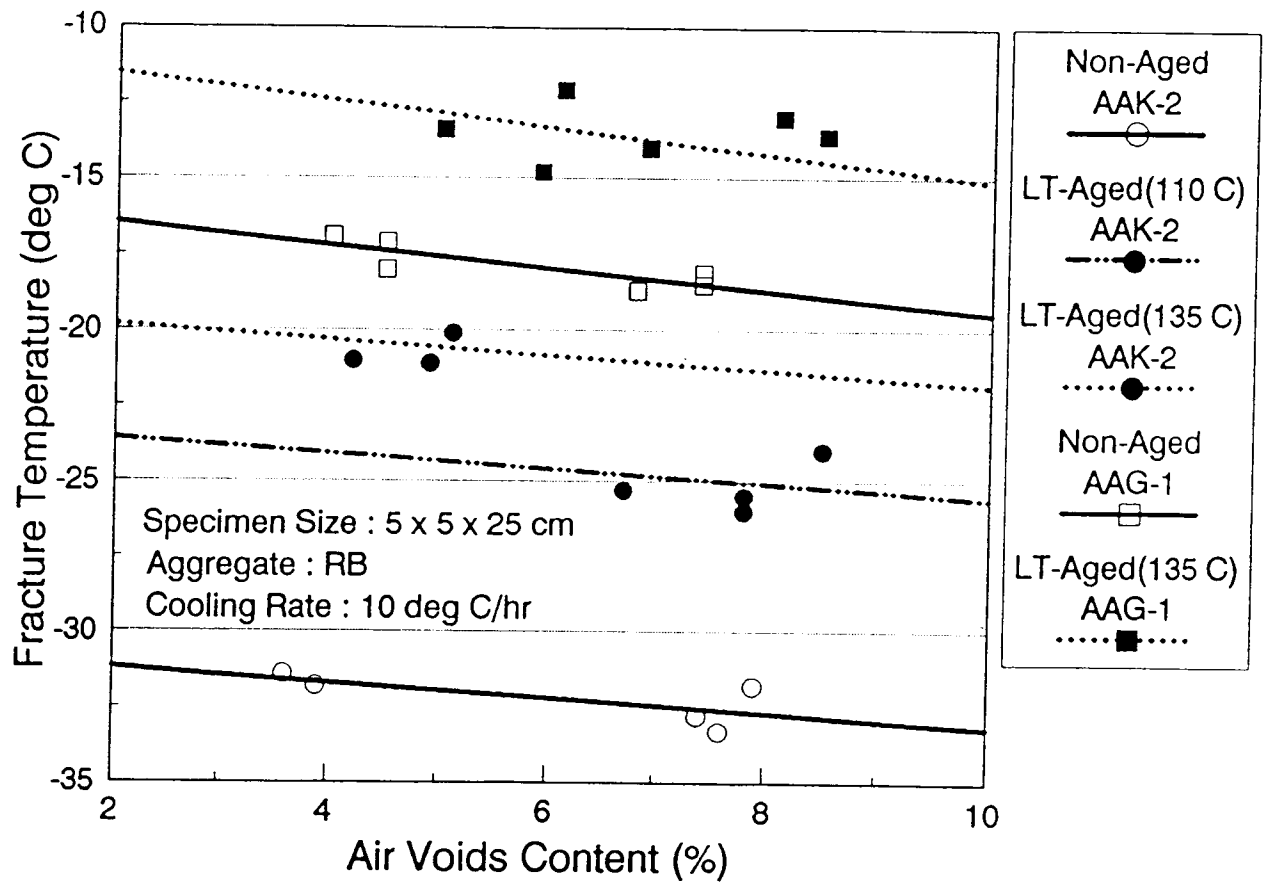
Figure 5.6 **Effect of Environmental Aging on Fracture Temperature (Vinson, et. al., 1992).**

intersects the lowest pavement temperature, cracking will result. A schematic illustration of this common low temperature cracking scenario is presented in Figure 5.7. This cracking mechanism does not exclude the occurrence of fatigue damage in the pavement due to thermal cycling. Small scale fatigue damage has been demonstrated to occur due to such loading (Gerritsen, 1988). However, the damaging effects of environmental aging are believed to overshadow any cumulative thermal fatigue damage. Thermal fatigue distress is believed to be insignificant with respect to the various other distress modes which simultaneously degrade the pavement structure. Similar conclusions were proposed by Anderson, et. al (1983), based on their analysis of recovered asphalt from distressed pavements in west Texas.

In addition to asphalt mixture properties, base and subgrade materials have been identified as primary causes of much of the so-called thermal fatigue cracking in west Texas. As far back as the late 1950's, an engineer with the Texas Highway Department by the name of Frank Frey recognized that pavements in west Texas did not experience severe transverse cracking where the roadways crossed areas of select subgrade soils, such as in river beds (Lytton, 1992). Extensive research on the soils in this region of Texas has demonstrated that the montmorillonite clays common to this area are extremely conducive of transverse cracking in pavements (Carpenter and Lytton, 1975). Thus, the role of thermally induced fatigue damage in the asphalt concrete pavement appears to be minor when compared with the various contributing factors leading to transverse cracking.
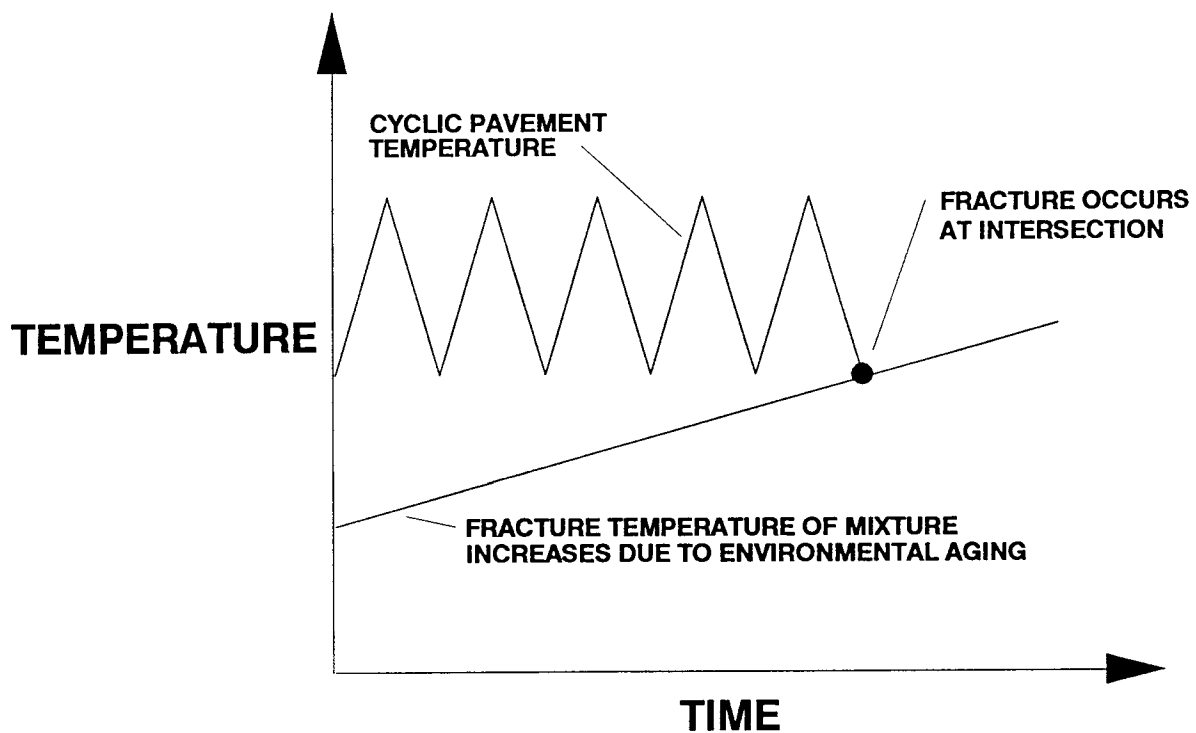
Figure 5.7   Schematic Illustration of Superimposed Low
Temperature Cracking and Environmental Aging
Effect on Fracture Temperature.

6.0 THERMAL FATIGUE PREDICTION ANALYSIS

6.1 Prediction Model

The primary objective of the prediction analysis conducted herein was to demonstrate the use of DTCT results in a mechanistic thermal cracking model. The development of a new mechanistic model to evaluate thermal fatigue cracking was beyond the scope of this study. An improved thermal cracking model is, however, currently being developed under a separate SHRP contract (Contract A-005). The model has not been verified at this time and was not available for this research program.

A slightly modified version of the Lytton, Shanmugham, and Garrett model was used in this study to predict the results observed in the TSRST device. Based on an extensive literature review, this model was identified as the most comprehensive existing model capable of predicting thermal fatigue cracking. The Lytton, Shanmugham, and Garrett model consists of the computer programs VISCO and THERM, developed at the Texas Transportation Institute. The model is based on fracture mechanics with thermal stresses calculated from visco-elastic theory.

The results of the DTCT program were used to develop visco-elastic input parameters for the modified THERM program. As presented in Chapter 5, Section 5.5, transformed stiffness curves were estimated with the DTCT results obtained in

this study. The DTCT results, at three different temperatures, were transformed to a standard temperature of -10°C (14°F). The standard temperature (T_m), the slope (m_1) and intercept(E_0) of the transformed curve, and the slope (m_2) and the power law constant (T_a) of the time-temperature shift factor curve make up the visco-elastic mixture properties required as input to the modified THERM program.

In addition to the visco-elastic parameters noted above, the THERM program utilizes various binder, aggregate and mixture properties, solar radiation, wind velocity, and thermal coefficients to estimate the effects of aging of the mixture. These input parameters are outlined in the first few pages of the program source code listing provided in Appendix D. Since the goal of this study was to evaluate thermal fatigue without the aging component, the aging computations were effectively turned off in this study by setting the solar radiation and wind velocity parameters to zero. The initial values for binder properties (i.e penetration and ring and ball softening point) were carried through the entire analysis period without change.

The THERM program was run with an assumed initial crack depth of 0.1 in. (.25 cm) and a full pavement depth of 1.125 in. (2.86 cm). The assumed pavement depth was based on the radius of the 2.25 in. (5.72 cm) diameter cylindrical specimens tested in this study. It was assumed that an initial flaw of 0.1 in. (.25 cm) would propagate diametrically from the perimeter to the center of the specimen.

The THERM program computes pavement temperatures on an hourly basis.

Temperatures are computed based on the daily maximum and minimum input temperatures with a 24 hour, sinusoidal function. Crack depth (YC) is printed along with the date, number of cycles (NF), cumulative number of cycles (NF1), and cumulative damage parameters (CDMG and CDMG1) for each month until a full-depth crack is computed. This information is also printed for the day when the full-depth crack is computed. A sample output file is listed at the end of the program source code listing in Appendix D.

It should be noted that the thermal regime described above corresponds to a rate of cooling which is somewhat slower than that observed in the laboratory with the TSRST device. This discrepancy could be accounted for with additional modifications to the THERM program. However, the error in the computations associated with this source is considered to be insignificant.

6.2   Prediction Results

The visco-elastic parameters presented in Table 6.1 were input into the THERM program along with the respective environmental boundary conditions applied in the TSRST program. Since none of the tests conducted with the TSRST device experienced cracking, it was not possible to precisely evaluate the computed predictions of fatigue cracking. However, numerous runs of the THERM program were performed for general comparison purposes. The computations performed with the THERM program indicate that a full-depth crack would not develop in the

mixtures evaluated herein even after experiencing over 3000 thermal cycles. An example output file is included at the end of the THERM program source code listing in Appendix D.

The results of this study tend to agree with the results of our laboratory TSRST program. That is, in the absence of environmental aging, a period of more than seven years would be required to develop a single thermal fatigue crack. The accuracy of this computation is somewhat debatable based on the various assumptions and simplifications involved in the use of the THERM model. Nevertheless, these computations reveal that an excessive period of time is required to induce thermal cracking in the unaged test specimens. As noted, these computations are in general agreement with the test results observed in the laboratory cyclic cooling study.

7.0 CONCLUSIONS

The objectives of this study were to investigate the possible occurrence of thermal fatigue cracking and identify a suitable laboratory test program to facilitate a mechanistic analysis of this mode of distress. To achieve these objectives, an extensive test program, including the Energy Rate Integral Test (ERIT), the Direct Tension Test (DTT), the Direct Tensile Creep Test (DTCT), and the Thermal Stress Restrained Specimen Test (TSRST) was conducted in the bituminous materials laboratory at OSU. A limited prediction analysis was also conducted to demonstrate how the results of the DTCT can be utilized in a mechanistic thermal cracking model. A slightly modified version of the Lytton, Shanmugham, and Garrett model was used in this study to predict the results observed in the TSRST program. The Lytton, Shanmugham, and Garrett model consists of the computer programs VISCO and THERM, developed at the Texas Transportation Institute. Conclusions based on the results of this study are summarized in the following paragraphs.

The results of this study suggest that the ERIT is not suitable for the evaluation of thermal distress. At low temperatures, generally in the temperature range of interest for thermal cracking, the controlling fracture parameter is most likely the J-Integral, J_{IC}, or more likely the Stress Intensity Factor, K_{IC}. The ERIT procedure followed in this study does not readily provide adequate small scale crack opening data necessary for the determination of such parameters.

The ERIT appears to be an appropriate test for investigating crack growth in asphalt concrete mixtures at moderate temperatures (Abdulshafi, et al., 1990). However, at temperatures below about 10°C (50°F), the results appear to be inconsistent with established patterns. Significantly decreasing the displacement rates may improve test response at lower temperatures, however the test procedure still requires modification to account for extremely rapid crack growth rates.

The DTT appears to provide sufficient information to facilitate an empirical analysis of thermal cracking of asphalt concrete mixtures. However, the results of this test are not suitable for a mechanistic analysis of thermal distress. Based on the relative ranking of the test data developed herein with respect to direct tensile strength and strain energy, the strain energy required to induce fracture was identified as a reliable parameter for correlation with low temperature performance. Ranking of the mixtures based on direct tensile strength does not consistently agree with the ranking based on critical fracture temperature or field observations. The failure of the tensile strength to adequately differentiate between mixtures is not surprising as noted by various researchers (Mahboub, 1985, Little and Mahboub, 1985, and Abdulshafi and Kaloush, 1988).

Ranking of the mixtures based on strain energy obtained from the DTT tends to be generally consistent with the ranking of the critical fracture temperature of the binder. The soft grade asphalt tends to require greater strain energy to produce fracture than the harder grade asphalt. In general, the DTT under constant rate of extension provides empirical information which is consistent with

existing analytical methods and field observations. The results of this test method can be utilized for relative comparisons of mixtures with respect to those of known field performance. However, fundamental material properties which can be implemented in an existing mechanistic analysis are not attainable from this test method.

Fundamental, visco-elastic material properties are attainable from the DTCT. The results of this study suggest that the DTCT, performed at three or more temperatures, provides sufficient information to proceed with a mechanistic analysis of thermal fatigue distress. Transformed creep modulus curves can be developed with DTCT data. This study demonstrates that such curves can be successfully used to estimate stiffness modulus in an existing thermal distress model. This approach is an improvement to existing empirical analyses and enables a mechanistic evaluation of a broader range of mixtures.

The TSRST is a phenomenological procedure which does not currently provide fundamental, mechanistic material properties. However, the TSRST does enable a direct analysis of thermal induced stresses. Both monotonic and cyclic cooling conditions can be approximated with the TSRST at a variety of cooling rates and thermal regimes. Due to the extensive time periods required to perform cyclic tests, the cyclic cooling procedure is recommended primarily for research applications. The TSRST with monotonic cooling is considered to be a realistic candidate for routine design with respect to low temperature cracking.

The most significant finding of this study was that fatigue cracking was not

observed in any of the cyclic cooling tests conducted. Stress relaxation was observed in lieu of cracking in all cases. The results of this study suggest that thermal fatigue cracking is not a significant mode of distress in the absence of environmental aging. It is proposed that distress typically attributed to thermal fatigue is actually the result of a special case of low temperature cracking or base and subgrade related problems. The damaging effects of environmental aging, base and subgrade problems, and vehicular distress modes were not evaluated herein. However, based on the results of this study, these distress mode are believed to overshadow any possible cumulative effects from thermal fatigue.

The Lytton, Shanmugham, and Garrett thermal fatigue cracking model was used to demonstrate the potential application of laboratory test data in an existing mechanistic analysis of thermal distress. This model is based on fracture mechanics with thermal stresses calculated from visco-elastic theory.

The DTCT results were used to develop visco-elastic input parameters for the Lytton, Shanmugham, and Garrett model. The program THERM was modified, as necessary, to accommodate direct input from the DTCT results. Numerous runs were performed with the program to compute the estimated number of cycles required to develop a full-depth crack in the specimens tested with the TSRST device.

In general, the results of the thermal fatigue prediction analysis reinforce the conclusions drawn from the phenomenological cyclic cooling TSRST program. That is, in the absence of environmental aging, or some other contributing factor,

the number of cycles (and thus the time) required to develop full-depth cracking is excessive. Consequently, it is believed that thermal fatigue distress due to thermal loading of semi-restrained pavements does not occur.

8.0 RECOMMENDATIONS FOR FURTHER RESEARCH

Based on the results of this study, it is recommended that future research efforts concentrate primarily on the effects of environmental aging with respect to thermal cracking. The cyclic cooling TSRST results documented herein suggest that thermal fatigue cracking is not of significant concern in the absence of environmental aging. However, low temperature cracking may be a serious concern once a mixture has been exposed to environmental aging. Results presented by previous researchers tend to agree with the this conclusion (Anderson and Epps, 1983).

A limited monotonic cooling TSRST program was conducted on oven aged specimens in the bituminous materials laboratory at OSU. The results of this work were presented in Figure 5.6. It is recommended that additional mixtures be tested in this fashion to establish specifications regarding aging susceptibility of asphalt concrete mixtures. Monotonic cooling tests should be conducted on samples of like mixture properties with differing degrees of aging. It is envisioned that a limiting change in fracture temperature observed in the TSRST can be established to avoid thermal cracking in the field over the design life of a given pavement.

REFERENCES

1.   Abdulshafi, A. and O. Abdulshafi, "Innovative techniques to distinguish performance of asphalt-aggregate interaction and mixtures," Strategic Highway Research Program Phase I Draft Report No. SHRP A-IIR-12, June, 1990.

2.   Abdulshafi, O.A., "Rational material characterization of asphalt concrete pavements," Research dissertation submitted to The Ohio State University, Columbus, Ohio, 1983, in partial fulfillment of the requirements for the degree of Doctor of Philosophy.

3.   Abdulshafi, A.A. and K.E. Kaloush, "Modifiers for asphalt concrete," ESL-TR-88-29, Air Force Engineering and Services Center, Tyndall Air Force Base, Florida, August, 1988.

4.   Abdulshafi, A.A. and K. Majidzadeh, "J-integral and cyclic plasticity approach to fatigue and fracture of asphaltic mixtures," Transportation Research Record No. 1034, 1985, pp. 112-123.

5.   Anderson, K.O. and J.A. Epps, "Asphalt Concrete Factors Related to Pavement Cracking in West Texas," Proceedings, AAPT, Vol. 52, 1983, pp. 151-197.

6.   Arand, W., "Influence of Bitumen Hardness on the Fatigue Behavior of Asphalt Pavements of Different Thickness Due to Bearing Capacity of Subbase, Traffic Loading, and Temperature," Proceedings, 6th International Conference on Structural Behavior of Asphalt Pavements, University of Michigan, 1987, pp. 65-71.

7.   Carpenter, S.H., "Thermal cracking in asphalt pavements: an examination of models and input parameters," USA CRREL, 1983.

8.   Carpenter, S.H. and R.L. Lytton, "Thermal Pavement Cracking in West Texas," Research Report 18-4F, Texas Transportation Institute, October, 1977.

9.   Carpenter, S.H. and R.L. Lytton, "Thermal Activity of Base Course Material Related to Pavement Cracking," Research Report 18-2, Texas Transportation Institute, December, 1975.

10. Carpenter, S.H., R.L. Lytton and J.A. Epps, "Environmental Factors Relevant to Pavement Cracking in West Texas," Research Report 18-1, Texas Transportation Institute, January, 1974.

11. Chaichanavong, T., "Dynamic properties of ice and frozen clay under cyclic triaxial loading conditions," Dissertation submitted to Michigan State University, 1976, in partial fulfillment of the requirements for the degree of Doctor of Philosophy.

12. Fabb, T.R.J., "The Influence of Mix Composition, Binder Properties and Cooling Rate on Asphalt Cracking at Low Temperature," Proceedings, AAPT, Vol. 43, 1974, pp. 285-331.

13. Findley, W.N., Lai, J.S., and Onaran, K., 1989, Creep and Relaxation of Nonlinear Viscoelastic Materials, Dover.

14. Germann, F.P., and Lytton, R.L., "Methodology for Predicting the Reflection Cracking Life of Asphalt Concrete Overlays," Research Report 207-5, Texas Transportation Institute, Texas A&M University, College Station, Texas, March, 1979.

15. Gerritsen, A.H., and D.J. Jongeneel, "Fatigue properties of asphalt mixes under conditions of very low loading frequencies," Shell International Petroleum Company Limited, Amsterdam, The Netherlands, 1988.

16. Haas, R., "A method for designing asphalt pavements to minimize low-temperature shrinkage cracking," RR-73-1, Asphalt Institute, 1973.

17. Hills, J.F., "Predicting the Fracture of Asphalt Mixes by Thermal Stresses," Institute of Petroleum Report No. IP 74-014, Institute of Petroleum, U.K., 1974.

18. Jacob, T.R., "Basic Limits of Overlay Performance During Simultaneous Thermal and Traffic Loading," Proceedings, AAPT, Vol. 59, 1990, pp. 383-395.

19. Jung, D.H., "A Thermal Stress Restrained Specimen Test To Evaluate Low Temperature Cracking in Asphalt Concrete Mixtures," Project Report submitted to Oregon State University, November, 1990, in partial fulfillment of the requirements for the degree of Master of Science.

20. Landes, J.D. and J.A. Begley, "A fracture mechanics approach to Creep Crack Growth," Mechanics of Crack Growth, ASTM STP 590, American Society for Testing and Materials, 1976, pp. 128-148.

21. Little, D.N. and K. Mahboub, "Engineering properties of first generation plasticized sulfur binders and low temperature fracture evaluation of plasticized sulfur paving mixtures," Transportation Research Record, No 1034, 1985, pp. 103-111.

22. Lytton, R.L., Personal Communication, June, 1992.

23. Lytton, R.L., U. Shanmugham, and B.D. Garrett, "Design of Asphalt Pavements For Thermal Fatigue Cracking," Research Report 284-4, Texas Transportation Institute, January, 1983.

24. Mahboub, K., "Low temperature fracture evaluation of plasticized sulfur paving mixtures," Thesis submitted to Texas A&M University, 1985, in partial fulfillment of the degree of Master of Science.

25. Majidzadeh, K., "Development and field verification of a mechanistic structural design system in Ohio," Proceedings of the 4th International Conference on Structural Design of Asphalt Pavements, University of Michigan, 1977.

26. Majidzadeh, K., C. Buranrom, and M. Karakomzian, "Applications of fracture mechanics for improved design of bituminous concrete," Report No. 76-91, FHWA, U.S. Department of Transportation, 1976.

27. Miner, M.A., "Cumulative Damage in Fatigue," Journal of Applied Mechanics, Vol. 12, No. 1, September, 1945.

28. Monismith, C.L., G.A. Secor, and K.E. Secor, "Temperature Induced Stresses and Deformations in Asphalt Concrete," Proceedings, AAPT, Vol. 34, 1965, pp. 248-285.

29. Painter, L.J., Personal Communication with T.S. Vinson, November, 1990.

30. Roque, R., and B.E. Ruth, "Mechanisms and Modeling of Surface Cracking in Asphalt Pavements," Proceedings, AAPT, Vol. 59, 1990, pp. 396-421.

31.   Salam, Y.M., "Characterization of Deformation and Fracture of Asphalt
        Concrete," Dissertation submitted to the University of California,
        Berkeley, California, 1971, in partial fulfillment of the requirements of the
        degree of Doctor of Philosophy.

32.   Stephanos, P.J., "A Computer Program for Determining Master
        Compliance Curves of Dynamic and Creep Moduli of Asphalt Concrete,"
        Scholarly Paper Submitted to the Graduate School of the University of
        Maryland in Partial Fulfillment of the Requirements for the Degree of
        Master of Science., 1990

33.   Sugawara, T., and A. Moriyoshi, "Thermal fracture of bituminous
        mixtures," Proceedings of the Paving in Cold Areas Mini-Workshop, 1984,
        pp. 291-320.

34.   Vinson, T.S., V.C. Janoo, and R.C.G. Haas, "Low Temperature and
        Thermal Fatigue Cracking" Strategic Highway Research Program
        Summary Report No. SR-OSU-A-003A-89-1, June, 1989.

35.   Vinson, T.S., N.M. Jackson, and D.H. Jung, "Thermal Cracking
        Resistance of Asphalt Concrete: An Experimental Approach," Proceedings,
        7th International Conference on Asphalt Pavements, University of
        Nottingham, Nottingham, England, 1992.

36.   Wilson, C.R., "Dynamic properties of naturally frozen Fairbanks silt,"
        Thesis submitted to Oregon State University, Corvallis, Oregon, 1982, in
        partial fulfillment of the requirements for the degree of Master of Science.

APPENDICES

APPENDIX A

ELECTRO-HYDRAULIC CLOSED LOOP TEST SYSTEM

APPENDIX A

ELECTRO-HYDRAULIC CLOSED LOOP TEST SYSTEM

The electro-hydraulic, closed loop test system utilized in this study consists of three primary components: (1) loading system, (2) data acquisition system, and (3) temperature control system. These components are summarized in the following paragraphs. The utilization of this system with respect to the performance of the ERIT, DTT, and DTCT procedures is outlined in Appendix B.

Loading System

The loading system utilized in this study consisted of an MTS Series 204 hydraulic actuator, MTS Series 252 servo-valve and MTS Series 506 hydraulic power supply. The load applied to the test specimen was monitored with a 2.27 kg (5 kip) Strainsert Model FL5U-2SGKT load cell. For all test procedures except for the DTT, the rate of extension of the actuator was controlled with the 15.24 cm (6 in) internal MTS Linear Variable Displacement Transducer (LVDT).

For the DTT procedure, the rate of extension of the actuator was controlled with a 0.635 cm (0.25 in) external LVDT. The spring loaded, gage head LVDT was mounted to one side of the specimen with an "anti-tilt" device. A schematic diagram of the "anti-tilt" device is shown in Figure A-1.

Appendix A (Continued)
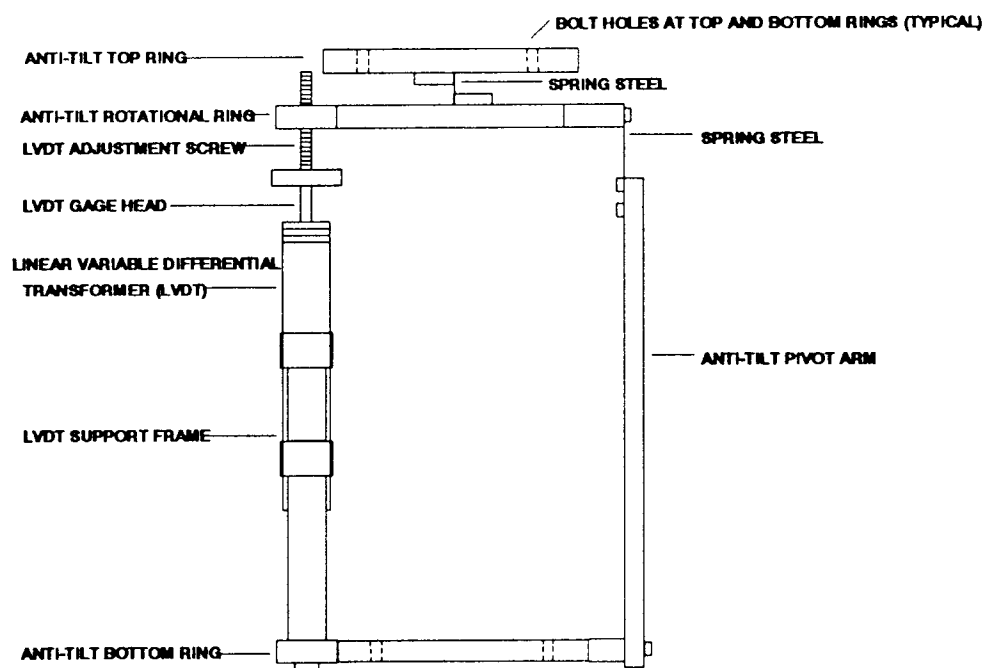
Figure A-1   **Schematic Diagram of the "Anti-Tilt" Device.**

Appendix A (Continued)

The "anti-tilt" device used at OSU was developed by Chaichanavong and Vinson (1976) for use in a triaxial testing apparatus to measure cyclic shear in frozen soils. The purpose of the "anti-tilt" device is to minimize the effects of slight tilting in the end platens on the displacement reading in the LVDT. The device causes the displacement measured in the LVDT at the side of the specimen to be effectively two times that at the sample centerline. Calibration tests performed on the specific device used in this study indicate the gage head output was increased by a factor of 1.98. This factor corresponds to an "anti-tilt ratio" of .505 (1/1.98) (Wilson, 1982).

Data Acquisition System

In general, all data pertaining to load and displacement was acquired with an IBM compatible personal computer (PC). Signal conditioning was obtained from the primary MTS 406 controller and a secondary signal conditioner used to step down the voltage. Voltages were converted to engineering units of load and displacement via calibrated relationships developed with the Digital Control Systems, ATS data acquisition software.

The MTS loading system described above is typically controlled entirely with the MTS Series 406 Controller. The MTS controller contains internal signal

Appendix A (Continued)

conditioning with output signals in the range of +/- 10 Volts. (20 Volt range). A

PC with the ATS software was used as the primary input/output device in this

study. The MTS 406 controller was used to convert resistance signals from the

load cell and LVDT's to voltages in the range of +/- 10 Volts. In order to link

the MTS system with the ATS software via a 16 channel data acquisition hardware

card (DAS-16), it was necessary to make use of a secondary signal conditioner to

divide the +/- 10 Volt signal by a factor of two (in effect producing a signal range

of 10 Volts). This secondary signal conditioning unit was developed by Andy

Brickman, OSU Civil Engineering Materials Lab Manager and Instrumentation

Specialist. A schematic diagram of the closed loop data acquisition system is

shown in Figure A-2.

<u>Temperature Control System</u>

An Applied Test Systems, Inc. (ATS) Series 3710 cryogenic environmental

chamber with a Model 2010 temperature controller was utilized in this study. The

chamber was equipped with an internal RTD temperature sensor capable of

measuring to +/- 0.1 C (.18 F). Thermistors were attached to the test specimens

at three different locations to monitor the relative temperature gradient across each

specimen. The environmental chamber was cooled with liquid nitrogen.

Appendix A (Continued)

P.C. WITH ATS SOFTWARE
AND DAS 16 CARD FOR
PROPORTIONAL COMMAND SIGNAL

MTS 406 CONTROLLER

MTS 204 HYDRAULIC ACTUATOR

DISPLACEMENT

+/- 10 Volt S.C.

LVDT

CRYOGENIC
ENVIRONMENTAL
CABINET

TEST SPECIMEN

+/- 5 Volt S.C.

DYVAL
23-5030
SERVO-CONTROLLER

CORRECTION

LOAD

STRAINSERT LOAD CELL

SECONDARY SIGNAL COND.

CHANNEL 0 = LOAD SIGNAL
CHANNEL 1 = DISPLACEMENT SIGNAL

MTS 252 SERVOVALVE

MTS 506 HYDRAULIC POWER SUPPLY

Figure A-2   **Schematic Diagram of the MTS Electro-Hydraulic Closed Loop Test System.**

APPENDIX B

LABORATORY TEST PROCEDURES

APPENDIX B-1

ENERGY RATE INTEGRAL TEST (ERIT) PROCEDURE

The step-by-step test procedure described below is based on the assumption that test specimens are properly fabricated and conditioned as described in Appendix C. This procedure applies specifically to the ERIT performed with an electro-hydraulic closed-loop testing system consisting of an MTS testing machine, the Applied Test Systems (ATS) cryogenic environmental chamber, and an IBM compatible personal computer (PC) equipped with Microsoft Windows, the Digital Control Systems ATS software package, and all associated hardware. The test system utilized for this study is described in Appendix A. For additional information pertaining to the specific equipment or software mentioned above, reference the respective equipment specification catalogs or contact the specific equipment manufactures.

1.   Prior to turning on the power to the MTS system, turn on the computer and execute Microsoft WINDOWS and Digital Control Systems ATS. At the DOS prompt, type "WIN ATS" and press the Enter key.

2.   Select the appropriate channel file. That is, under Setup, click on Channels and then open the appropriate channel (Energy.SET) file.

Appendix B-1 (Continued)

3.　Under Setup, click on Edit and check to ensure that the appropriate

　　channel file name is displayed at the top of the activated window.

4.　Select the appropriate test to be run.　Under Test click on Edit and then

　　open the appropriate Test (Ramp.TST) file.

5.　Check to be sure all settings in the test file are appropriate.　Edit

　　these settings as necessary, choose Save or Save as if desired, and

　　click on Run.

6.　Enter a name for the file to contain the test results and click on

　　Save.　Note that the default file name can also be accepted or edited.　If the

　　name given to the file for the test results already exists, a warning is

　　displayed.　Answering Yes replaces the existing contents of the file with the

　　new data, while answering No returns control to the previous window.

7.　Select (OPEN) to open the appropriate specimen (Briquette.SPC) file.

Appendix B-1 (Continued)

8.   Select the appropriate channels for which data is to be recorded. An X in

the box adjacent to the appropriate channel name indicates which channels

will be saved (recorded) on the disk. Click on (OK) when all appropriate

channels have been selected.

9.   The Control Panel window is then displayed. However, before

starting the test, proceed with steps 10 through 15.

10. Activate the monitor window and set its display to units. That is,

under Display select Monitor and under the (*) select Units.

11. Activate the scope window and set the display such that Channel A is load

and Channel B is disp_1. That is, under Display in ATS select Scope and

select the appropriate Display and Channel options.

12. Activate the manual control window for the servo valve (sv0) and set the

feedback channel to (1) and click on (+) for compressive loading.

Manually set the position of the MTS actuator near the low end of the scale

(It is important that this be done prior to turning the power on to the MTS

system.)

13.   Place the test specimen on the load cell platen. Position the top

loading platens on the notched specimen with teflon strips between the

platens and the specimen.

14.   Turn the MTS hydraulic power supply on and manually position the

specimen and loading platens under a small static load. The magnitude of

this load is displayed in the monitor window.

15.   Close the door to the environmental chamber and turn on the

temperature control system. Allow the specimen to thermally condition for

a period of no less than one hour. This period will provide sufficient time

for the MTS system to warm up as well.

16.   After the prescribed time period has passed, Reactivate the Control

Panel. Click on Ramp, and click on Start to begin the test.

17.   Reactivate Scope to ensure that the load and displacement are being

properly administered and recorded.

Appendix B-1 (Continued)

18. Manually observe the crack propagation via the view port on the door to the

   environmental chamber and click the appropriate switch as the crack

   proceeds past the predetermined intervals scaled on opposite faces of the

   specimen.

19. The ATS software is not currently equipped with an analysis routine for the

   Energy Rate Integral Test. Thus, the test data must be manipulated

   externally upon completion of the test. One approach is to import the data

   into a spreadsheet program for data reduction and analysis. Microsoft

   Excel for Windows was utilized in this study.

APPENDIX B-2

DIRECT TENSION TEST (DTT) PROCEDURE

The test procedure for the DTT program conducted at OSU was similar to that for the ERIT program. The MTS electro-hydraulic closed loop test system was utilized. However, a few distinct changes from the ERIT procedure were necessary to perform the DTT. The procedure described below is based on the assumption that the test specimens are properly prepared, instrumented, and thermally conditioned. This procedure applies specifically to the DTT performed on the electro-hydraulic closed-loop testing system consisting of the MTS testing machine, the Applied Test Systems (ATS) cryogenic environmental chamber, and a Personal Computer (PC) equipped with Microsoft Windows, the Digital Control Systems ATS software package, and associated hardware.

1. Prior to turning on the power to the MTS system, turn on the computer and execute Microsoft WINDOWS and Digital Control Systems ATS. At the DOS prompt, type "WIN ATS" and press the Enter key.

2. Select the appropriate channel file. That is, under Setup, click on Channels... and then open the appropriate channel (Tension.SET) file.

Appendix B-2 (Continued)

3. Under §etup, click on £dit and check to ensure that the appropriate channel file name is displayed at the top of the activated window.

4. Select the appropriate test to be run. Under Test click on £dit and then open the appropriate Test (Ramp.TST) file.

5. Check to be sure all settings in the test file are appropriate. Edit these settings as necessary, choose §ave or Save as if desired, and click on Run.

6. Enter a name for the file to contain the test results and click on §ave. Note that the default file name can also be accepted or edited. If the name given to the file for the test results already exists, a warning is displayed. Answering Yes replaces the existing contents of the file with the new data, while answering No returns control to the previous window.

7. Select (OPEN) to open the appropriate specimen (Beam.SPC) file.

Appendix B-2 (Continued)

8.   Select the appropriate channels for which data is to be recorded. An X in

the box adjacent to the channel names indicates which channels will be

saved (recorded) on the disk. Click on (OK) when all appropriate channels

have been selected.

9.   The Control Panel window is then displayed. However, before starting the

test, proceed with steps 10 through 18.

10.   Activate the monitor window and set its display to units. That is, under

Display select Monitor and under the (*) select Units.

11.   Activate the scope window and set the display such that Channel A is load

and Channel B is disp_1. That is, under Display in ATS select Scope and

select the appropriate Display and Channel options.

12.   Activate the manual control window for the servo valve (sv0) and set the

feedback channel to (1) and click on (-) for tensile loading. Manually set

the position of the MTS actuator near the low end of the scale (It is

important that this be done prior to turning the power on to the MTS

system.)

Appendix B-2 (Continued)

13. Turn the MTS hydraulic power supply on.

14. Place the specimen in the environmental chamber and connect the top and bottom load platens to the respective swivel connections (Note: the specimen is free to hang from the top swivel connection, thus the restraining rods must remain in place to support all tension until the specimen has sufficiently cooled).

15. Close the door to the environmental chamber and turn on the temperature control system. Allow the specimen to condition for a period of no less than thirty minutes.

16. Turn the temperature control system off and quickly open the environmental chamber and loosen the restraining rods to allow free extension of the end platens during testing. It is also important to make any necessary adjustments to the external LVDT with the appropriate adjustment screw at this time.

Appendix B-2 (Continued)

17. Close the door to the environmental chamber and turn the temperature

control system back on. Allow the specimen to condition for a additional

period of no less than thirty minutes prior to proceeding with the test.

18. After the prescribed time period has passed, manually set the position of the

MTS actuator to apply a small static tensile load to the specimen.

19. Reactivate the Control Panel. Click on Ramp, and click on Start to

begin the test.

20. Reactivate Scope to ensure that the load and displacement are being

properly administered and recorded.

21. Upon completion of the test, import the test data into a suitable

spreadsheet program or analysis program for data reduction and

analysis.

APPENDIX B-3

DIRECT TENSILE CREEP TEST (DTCT) PROCEDURE

The DTCT program was also conducted with the MTS electro-hydraulic closed loop test system. Thus, the procedure followed for the this test was similar to those for the ERIT and the DTT. Several slight changes in the procedure were necessary, however. The step-by-step procedure described below is based on the assumption that test specimens are properly prepared, instrumented, and thermally conditioned prior to testing. This procedure applies specifically to the DTCT performed on the electro-hydraulic closed loop testing system at OSU. The OSU test system consists of the MTS electro-hydraulic testing machine, the Applied Test Systems (ATS) cryogenic environmental chamber, and an IBM compatible PC equipped with Microsoft Windows, the Digital Control Systems ATS software package, and associated hardware.

1.   Prior to turning on the power to the MTS system, turn on the computer and execute Microsoft WINDOWS and Digital Control Systems ATS. At the DOS prompt, type "WIN ATS" and press the Enter key.

2.   Select the appropriate channel file. That is, under Setup, click on Channels... and then open the appropriate channel (Creep.SET) file.

Appendix B-3 (Continued)

3.   Under <u>S</u>etup, click on <u>E</u>dit and check to ensure that the appropriate

      channel file name is displayed at the top of the activated window.

4.   Select the appropriate test to be run. Under <u>T</u>est click on <u>E</u>dit and then

      open the appropriate Test (Creep.TST) file.

5.   Check to be sure all settings in the test file are appropriate. Edit these

      settings as necessary, choose <u>S</u>ave or S<u>a</u>ve as if desired, and click on

      <u>R</u>un.

6.   Enter a name for the file to contain the test results and click on <u>S</u>ave.

      Note that the default file name can also be accepted or edited. If the

      name given to the file for the test results already exists, a warning is

      displayed. Answering <u>Y</u>es replaces the existing contents of the file with the

      new data, while answering <u>N</u>o returns control to the previous window.

7.   Select (OPEN) to open the appropriate specimen (Cylinder.SPC) file.

Appendix B-3 (Continued)

8. Select the appropriate channels for which data is to be recorded. An X in the box adjacent to the channel names indicates which channels will be saved (recorded) on the disk. Click on (OK) when all appropriate channels have been selected.

9. The Control Panel window is then displayed. However, before starting the test, proceed with steps 10 through 18.

10. Activate the monitor window and set its display to units. That is, under Display select Monitor and under the (*) select Units.

11. Activate the scope window and set the display such that Channel A is disp_1 and Channel B is disp_2. That is, under Display in ATS select Scope and select the appropriate Display and Channel options.

12. Activate the manual control window for the servo valve (sv0) and set the feedback channel to (1) and click on (-) for tensile loading. Manually set the position of the MTS actuator near the low end of the scale (It is important that this be done prior to turning the power on to the MTS system.)

Appendix B-3 (Continued)

13.   Turn the MTS hydraulic power supply on.

14.   Place the specimen in the environmental chamber and connect the top and

bottom load platens to the respective swivel connections.

15.   Manually set the position of the MTS actuator to support the test

specimen from the bottom swivel without introducing any compressive or

tensile stresses to the specimen.

16.   Close the door to the environmental chamber and turn on the

temperature control system. Allow the specimen to condition for a

period of no less than one hour.

17.   After the prescribed time period has passed, manually set the position of the

MTS actuator to apply a small static tensile load to the specimen.

18.   Reactivate the Control Panel. Click on Creep, and click on Start to

begin the test.

Appendix B-3 (Continued)

19.   Reactivate Scope to ensure that the external LVDT displacement gages are being properly administered and recorded.

20.   Upon completion of the test, import the test data into a suitable spreadsheet program or analysis program for data reduction and analysis.

APPENDIX C

SAMPLE PREPARATION PROTOCOLS

APPENDIX C

SAMPLE PREPARATION PROTOCOLS

Test specimens were prepared in general accordance with the procedures outlined in the document entitled "Asphalt Concrete Specimen Preparation Protocol, SHRP Asphalt Project A-003A," prepared by John Harvey, Research Assistant, University of California - Berkeley, and dated May 8, 1990. This document includes protocols for: 1) aggregate batching and handling, 2) asphalt concrete mixing and curing, 3) compaction methods, and 4) procedures for the determination of air voids content. The sample preparation procedures, as applied in this study, are briefly summarized in the following paragraphs.

Aggregate Processing

The RB aggregate was handled and processed in general accordance with ASTM procedures and the above-referenced SHRP MRL protocols. The aggregate was initially oven-dried upon arrival to the OSU facilities and then passed through a series of standard ASTM sieves consisting of the 3/4", 1/2", 3/8", #4, #8, #16, #30, #50, and #100 sieves. The material retained on each of the above sieves, and that passing the #100 sieve, was then stored in separate containers and batched according to the target gradation. Wet sieve analyses were performed on

Appendix C (Continued)

representative batches of the processed aggregate in order to adjust the batch

gradation to achieve the actual target gradation. The target gradation used in this

study is provided in Table C-1. As noted, the material larger than that passing the

1/2-inch sieve was scalped and replaced with material retained on the 3/8-inch

sieve for this study. This precaution was taken to increase the ratio of the sample

outside diameter (2-1/4 inch) to the largest aggregate diameter size (1/2 inch) to a

value greater than at least four.

Mixing and Compacting

Test specimens were fabricated in the bituminous materials laboratory at

OSU in accordance with ASTM procedures D 1560-81a, D 1561-81a, and D 3202

and modified as provided in the SHRP technical publication "Protocol for Mixing

and Compacting Laboratory Samples Using the Hveem Method (Kneading

Compactor)," (Bell, 1989). The California kneading compactor was utilized to

compact specimens to the prescribed void contents. Marshall-shaped specimens of

dimensions 10 cm. (4 in.) diameter by 10 cm. (4 in.) thick were compacted for the

ERIT. Asphalt concrete beams of dimensions 15.25 cm. (6 in.) by 15.25 cm. (6

in.) by 40.65 cm. (16 in.) were compacted for all other test procedures evaluated

herein. Void contents were evaluated based on the bulk and theoretical maximum

Appendix C (Continued)

Table C-1   Target Aggregate Gradation Utilized in This Study.

NOMINAL SIZE	PERCENT RETAINED*	PERCENT PASSING*
1"	0.0	100.0
3/4"	5.0	95.0
1/2"	15.0	80.0
3/8"	12.0	68.0
#4	20.0	48.0
#8	13.0	35.0
#16	10.0	25.0
#30	8.0	17.0
#50	5.0	12.0
#100	4.0	8.0
#200	2.5	5.5
PAN	5.5	0.0

*   Aggregate of nominal size larger than 1/2-inch was scalped and replaced with material of nominal size between 1/2-inch and 3/8-inch.

Appendix C (Continued)

specific gravities of the mixtures as determined by the Chevron Research Company method, "Procedure - Bulk Specific Gravity of Compacted Bituminous Mixtures Using Parafilm-Coated Specimens," (Del Valle, 1985) and ASTM procedure D 2041-78.

Saw Cutting and Coring

Specimens were cut and/or cored to different geometric shapes and dimensions for the different tests conducted in this study. All coring and saw cutting was performed with water cooled, diamond abrasion rotary equipment. Care was taken to provide symmetry of all cut surfaces. After coring and cutting to the prescribed dimensions, void contents were determined based on the bulk and theoretical maximum specific gravities, as noted in the preceding section.

The cylindrical ERIT specimens were notched and cut to approximately 10 cm. (4 in.) diameter by 10 cm. (4 in.) thick. These dimensions were analyzed to be compatible with the assumption of plane strain loading conditions (Abdulshafi, 1990). The ends of the specimens were cut to provide a smooth crack surface. The right-angle notch was cut into the specimens to accommodate the loading platens. The notch was cut not to exceed a depth of 1.9 cm. (0.75 in.) and extended the full thickness of the specimen. Care was taken to ensure symmetry

Appendix C (Continued)

Figure C-1 **Typical Notched Cylindrical Energy Rate Integral Test Specimen and Loading Platens.**

Appendix C (Continued)

of the notch and smoothness of the saw cut surfaces for proper contact with the loading platens. A typical notched cylindrical specimen with loading platens is displayed in Figure C-1.

Rectangular beam specimens were utilized to evaluate the DTT. The DTT specimens were saw cut from the larger compacted beams in the transverse direction relative to compaction. The beam specimens, were saw cut to approximate dimensions of 5 cm. (2 in.) by 5 cm. (2 in.) by 25.4 cm. (10 in.). All faces of the specimens were cut to provide relatively square, uniform surfaces. Typical DTT beam specimens are pictured in Figure C-2.

Cylindrical specimens were utilized in the evaluation of the DTCT and TSRST. The specimens were cored from the 15.25 cm. (6 in.) by 15.25 cm. (6 in.) by 40.65 cm. (16 in.) compacted beams in the transverse direction relative to compaction. The ends of the core specimens were cut to provide relatively square surfaces. Specimens of dimensions 5.72 cm. (2.25 in.) outside diameter and 25.4 cm. (10 in.) length were used. These dimensions were selected to provide approximately equivalent length and cross-sectional area to the beam specimens tested in the DTT study. Typical cylindrical DTCT specimens are pictured in Figure C-3.

Appendix C (Continued)
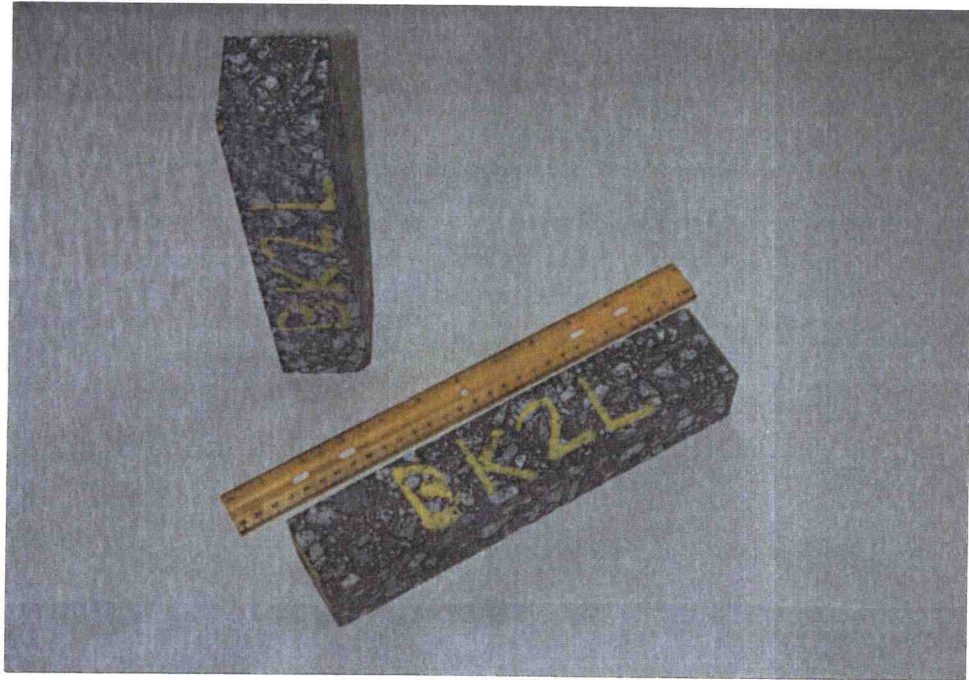
Figure C-2   Typical Rectangular Beam Direct Tension
                    Test Specimens.

Appendix C (Continued)

Figure C-3   Typical Cylindrical Direct Tensile Creep
Test Specimens.

Appendix C (Continued)

Thermal Conditioning

After compaction, the specimens were stored in an environmentally controlled room at 0% relative humidity and a constant temperature of 10 C (50 F). Prior to testing, the specimens were thermally conditioned at the respective initial test temperatures to provide a relatively uniform temperature distribution throughout. This was accomplished by placing the specimens in the environmental chamber, set at the prescribed test temperature, for a period of no less than 1 hour prior to testing. The period of 1 hour was established by monitoring the temperature at the core of a representative test specimen during cooling from 25 C (77 F) to a constant chamber temperature of -30 C (-22 F). This time period may vary with differing test conditions and it is recommended that the specific conditioning period be established for each case via a thermistor placed at the center of a dummy specimen.

Additional Preparation and Instrumentation Requirements

A thin coat of light-colored, non-detrimental paint was applied to the faces of the ERIT specimens to enable clear observation of crack initiation and propagation. Both faces of the specimens were then marked with a vertical scale

Appendix C (Continued)

extending from the notch tip to the base of the specimen. An initial crack, no greater than 0.05 cm. (0.02 in.) long, was introduced to the specimen by applying a low intensity cyclic load to the sample until the initial crack was visible to the naked eye. The tip of the initial crack was clearly marked to define the starting point for the test. The scale scribed on opposite faces of the specimen was used to monitor crack propagation.

The DTT, DTCT, and TSRST specimens were affixed to load platens with epoxy. Thermoset Plastics, Inc. DC-80 epoxy was utilized in this study with a 1:1 mixture ratio of resin to hardener. The specimens were affixed to the end platens in alignment devices in order to ensure verticality and subsequently minimize applied bending moments during testing. A sketch of the alignment device utilized in this study is presented in Figure C-4. The epoxy was allowed to harden at room temperature for a period of 12 hours prior to disturbing or moving the specimens.

During testing, the surface temperature was monitored with at least three thermistors attached at different locations around the perimeter and along the length of the test specimens. The thermistors were adhered to the specimens with common household modeling clay. The modeling clay was used to provide a buffer from fluctuations in the air temperature within the environmental chamber. Thus, a relatively continuous estimate of the surface temperature of the test specimen was obtained during testing.

Appendix C (Continued)

SHAFT AND COLLAR ASSEMBLY

TOP LOAD PLATEN

RESTRAINING RODS

BEAM TEST SPECIMEN

THERMASET EPOXY

BOTTOM LOAD PLATEN

(a) Front View

(b) Side View
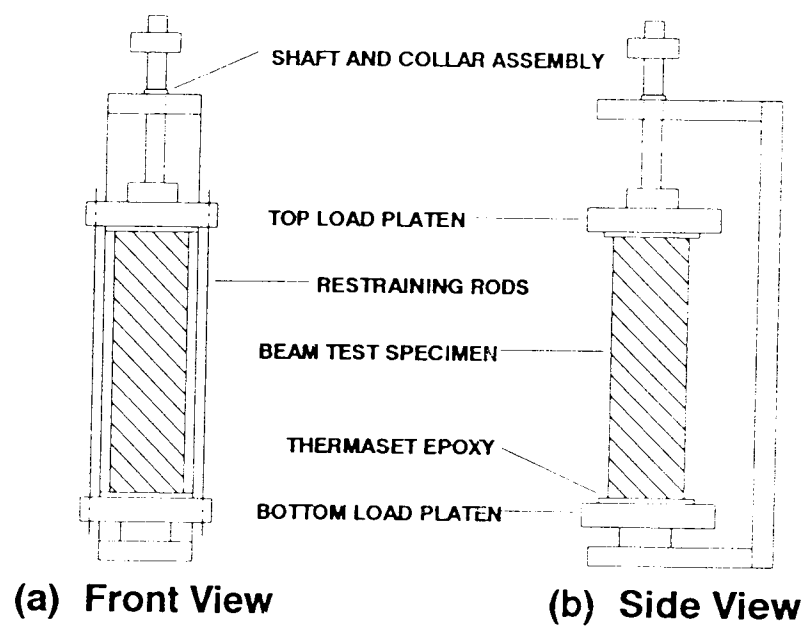
Figure C-4   Sketch of the Alignment Device Used to Epoxy
                    the End Platens to the Test Specimens.

APPENDIX D

LISTING OF THE FORTRAN SOURCE
CODE FOR THE COMPUTER PROGRAM THERM

APPENDIX D

LISTING OF THE FORTRAN SOURCE
CODE FOR THE COMPUTER PROGRAM THERM

```
C
C     *************************************************************
C
C     COMPUTER PROGRAM FOR THERMAL CRACKING MODEL (THERM)
C              (USING THE RESULTS FROM VISCO)
C
C     *************************************************************
C
C              THE BITUMEN AGES WITH TIME.
C
C     *************************************************************
C
C              AUTHORS  :  DR. ROBERT L. LYTTON
C                          MS. ULPALA L. SHANMUGHAM
C
C                          TEXAS TRANSPORTATION INSTITUTE
C                          TEXAS A&M UNIVERSITY
C                          COLLEGE STATION, TEXAS 77843
C
C     *************************************************************
C
C     RESULTS PRINTED EVERY MONTH
C
C     *************************************************************
C
C     DESCRIPTION OF INPUT VARIABLES
C
C     *************************************************************
C
C     TITL   = TITLE OF THE PROBLEM.
C     W      = DENSITY OF THE ASPHALT CONCRETE,PCF.
C     S      = SPECIFIC HEAT OF THE ASPHALT CONCRETE,BTU/LB,
C              DEGREE FAHRENHEIT.
C     AK     = THERMAL CONDUCTIVITY OF THE ASPHALT CONCRETE,
C              BTU/SQUARE FOOT/HR, DEGREE FAHRENHEIT PER FOOT.
C     B      = THE ABSORBTIVITY OF THE ASPHALT CONCRETE.
C     D0     = INITIAL CRACK LENGTH, INCHES (CRACK IS PROPAGATING
C              DOWNWARDS).
C     DF     = DEPTH OF THE ASPHALT CONRETE, INCHES.
C     VMPH   = AVERAGE WIND VELOCITY, MPH.
C     NSEL   = STARTING DATE: YR/MO/DY
```

Appendix D (Continued)

```
C    SR1    = THE AVERAGE SOLAR RADIATION FOR JULY,LANGLEYS PER DAY.
C    SRM    = THE YEARLY AVERAGE SOLAR RADIATION,LANGLEYS PER DAY.
C    IMODE  = MODES, 1, 2,& 3
C    IAGE   = (NUMBER OF YEARS TO BE RUN) OR (THE NUMBER OF YEARS
C             THE BITUMEN TO BE AGED), USUALLY BOTH ARE SAME.
C    CV     = AGGREGATE VOLUME / ( AGGREGATE VOL + ASPHALT VOL )
C    SPRB   = ORIGINAL SOFTENING POINT RING AND BALL TEMPERATURE,
C             DEGREES C. ( IMODE = 1 OR 2 )
C    TPEN2  = TEMPERATURE OF REFERENCE PENETRATION, DEGREES C.
C             ( IMODE = 3 )
C    PI     = ORIGINAL PENETRATION INDEX.( IMODE = 1 )
C    PEN1   = PENETRATION AT 25 DEGREES C. ( IMODE = 2 OR 3 )
C    PEN2   = REFERENCE PENETRATION AT TPEN2. ( IMODE = 3 )
C    IYR    = THE NUMBER OF YEARS THE BITUMEN HAS AGED.
C             ( IYR = 0 ( AGED 6 MONTHS, FOR FIRST YEAR ),
C             IYR = 1 (AGED 18 MONTHS, FOR SECOND YEAR ), ETC )
C    SPRBI  = SOFTENING POINT RING & BALL TEMPERATURE FOR THE
C             CURRENT YEAR, DEGREES C.
C    CN     = THE SLOPE OF THE MASTER RELAXATION MODULUS CURVE.
C    D1     = THE POWER OF THE INTERCEPT VALUE FOR LOG T=0 OF THE
C             MASTER RELAXATION MODULUS CURVE.
C    TA     = THE POWER LAW CONSTANT FOR THE SHIFT FACTOR.
C    CM     = THE SLOPE OF THE POWER LAW CURVE FOR THE SHIFT FACTOR.
C    NDATE  = DATE, YR/MO/DY, IN THE WEATHER DATA TAPE.
C             (SCAN DOWN TAPE TO SELECTED DATE)
C    NYEAR  = YEAR.(2 DIGITS)
C    LL     = MONTH.(2 DIGITS)
C    DAY(I) = DAY.(2 DIGITS)
C    TMAX(I) = MAXIMUM TEMPERATURE DURING DAY(I),DEGREE FAHRENHEIT.
C    TMIN(I) = MINIMUM TEMPERATURE DURING DAY(I),DEGREE FAHRENHEIT.
C
C    ***********************************************************************
C
C    INPUT DATA INFORMATION:
C    ----------------------
C
C    DATA FROM TAPE50
C    ----------------
C    CARD   COLUMNS/FORMAT   VARIABLE
C    NO.              NAME
C
C    01    01-60   (15A4)   TITL
C
C    02    01-10   F10.0    W
C    02    11-20   F10.0    S
C    02    21-30   F10.0    AK
C    02    31-40   F10.0    B
```

Appendix D (Continued)

```
C   03    01-10    F10.0    DO
C   03    11-20    F10.0    DF
C   03    21-30    F10.0    VMPH
C
C   04    01-10    I10      NSEL
C
C   05    01-10    F10.0    SR1
C   05    11-20    F10.0    SRM
C
C   06    01-10    F10.0    TR
C   06    11-20    F10.0    TM
C   06    21-30    F10.0    SCFT
C
C   DATA FROM TAPE20 (RESULTS FROM VISCO PROGRAM)
C   ---------------------------------------------
C
C   CARD   COLUMNS/FORMAT    VARIABLE
C   NO.                      NAME
C
C   01    01-02    I2       IMODE
C   01    03-04    I2       IAGE
C   01    05-14    F10.3    CV
C   01    15-24    F10.3    SPRB (IMODE=1,2) OR TPEN2 (IMODE=3)
C   01    25-34    F10.3    PI (IMODE=1) OR PEN1 (IMODE=2,3)
C   01    35-44    F10.3    PEN2 ( FOR IMODE=3 ONLY )
C
C   02    01-02    I2       IYR
C   02    03-12    F10.3    PEN1
C   02    13-22    F10.3    SPRBI
C
C   03    01-10    F10.5    CN
C   03    11-20    F10.5    D1
C
C   04    01-10    F10.5    TA
C   04    11-20    F10.5    CM
C
C
C   NOTE: CARDS 02-04 MUST BE REPEATED FOR EACH YEAR I,
C         I = 1, ..., IAGE
C
C   DATA FROM TAPE10 (WEATHER TAPE)
C   -------------------------------
C
C   CARD   COLUMNS/FORMAT    VARIABLE
C   NO.                      NAME
C
C   01    12-17    I6       NDATE
```

Appendix D (Continued)

```
C
C   02   12-13   I2       NYEAR
C   02   14-15   I2       LL
C   02   16-17   I2       DAY(1)
C   02   20-23   F4.0     TMAX(1)
C   02   24-27   F4.0     TMIN(1)
C
C   03   12-13   I2       NYEAR
C   03   16-17   I2       DAY(I)
C   03   20-23   F4.0     TMAX(I)
C   03   24-27   F4.0     TMIN(I)
C
C   NOTE:  CARD 03 MUST BE REPEATED FOR EACH DAY OF THE
C          ANALYSIS PERIOD.
C          FORMAT OF THE CARDS 1, 2, & 3 MUST BE CHANGED
C          ACCORDING TO THE FORMAT OF WEATHER DATA TAPE.
C
C   ***************************************************************
C
      IMPLICIT REAL*8 (A-H, O-Z)
      DIMENSION   XX(3),TE(3,24),TI(3,24)
      DIMENSION   TMAX(31),TMIN(31),AL(372),N(12)
      DIMENSION   DAY(31)
      DIMENSION   YC(2500), DYC(2500), K1(2500)
      DIMENSION   NF(2500), DN(2500), TITL(15), NF1(2500)
      COMMON /A1/ CN, CM, TM, TR, TA, E1, EE
      COMMON /A2/ SA1, SA2, SB1, SB2
      COMMON /A3/ M1, M2, M3, M4
      COMMON /A4/ TC(12), TH(12)
      INTEGER     DAY
      INTEGER MOS(12)/'JAN','FEB','MAR','APR','MAY','JUN',
     1            'JUL','AUG','SEP','OCT','NOV','DEC'/
      REAL*8      M1, M2, M3, M4, K1, NF, KTMX, KTMN, NF1
  500 FORMAT ( 15A4 )
  520 FORMAT ( 8F10.0 )
  530 FORMAT ( 8I10 )
C********* INPUT DATA FOR NEW PROBLEM **********
      OPEN (50,FILE = 'INPUT.DAT')
      REWIND 50
      OPEN (60,FILE = 'OUTPUT.DAT')
      REWIND 60
    8 READ(50,500,END = 999)TITL
      READ  (50,520) W, S, AK, B
      READ  (50,520) DO, DF, VMPH
      READ  (50,530) NSEL
      READ  (50,520) SR1, SRM
      READ  (50,520) TR, TM, SCFT
```

Appendix D (Continued)

```
C*******************************************
C    TM IS THE REFERENCE TEMPERATURE OF THE MASTER
C    RELAXATION CURVE, DEGREE FAHRENHEIT.
C    TR IS THE TEMPERATURE OF THE STRESS FREE STATE,
C    DEGREE FAHRENHEIT.
C*******************************************
C   TM =77.  REVISED TO INPUT DATA BY NMJ
C   TR =75.  REVISED TO INPUT DATA BY NMJ
    DZ =1.0
C
C*****READ ORIGINAL PROPERTIES OF BITUMEN FROM VISCO FOR
C*****DIFFERENT MODES 1, 2, OR 3.
    OPEN (20,FILE ='VISCO.DAT')
    REWIND 20
    READ  (20,208) IMODE, IAGE, CV, SPRB, PI, PEN2
    SPRB =(SPRB*9./5.) +32.
    TPEN2 = SPRB
 208 FORMAT ( 2I2, 4F10.3 )
    WRITE(60,600)TITL
 600 FORMAT('1', 10(/), 10X, 'THERMAL CRACKING ANALYSIS FOR ',15A4)
    WRITE(60,601)NSEL,IAGE
 601 FORMAT(/,10X,'THIS ANALYSIS BEGINS AFTER ',I6,' AND RUNS FOR ',I2,
    +        ' YEARS.')
    WRITE(60,602)
 602 FORMAT(/,10X,'THE BITUMEN USED HAS THE FOLLOWING ORIGINAL ',
    1 'PROPERTIES:' )
    IF(IMODE.EQ.1)WRITE(60,603)PI
 603 FORMAT( 15X, 'PENETRATION INDEX      = ',F10.3)
    IF(IMODE.EQ.2)WRITE(60,605)PI
 605 FORMAT( 15X, 'PENETRATION AT 77 DEG F   = ',F10.3)
    IF ( IMODE .EQ. 3 ) WRITE (60,6051) PI, TPEN2, PEN2
6051 FORMAT (15X, 'PENETRATION AT  77.0 DEG F = ', F10.3, /,
    1       15X, 'PENETRATION AT', F6.1, ' DEG F = ', F10.3 )
    IF ( IMODE .LT. 3 ) WRITE(60,606)SPRB
 606 FORMAT(15X,'SOFTENING POINT RING & BALL TEMP = ',F10.3,' DEG F')
    IF ( IMODE .EQ. 3 ) WRITE (60,6065) TPEN2
6065 FORMAT ( 15X, 'TEMPERATURE OF REFERENCE PENETRATION = ', F10.3,
    1 ' DEG F' )
    WRITE(60,607)DF,D0
 607 FORMAT(10X,'THE ASPHALT CONCRETE LAYER IS ',F10.3,' INCHES THICK'
    + /, 10X, 'AND IS ASSUMED TO HAVE AN INITIAL CRACK OF ',F10.3,
    + /10X, 'INCHES EXTENDING FROM THE SURFACE.')
    WRITE(60,608)
 608 FORMAT(10X,'THE ASPHALT CONCRETE HAS THE FOLLOWING MIX ',
    1 'PROPERTIES:' )
    WRITE(60,609)CV,W,S,AK,B
 609 FORMAT(15X, 'AGGREGATE VOLUME CONCENTRATION = ',F10.3,
```

Appendix D (Continued)

```
      +/, 15X, 'DENSITY = ',F10.3,' LBS/FT**3'
      +/, 15X, 'SPECIFIC HEAT = ',F10.3,' BTU/LB DEG F'
      +/, 15X,'THERMAL CONDUCTIVITY = ',F10.3,' BTU/FT**2/HR,DEG F/FT'
      +/, 15X,'ABSORPTIVITY = ',F10.3)
      WRITE(60,610)VMPH,SRM,SR1
  610 FORMAT(/, 10X, 'THE PAVEMENT IS ASSUMED TO BE SUBJECTED TO THE'
      +/, 10X, 'FOLLOWING AVERAGE ENVIRONMENTAL CONDITIONS:'
      +/, 15X,'WIND VELOCITY = ',F10.3,' MILES PER HOUR'
      +/, 15X,'AVERAGE ANNUAL SOLAR RADIATION = ',F10.3,' LANGLEYS/DAY'
      +/, 15X,'AVERAGE JULY SOLAR RADIATION = ',F10.3,' LANGLEYS/DAY')
C********* INITIALIZE CONSTANTS *********
      ACON = 1.0D0
      ID      = 0
      YC(1)   = D0
      CDMG    = 0.0D0
      CDMG1   = 0.0D0
      IKOUNT  = 1
C********* DAYS IN THE MONTH *********
      N(1) = 31
      N(2) = 28
      N(3) = 31
      N(4) = 30
      N(5) = 31
      N(6) = 30
      N(7) = 31
      N(8) = 31
      N(9) = 30
      N(10) = 31
      N(11) = 30
      N(12) = 31
      XYZTIM = 14.0
      XYZTEM = 80.0D0
      DZ = 10.D0**DZ
      EE = DZ
   18 CONTINUE
      DO 109 IJK = 1,360
      F = IJK/57.2958
      AL(IJK) = SRM + (SR1-SRM) * DCOS( F )/0.966
  109 CONTINUE
      DO 108 IJK = 361,366
      AL(IJK) = AL(360)
  108 CONTINUE
  138 CONTINUE
C****** THE UPPER LIMIT ON THE RELAXATION MODULUS CURVE IS SPECIFIED
      SBTMAX = 3.625D+05
      ESSM   = SBTMAX * (1.0D0 + 2.52D0 * (CV/(1.0-CV))) ** 0.9923D0
```

Appendix D (Continued)

```
C********** SCAN DOWN TAPE TO SELECTED DATE ***********
      OPEN (10,FILE='WEATH.DAT')
      REWIND 10
    9 READ(10,101)NDATE
  101 FORMAT(11X,I6)
      IF(NDATE.LT.NSEL)GOTO9
C********** TAPE NOW IS AT STARTING POINT *************
C********** DO ONE YEAR AT A TIME **********
      DO 3 I3=1,IAGE
C********** READ VARIABLES FROM VISCO *********
      READ(20,201)IYR,PEN1,SPRBI
      SPRBI=(SPRBI*9./5.)+32
  201 FORMAT(I2,2F10.3)
      READ(20,200)CN,D1
      READ(20,200)TA,CM
  200 FORMAT(2F10.5)
      CN=-CN
      CM=-CM
      D1=10.0D0**D1
   16 E1=D1
      I3M1=I3-1
C****** FATIGUE PARAMETERS, CA & FN, ARE CALCULATED *****
C SCFT IS THE SCALING FACTOR TO CALCULATE FN
C AFAT AND BFAT ARE EMPIRICAL CONSTANTS THAT
C RELATE CA AND FN.
C*********************************************************
C    SCFT= 2.5  REVISED TO INPUT DATA BY NMJ
      FN=(1.+1./CN)*(2./SCFT)
      AFAT=0.69
      BFAT=-0.511
      CA=10.**((AFAT+FN)/BFAT)
      WRITE (60,667)
  667 FORMAT ( // )
      IF ( MOD(IYR,2) .EQ. 0 ) WRITE (60,666)
  666 FORMAT ( 1H1, //// )
      WRITE(60,604)IYR,PEN1,SPRBI,CA,FN
  604 FORMAT( 10X, ' *** YEAR ',I2,' ***'/,
     1 10X, ' IN PLACE BITUMIN PROPERTIES:',
     +    /, 15X, 'PENETRATION AT 77 DEG F    = ',F10.3
     + /,15X,'SOFTENING POINT RING & BALL TEMP = ',F10.3,' DEG F',
     + //, 10X, ' FATIGUE PARAMETERS OF THE MIX:',
     + /, 15X, 'A = ', E10.3, '    N = ', F8.3, // )
      WRITE (60,3457)
      CALL CURVE(TH,TC)
      TC(12) = TC(11)
      TH(12) = TH(11)
```

Appendix D (Continued)

```
C********* DO ONE MONTH AT A TIME *********
      DO  1 LJ = 1, 12
  997 READ  (10,1233) NYEAR, LL, DAY(1), TMAX(1), TMIN(1)
 1233 FORMAT (11X,3I2,2X,2F4.0)
      IF(TMAX(1).EQ.999)GOTO997
      M      = MOD(NYEAR,4)
      N(2)   = 28
      IF ( M .EQ. 0 ) N(2) = 29
      JYR    = N(LL)
      DO 3333 I = 2,JYR
      READ (10,1234) NYEAR, DAY(I), TMAX(I), TMIN(I)
 1234 FORMAT(11X,I2,2X,I2,2X,2F4.0)
 3333 CONTINUE
C********* ADD A DAY IF LEAP YEAR *********
      MAXDAY   = 365 + N(2) - 28
C********* TEMPORARY DEBUG OUTPUT *********
C********* DO ONCE FOR EACH DAY IN MONTH *********
      DO 2 NI = 1,JYR
      TRANG    = 0.0D0
      IF ( TMIN(NI) .GE. TR ) GO TO 2
      TAVG = 0.5*(DMIN1(TR,TMAX(NI)) + DMIN1(TR,TMIN(NI)))
      TRANG    = DMIN1( TR,TMAX(NI) ) - DMIN1(TR,TMIN(NI))
      AH = 1.3 + 0.62*(VMPH/24.)**0.75
      H = AH/AK
      AC = AK/(S*W)
      C = (0.131/AC)**0.5
      R = 0.67*B*3.69*AL(IKOUNT)/(24.*AH)
C*****************************************************
C SET UP TO CALCULATE TEMPERATURE OF TOP, MIDDLE, AND
C BOTTOM OF PAVEMENT.
C   XX(1) = BOTTOM TEMPERATURE
C   XX(2) = MIDDLE TEMPERATURE
C   XX(3) = TOP TEMPERATURE
C TEMPERATURE CALCULATED EACH HOUR FOR A COMPLETE DAY
C*****************************************************
      DO 10 ITHCK = 1,3
      XX(ITHCK) = DF/ITHCK
      IF(ITHCK.EQ.3)XX(3) = 0.0D0
      Z2 = (-XX(ITHCK))*C/12.0
      Z3 = DEXP(Z2) * H/(( H + C)**2. + C**2.) ** 0.5
      DO 10 J = 2,25
      TIM = J
      IF(J.GT.9) GO TO 31
      Z4 = 6.8176*(.0576*TIM + 0.144*Z2-0.288)
      GO TO 35
   31 IF(J.GT.14) GO TO 32
      Z4 = +14.7534*(0.02057*TIM + 0.075*Z2-0.288)
```

Appendix D (Continued)

```
      GO TO 35
   32 Z4 = -6.94274*(0.02057*TIM + 0.12*Z2-0.288)
   35 Z5 = DSIN(Z4)
      IF(Z5) 21,22,22
   21 TMEAN = TAVG + 0.5*R
      TV = .5*TRANG
      GO TO 23
   22 TV = .5*TRANG + 3.*R
      TMEAN = TAVG + R
   23 TEMP = TMEAN + TV*Z3*Z5
      IF(J.GT.19) TIM = TIM-24
      ITM = TIM + 5
      TE(ITHCK,ITM) = TEMP
      TI(ITHCK,ITM) = ITM
   10 CONTINUE
C********* 1 DAYS CALCULATIONS COMPLETE *********
   20 IKOUNT = IKOUNT + 1
      IF(IKOUNT.EQ.MAXDAY) IKOUNT = 1
      DO 110 L1 = 1,3
      DO 110 L = 2,23
      IF(TE(L1,L).LE.TE(L1,L-1).AND.TE(L1,L).LE.TE(L1,L + 1)) GO TO 112
      GO TO 118
  112 CONTINUE
C********* MINIMUM TEMPERATURES HAVE BEEN CALCULATED *********
      IF(L1.EQ.1)TEMP1 = TE(1,L)
      IF(L1.EQ.2)TEMP2 = TE(2,L)
      IF(L1.EQ.3)TEMP3 = TE(3,L)
C********* TIME FOR MINIMUM TEMPERATURES *********
      IF(L1.EQ.1)TIM1 = TI(1,L)
      IF(L1.EQ.2)TIM2 = TI(2,L)
      IF(L1.EQ.3)TIM3 = TI(3,L)
  118 CONTINUE
C********* NOW CALCULATE MAX TEMPERATURES *********
      IF(TE(L1,L).GT.TE(L1,L-1).AND.TE(L1,L).GT.TE(L1,L + 1)) GO TO 113
      GO TO 110
  113 CONTINUE
      IF(L1.EQ.1)TEMP4 = TE(L1,L)
      IF(L1.EQ.2)TEMP5 = TE(L1,L)
      IF(L1.EQ.3)TEMP6 = TE(L1,L)
      IF(L1.EQ.1)TEMP7 = TE(L1,L + 1)
      IF(L1.EQ.2)TEMP8 = TE(L1,L + 1)
      IF(L1.EQ.3)TEMP9 = TE(L1,L + 1)
C********* TIME FOR MAXIMUM TEMPERATURES *********
      IF(L1.EQ.1)TIM4 = TI(L1,L)
      IF(L1.EQ.2)TIM5 = TI(L1,L)
      IF(L1.EQ.3)TIM6 = TI(L1,L)
  110 CONTINUE
```

Appendix D (Continued)

```
C*************************************************************
C IF THE MAX TEMPERATURE IS ABOVE 75 F, FIND TIME AT WHICH
C 75 F OCCURS.  DEL IS TEMP DROP PER HOUR
C*************************************************************
      DEL1 = (TEMP4-TEMP1)/(-TIM4 + TIM1)
      DEL2 = (TEMP5-TEMP2)/(-TIM5 + TIM2)
      DEL3 = (TEMP6-TEMP3)/(-TIM6 + TIM3)
      IF(TEMP4.GT.TR) TIM4 = TIM4 + (TEMP4-TR)/DEL1
      IF(TEMP5.GT.TR) TIM5 = TIM5 + (TEMP5-TR)/DEL2
      IF(TEMP6.GT.TR) TIM6 = TIM6 + (TEMP6-TR)/DEL3
C***** CALCULATE AVG MIN TEMP OF PAVEMENT******
      TMEN = (1./3.)*(TEMP1 + TEMP2 + TEMP3)
      IF ( TMEN .LT. TR ) GO TO 231
      TRANG    = 0.0D0
      GO TO 2
  231 CONTINUE
      ID    = ID + 1
      DN(ID) = 1.0D0
C**** CALCULATE AVG MAX TEMP OF PAVEMENT ******
      TMEX = (1./3.)*(TEMP4 + TEMP5 + TEMP6)
      IF(TMEX.GT.TR) TMEX = TR
C**** CALCULATE AVG TIME FOR MIN TEMP AND MAX TEMP *******
      TIMMIN = (TIM1 + TIM2 + TIM3)/3.0
      TIMMAX = (TIM4 + TIM5 + TIM6)/3.
      PERIOD = 24.0-XYZTIM + TIMMIN
      XYZTIM = TIMMAX
      DLTN = TMEN-TR
      DLTX = TMEX-TR
      XYZTEM = TMEX
 1000 CONTINUE
      KTMX     = 0.0D0
      KTMN     = 0.0D0
      TRMX     = DMAX1 ( 0.0D0, TR-TMAX(NI) )
      TRMN     = TR - TMIN(NI)
C*** CALCULATE STRESS INTENSITY FACTOR FOR MIN & MAX TEMP ****
      CALL FACTOR ( DF, DLTX, PERIOD, TRMX, ID, YC, SA1, SB1, KTMX,
     *          NYEAR, LJ, ESSM )
      CALL FACTOR ( DF, DLTN, PERIOD, TRMN, ID, YC, SA2, SB2, KTMN,
     *          NYEAR, LJ, ESSM )
      K1(ID)    = KTMN - KTMX
      DYC(ID)   = 0.0D0
      IF (K1(ID) .GT. 0.0D0) GO TO 875
      ID = ID-1
      GO TO 2
```

Appendix D (Continued)

```
  875 CONTINUE
      Z0      = YC(ID)
      Z1      = DF
      Z01     = 0.0D0
      IF ( Z0 .LT. Z1 ) CALL SIMPSN ( CA, FN, Z0, Z1, Z01 )
      NF(ID)  = ACON + Z01
      ACON = 0.0D0
      IF ( NF(ID) .GT. 0.0D0 ) CDMG = CDMG + DN(ID)/NF(ID)
      DYC(ID)  = DN(ID) * CA * (K1(ID) ** FN)
      IF(NF(ID).LE.0.0D0)DYC(ID) = 0.
  876 YC(ID + 1)  = YC(ID)  + DYC(ID)
      Z01     = 0.0D0
      CALL SIMPSN ( CA, FN, D0, DF, Z01 )
      NF1(ID)  = 1.00 + Z01
      CDMG1      = CDMG1 + DN(ID)/NF1(ID)
      IF ( YC(ID + 1) .LE. DF ) GO TO 9880
      WRITE (60,3456) IYR, MOS(LL), DAY(NI), NYEAR,
     1          ID, NF(ID), NF1(ID), YC(ID), CDMG, CDMG1
      IF ( YC(ID + 1) .LE. DF ) GO TO 9880
      YC(ID + 1)  = DF
 9880 CONTINUE
    2 CONTINUE
      YCID = YC(ID)
      IF ( ID .EQ. 0 ) YCID = D0
      WRITE (60,3456) IYR, MOS(LL), JYR,     NYEAR,
     1          ID, NF(ID), NF1(ID), YCID, CDMG, CDMG1
 3456 FORMAT ( 11X, I2, 2X, A4, I2, ', 19', I2,
     1      1X, I5, 5E13.6 )
 3457 FORMAT ( 11X, 'NO', 6X, 'DATE',
     1      8X, 'ID', 6X, 'NF', 10X, 'NF1', 11X,
     2      'YC', 10X, 'CDMG',  9X, 'CDMG1', / )
    1 CONTINUE
    3 CONTINUE
C ********* REWIND FILE AND PROCESS NEXT PROBLEM *********
      REWIND 1
      GOTO 8
  999 STOP
      END
      SUBROUTINE CURVE(TH,TC)
C*** CURVE CALCULATES TH AND TC, HEATING AND COOLING TEMPS ***
      IMPLICIT REAL*8 (A-H,O-Z)
      DIMENSION TH(11),TC(11)
      COMMON /A1/ CN,CM,TM,TR,TA,E1,EE
      COMMON /GT/ GAB1
      DIMENSION F(50)
      COMMON     HH(11),ZZ
      COMMON /KK/ I
```

Appendix D (Continued)

```
100 CONTINUE
    INT = 40
    A = CM/(CM + 1.0) + CN-2.0
    B = -CN
    DM = (1.0-CN)/(CM + 1.0)**(1.0-CN)
    GA = DGAMMA(A + 1.0)
    GB1 = DGAMMA(B + 1.0)
    GAB1 = GA*GB1/DGAMMA(A + B + 2.0)
    TH(1) = 1.0
    TC(1) = 1.0
    TC(11) = 0.0D0
    DO 40 INDEX = 1,2
    HH(1) = 1.0
    AREA = 0.0D0
    ZZ = 0.0D0
    DTN = 0.0D0
    DO 10 I = 1,10
    DTN = DTN + 0.1
    DTR = DABS(DTN)
    IF(INDEX.EQ.1) GO TO 21
    H = (DTN + 1.0)**(CM + 1.0)
    HH(I + 1) = H
    HS = (HH(I + 1)-HH(I))/(INT-1)
    CALL HEAT(A,B,H,INT,F,AREA,HS)
    CONS = DM*(1.0 + 1.0/DTN)**(1.0-CN)
    TII = CONS*AREA
    TH(I + 1) = TII
    GO TO 25
21 CONTINUE
    IF(I.EQ.10) GO TO 10
    RR = -DTR
    H = (1.0 + RR)**(CM + 1.0)
    HH(I + 1) = H
    HS = (HH(I)-HH(I + 1))/(INT-1)
    CALL COOL(A,B,H,AREA)
    CONS = DM*(-1.0-1.0/RR)**(1.0-CN)
    TII = CONS*AREA
    TC(I + 1) = TII
25 CONTINUE
10 CONTINUE
40 CONTINUE
    RETURN
    END
    SUBROUTINE HEAT(A,B,H,INT,F,AREA,HS)
    IMPLICIT REAL*8 (A-H,O-Z)
    DIMENSION F(INT)
```

Appendix D (Continued)

```
      COMMON    HH(11),ZZ
      COMMON /KK/ I
      DA = H**(A + 1.0)*(-1.0 + H)**(B + 1.0)/(B + 1.0)
      DB = -(A + B + 2.0)/(B + 1.0)
      DO 10 J = 1,INT
      XX = HH(I) + HS*(J-1)
   10 F(J) = XX**A*(-1.0 + XX)**(B + 1.0)
      CALL INTGRT(INT,F,HS,AR)
      ZZ = ZZ + AR
      AREA = DA + ZZ*DB
      RETURN
      END
      SUBROUTINE INTGRT(N,F,H,AREA)
      IMPLICIT REAL*8 (A-H,O-Z)
      DIMENSION F(N)
      AREA = 0.0D0
      S = 0.5*H
      DO 10 I = 2,N
      AREA = AREA + S*(F(I-1) + F(I))
   10 CONTINUE
      RETURN
      END
      SUBROUTINE COOL (A,B,H,AREA)
      IMPLICIT REAL*8 (A-H,O-Z)
      REAL*4 SH,SA1,SB2,SP
      REAL*4 SNGL
      COMMON /GT/ GAB1
      A1 = A + 1.0
      B1 = B + 1.0
      P = 0.0D0
      SH = SNGL(H)
      SA1 = SNGL(A1)
      SB2 = SNGL(B1)
      SP = SNGL(P)
   10 CONTINUE
      P = DBLE(SP)
      H = DBLE(SH)
      A1 = DBLE(SA1)
      B2 = DBLE(SB2)
      AREA = GAB1*(1.D0-P)
      RETURN
      END
```

Appendix D (Continued)

```
      SUBROUTINE FACTOR ( DF, DELT, PERIOD, TRG, ID, YC, SA, SB, XXX,
     *            NYEAR, LJ, ESSM )
C****************************************************************
C* CALCULATES STRESS INTENSITY FACTOR FOR A GIVEN PAVEMENT     *
C*                                        *
C*  DF   = DEPTH OF ASPHALT LAYER                  *
C*  DELT = PAVEMENT TEMP - STRESS FREE TEMP          *
C*  PERIOD LOADING TIME                         *
C*  TRG  = STRESS FREE TEMP - MAX AIR TEMP           *
C*  ID   = DAY COUNTER                      *
C*  YC   = CRACK LENGTH                      *
C*  SA,SB= CONSTANTS TO CALCULATE STRESS INTENSITY FACTOR   *
C*  XXX  = STRESS INTENSITY FACTOR              *
C****************************************************************
      IMPLICIT REAL*8 (A-H,O-Z)
      REAL*8    M1, M2, M3, M4
      DIMENSION  YC(2500)
      COMMON /A1/ CN, CM, TM, TR, TA, E1, EE
      COMMON /A3/ M1, M2, M3, M4
      COMMON /A4/ TC(12), TH(12)
      SA      = 0.0D0
      SB      = 0.0D0
      XXX     = 0.0D0
      DT = DELT
      IF (PERIOD.LT.1.0) PERIOD = 1.0
      TIME = PERIOD*3600.
      TTN = TIME**(-CN)
      T = TR + DT
      AT = ((TM-TA)/(T-TA))**CM
      ATN = AT**CN
      DTN = DT/(TR-TA)
      DTR = DABS(DTN*10.0)
      NN = IDINT(DTR)
      DIF = DTR-NN
      NG = NN + 1
      IF ( NG .LE. 11 ) GO TO 99
      WRITE (60,654)
 654 FORMAT ( 5X, 'NG IS GREATER THAN 11. SET NG = 11', // )
      NG = 11
 99 CONTINUE
C** CALCULATION OF EFF MODULUS. SEE P. 17, REPORT 18-3 ***
      IF(DELT) 90,29,30
 90 RATIO = (TC(NG+1) - TC(NG)) * DIF + TC(NG)
      J = 1
      GO TO 120
 29 RATIO = 1.D0
      J = 3
```

Appendix D (Continued)

```
      GO TO 120
   30 RATIO = (TH(NG + 1) - TH(NG)) * DIF  +  TH(NG)
      J = 2
  120 CONTINUE
      ESS = ATN*E1*TTN/(1.D0-CN)
      IF (ESS .GT. ESSM) ESS = ESSM
      EEF    = EE + RATIO * ( ESS - EE )
      M1     = 8.8988D + 00
      M2     = 2.0599D + 00
      M3     = 0.8481D + 00
      M4     =-0.00157D + 00
      IF ( EEF .GE. 1.000D + 05 ) GO TO 978
      M1     = M1 + ( 29.1063D + 00 - DF ) * ( 1.3573D + 00
     1         - 0.013573D + 00 * ( EEF / 1000.0D0) )
      M2     = M2 - ( 129.3215D + 00 - DF ) * ( 0.01687 + 00
     1         - 0.0001687D + 00 * ( EEF / 1000.0D0) )
      IF ( DF .GT. 4.0D0 ) GO TO 988
      M3     = M3 + ( 2.7811D + 00 - DF ) * ( 0.2738D + 00
     1         - 0.002738D + 00 * ( EEF / 1000.0D0) )
      GO TO 987
  988 CONTINUE
      M3     = M3 - ( 6.5835D + 00 - DF ) * ( 0.12919D + 00
     1         -0.0012919D + 00 * ( EEF / 1000.0D0))
  987 CONTINUE
      M4     = M4 + ( 5.0472D + 00 - DF ) * ( 0.001129D + 00
     1         - 0.00001129D + 00 * ( EEF / 1000.0D0) )
  978 IF ( TRG .LE. M1 ) RETURN
      SA     = M2 * ( TRG - M1 )
      SB     = M3 + M4 * TRG
      XXX    = SA * YC(ID) ** SB
      RETURN
      END
      SUBROUTINE SIMPSN ( CA, FN, XF, XL, AREA )
      IMPLICIT REAL*8 (A-H,O-Z)
      REAL*8    KMIN, KMAX
      DIMENSION  Y(7)
      COMMON /A2/ SA1, SA2, SB1, SB2
      NS     = 6
      NP     = 7
      XINC   = ( XL - XF ) / 6.000D + 00
      X      = XF
      DO 1100 I = 1, NP
      F      = SA2 * X ** SB2 - SA1 * X ** SB1
      YI     = CA * DABS(F) ** FN
      Y(I)   = 1.000D + 00 / YI
      X      = X + XINC
 1100 CONTINUE
```

Appendix D (Continued)

```
      AREA     = 0.0D0
      DO 1200 I = 1, NS, 2
      A        = Y(I) + 4.000D+00 * Y(I+1) + Y(I+2)
      A        = A * XINC / 3.000D+00
      AREA     = AREA + A
 1200 CONTINUE
      RETURN
      END
C*****************************************************************
      FUNCTION DGAMMA(A)
C*****************************************************************
C
      IMPLICIT REAL*8 (A-H,O-Z)
C
      G        = 0.
      GLAST    = 0.


      DO 1000 I = 1, 3480
      X        = 0.05*I
      G        = GLAST+0.05*(X**(A-1)*DEXP(-X))
      IF( DABS((G-DLAST)/G) .LT. 0.000001) GO TO 2000
      GLAST    = G
 1000 CONTINUE
 2000 CONTINUE
      DGAMMA     = G
      RETURN
      END
```

Appendix D (Continued)

EXAMPLE LISTING OF PROGRAM THERM OUTPUT

THERMAL CRACKING ANALYSIS FOR BG1L

THIS ANALYSIS BEGINS AFTER 411231 AND RUNS FOR 17 YEARS.

THE BITUMEN USED HAS THE FOLLOWING ORIGINAL PROPERTIES:
    PENETRATION INDEX   =   8.500
    SOFTENING POINT RING & BALL TEMP =   120.200 DEG F
THE ASPHALT CONCRETE LAYER IS   1.125 INCHES THICK
AND IS ASSUMED TO HAVE AN INITIAL CRACK OF   .100
INCHES EXTENDING FROM THE SURFACE.
THE ASPHALT CONCRETE HAS THE FOLLOWING MIX PROPERTIES:
    AGGREGATE VOLUME CONCENTRATION =   .880
    DENSITY =   140.000 LBS/FT**3
    SPECIFIC HEAT =   .220 BTU/LB DEG F
    THERMAL CONDUCTIVITY =   .700 BTU/FT**2/HR,DEG F/FT
    ABSORPTIVITY =   .950

THE PAVEMENT IS ASSUMED TO BE SUBJECTED TO THE
FOLLOWING AVERAGE ENVIRONMENTAL CONDITIONS:
    WIND VELOCITY =   .000 MILES PER HOUR
    AVERAGE ANNUAL SOLAR RADIATION =   .000 LANGLEYS/DAY
    AVERAGE JULY SOLAR RADIATION =   .000 LANGLEYS/DAY

*** YEAR 0 ***
IN PLACE BITUMIN PROPERTIES:
    PENETRATION AT 77 DEG F   =   53.000
    SOFTENING POINT RING & BALL TEMP =   120.200 DEG F

FATIGUE PARAMETERS OF THE MIX:
    A = .862E-10   N =   4.453

NO	DATE	ID	NF	NF1	YC	CDMG	CDMG1
0	JAN 31, 1942	31	.132180E+07	.132187E+07	.100001E+00	.234522E-04	.234516E-04
0	FEB 28, 1942	59	.132174E+07	.132187E+07	.100003E+00	.446359E-04	.446337E-04
0	MAR 31, 1942	90	.132167E+07	.132187E+07	.100004E+00	.680904E-04	.680853E-04
0	APR 30, 1942	120	.132161E+07	.132187E+07	.100006E+00	.907894E-04	.907804E-04
0	MAY 31, 1942	151	.132154E+07	.132187E+07	.100007E+00	.114246E-03	.114232E-03
0	JUN 30, 1942	181	.132147E+07	.132187E+07	.100009E+00	.136948E-03	.136927E-03
0	JUL 31, 1942	212	.132141E+07	.132187E+07	.100010E+00	.160407E-03	.160379E-03
0	AUG 31, 1942	243	.132134E+07	.132187E+07	.100012E+00	.183867E-03	.183830E-03
0	SEP 30, 1942	273	.132127E+07	.132187E+07	.100013E+00	.206572E-03	.206525E-03
0	OCT 31, 1942	304	.132120E+07	.132187E+07	.100015E+00	.230035E-03	.229977E-03
0	NOV 30, 1942	334	.132114E+07	.132187E+07	.100016E+00	.252742E-03	.252672E-03

Appendix D (Continued)

```
*** YEAR  1 ***
IN PLACE BITUMIN PROPERTIES:
    PENETRATION AT 77 DEG F    =    53.000
    SOFTENING POINT RING & BALL TEMP  =    120.200 DEG F

FATIGUE PARAMETERS OF THE MIX:
    A  =  .862E-10    N  =    4.453
```

NO	DATE	ID	NF	NF1	YC	CDMG	CDMG1
1	DEC 31, 1942	365	.132107E+07	.132187E+07	.100018E+00	.276208E-03	.276124E-03
1	JAN 31, 1943	396	.132100E+07	.132187E+07	.100019E+00	.299674E-03	.299575E-03
1	FEB 28, 1943	424	.132094E+07	.132187E+07	.100021E+00	.320870E-03	.320757E-03
1	MAR 31, 1943	455	.132087E+07	.132187E+07	.100022E+00	.344339E-03	.344209E-03
1	APR 30, 1943	485	.132081E+07	.132187E+07	.100023E+00	.367052E-03	.366904E-03
1	MAY 31, 1943	516	.132074E+07	.132187E+07	.100025E+00	.390523E-03	.390356E-03
1	JUN 30, 1943	546	.132067E+07	.132187E+07	.100026E+00	.413238E-03	.413051E-03
1	JUL 31, 1943	577	.132060E+07	.132187E+07	.100028E+00	.436712E-03	.436502E-03
1	AUG 31, 1943	608	.132054E+07	.132187E+07	.100029E+00	.460187E-03	.459954E-03
1	SEP 30, 1943	638	.132047E+07	.132187E+07	.100031E+00	.482905E-03	.482649E-03
1	OCT 31, 1943	669	.132040E+07	.132187E+07	.100032E+00	.506382E-03	.506101E-03
1	NOV 30, 1943	699	.132034E+07	.132187E+07	.100034E+00	.529103E-03	.528796E-03

```
                              *                    *
                              *                    *
                              *                    *
                              *                    *
                              *                    *
```

```
*** YEAR  7 ***
IN PLACE BITUMIN PROPERTIES:
    PENETRATION AT 77 DEG F    =    53.000
    SOFTENING POINT RING & BALL TEMP  =    120.200 DEG F

FATIGUE PARAMETERS OF THE MIX:
    A  =  .862E-10    N  =    4.453
```

NO	DATE	ID	NF	NF1	YC	CDMG	CDMG1
7	JUL 31, 1946	1642	.131826E+07	.132187E+07	.100080E+00	.124388E-02	.124218E-02
7	AUG 31, 1946	1673	.131820E+07	.132187E+07	.100081E+00	.126739E-02	.126563E-02
7	SEP 30, 1946	1703	.131813E+07	.132187E+07	.100083E+00	.129015E-02	.128833E-02
7	OCT 31, 1946	1734	.131806E+07	.132187E+07	.100084E+00	.131367E-02	.131178E-02
7	NOV 30, 1946	1764	.131800E+07	.132187E+07	.100086E+00	.133643E-02	.133447E-02
7	DEC 31, 1946	1795	.131793E+07	.132187E+07	.100087E+00	.135995E-02	.135792E-02
7	JAN 31, 1947	1826	.131786E+07	.132187E+07	.100089E+00	.138348E-02	.138137E-02
7	FEB 28, 1947	1854	.131780E+07	.132187E+07	.100090E+00	.140472E-02	.140256E-02
7	MAR 31, 1947	1885	.131773E+07	.132187E+07	.100092E+00	.142825E-02	.142601E-02
7	APR 30, 1947	1915	.131766E+07	.132187E+07	.100093E+00	.145101E-02	.144870E-02
7	MAY 31, 1947	1946	.131760E+07	.132187E+07	.100094E+00	.147454E-02	.147216E-02
7	JUN 30, 1947	1976	.131753E+07	.132187E+07	.100096E+00	.149731E-02	.149485E-02

APPENDIX E

LABORATORY TEST DATA

APPENDIX E-1

ENERGY RATE INTEGRAL TEST DATA

Table E-1.1   Summary Table of Energy Rate Integral Test Results.

Sample I.D.	Disp. Rate (in/min)	C*-Integral (lbs/in-min)	Crack Rate (in/min)	Slope (psi)
BG2H10 1	0.012	0.657	1.079	0.714
	0.030	2.292	4.183	
	0.048	3.553	4.563	
BG2L20 1	0.012	0.780	0.616	1.404
	0.030	3.758	1.435	
	0.048	8.993	5.977	
BK1H10 1	0.012	BRITTLE	***	***
	0.030	FRACTURE	***	
	0.048	***	***	
BK1L20 1	0.012	0.734	0.974	1.659
	0.030	5.931	3.505	
	0.048	14.492	9.130	
BG1H20 1	0.003	0.134	0.115	0.714
	0.012	0.374	0.375	
	0.030	3.098	4.235	
BG1L10 1	0.003	0.110	0.125	0.026
	0.012	0.136	0.287	
	0.030	0.249	5.027	
BK2H20 1	0.012	0.208	0.650	0.706
	0.030	1.020	2.335	
	0.048	2.143	3.283	
BK2L10 1	0.012	0.796	1.095	0.960
	0.030	2.259	5.000	
	0.048	6.643	6.058	

Table E-1.1 (Continued)

Sample I.D.	Disp. Rate (in/min)	C*-Integral (lbs/in-min)	Crack Rate (in/min)	Slope (psi)
BG2H10 2	0.012	0.852	0.683	0.640
	0.030	3.120	4.046	
	0.048	3.895	5.492	
BG2L20 2	0.012	0.663	0.674	2.025
	0.030	2.595	2.207	
	0.048	6.607	3.589	
BK1H10 2	0.012	BRITTLE	* * *	* * *
	0.030	FRACTURE	* * *	
	0.048	* * *	* * *	
BK1L20 2	0.012	0.804	1.471	0.763
	0.030	3.156	4.532	
	0.048	4.382	6.163	
BG1H20 2	0.012	1.012	0.616	0.681
	0.030	3.575	1.435	
	0.048	5.414	5.977	
BG1L10 2	0.012	BRITTLE	* * *	* * *
	0.030	FRACTURE	* * *	
	0.048	* * *	* * *	
BK2H20 2	0.012	0.466	0.655	1.354
	0.030	1.510	1.394	
	0.048	3.113	2.606	
BK2L10 2	0.012	0.865	2.495	0.322
	0.030	2.902	4.876	
	0.048	3.853	10.800	

Table E-1.1 (Continued)

Sample I.D.	Disp. Rate (in/min)	C*-Integral (lbs/in-min)	Crack Rate (in/min)	Slope (psi)
BG2H20 1	0.012	0.064	0.661	4.234
	0.030	1.790	0.982	
	0.048	5.356	1.887	
BG2L10 1	0.012	BRITTLE	***	***
	0.030	FRACTURE	***	
	0.048	***	***	
BK1H20 1	0.003	0.111	0.070	2.219
	0.006	0.504	0.305	
	0.009	1.073	0.500	
BK1L10 1	0.003	BRITTLE	***	***
	0.012	FRACTURE	***	
	0.030	***	***	
BG1H10 1	0.003	0.060	0.289	0.267
	0.012	0.223	0.764	
	0.030	2.271	8.502	
BG1L20 1	0.012	0.360	0.688	0.802
	0.030	1.000	0.886	
	0.048	5.030	6.226	
BK2H10 1	0.012	0.564	0.576	0.626
	0.030	2.068	3.498	
	0.048	2.999	2.561	
BK2L20 1	0.012	0.587	0.651	6.465
	0.030	2.548	1.059	
	0.048	5.820	1.460	

Table E-1.1 (Continued)

Sample I.D.	Disp. Rate (in/min)	C*-Integral (lbs/in-min)	Crack Rate (in/min)	Slope (psi)
BG2H20 2	0.012	0.131	0.390	1.502
	0.030	1.563	1.041	
	0.048	4.326	3.093	
BG2L10 2	0.012	BRITTLE	* * *	* * *
	0.030	FRACTURE	* * *	
	0.048	* * *	* * *	
BK1L10 2	0.012	BRITTLE	* * *	* * *
	0.030	FRACTURE	* * *	
	0.048	* * *	* * *	
BG1H10 2	0.012	BRITTLE	* * *	* * *
	0.030	FRACTURE	* * *	
	0.048	* * *	* * *	
BK2H10 2	0.012	0.790	0.852	1.042
	0.030	3.430	3.656	
	0.048	6.100	5.928	

APPENDIX E-2

DIRECT TENSION TEST DATA

Table E-2.1   Summary of Direct Tension Test Results (OSU Study).

Sample I.D.	Peak Stress (psi)	Peak Strain (10^{-3})	Secant Modulus (10^6 psi)	Strain Energy at Fracture (10^6 psi)
BG1H-34 1	204	0.22	0.93	0.094
BG1H-34 2	228	0.22	1.05	0.091
BG2H-34 1	229	0.39	0.59	0.060
BG2H-34 2	229	0.20	1.14	0.030
BK1H-34 1	263	0.41	0.64	0.147
BK1H-34 2	279	0.33	0.85	0.214
BK2H-34 1	231	0.23	1.00	0.172
BK2H-34 2	151	2.36	0.64	0.287
BG1L-34 1	343	0.44	0.79	0.090
BG1L-34 2	375	0.43	0.88	0.095
BG2L-34 1	265	0.26	1.00	0.042
BG2L-34 2	324	0.40	0.80	0.085
BK1L-34 1	448	0.63	0.71	0.159
BK1L-34 2	387	0.44	0.88	0.110
BK2L-34 1	531	0.49	1.09	0.151
BK2L-34 2	664	0.41	1.64	0.173

Table E-2.1 (Continued)

Sample I.D.	Peak Stress (psi)	Peak Strain (10^{-3})	Secant Modulus (10^6 psi)	Strain Energy at Fracture (10^6 psi)
BG1H-18 1	270	0.23	1.16	0.167
BG1H-18 2	418	0.36	1.16	0.086
BG2H-18 1	272	0.30	0.92	0.049
BG2H-18 2	323	0.49	0.66	0.091
BK1H-18 1	313	0.88	0.35	0.330
BK1H-18 2	289	1.06	0.27	0.223
BK2H-18 1	147	2.38	0.62	0.286
BK2H-18 2	170	2.47	0.07	0.329
BG1L-18 1	452	0.26	1.75	0.391
BG1L-18 2	382	0.49	0.78	0.215
BG2L-18 1	406	0.34	1.19	0.092
BG2L-18 2	485	0.63	0.77	0.177
BK1L-18 1	486	0.69	0.70	0.204
BK1L-18 2	438	1.54	0.28	0.401
BK2L-18 1	290	1.57	0.18	0.509
BK2L-18 2	289	1.42	0.20	0.460

Table E-2.2   **Summary of Direct Tension Test Results (University of Waterloo Study).**

Sample I.D.	Peak Stress (psi)	Peak Strain (10^{-3})	Secant Modulus (10^6 psi)	Strain Energy at Fracture (10^6 psi)
BG1H-34 1	413	0.20	2.09	0.073
BG1H-34 2	268	0.09	3.07	0.040
BG1H-34 3	279	0.16	1.77	0.037
BG2H-34 1	372	0.15	2.50	0.044
BG2H-34 2	338	0.15	2.31	0.124
BG2H-34 3	298	0.11	2.80	0.039
BK1H-34 1	430	0.23	1.89	0.093
BK1H-34 2	365	0.21	1.77	0.080
BK1H-34 3	451	0.22	2.01	0.074
BK2H-34 1	490	0.26	1.91	0.095
BK2H-34 2	509	0.27	1.88	0.096
BK2H-34 3	353	0.18	1.97	0.081
BG1L-34 1	332	0.12	2.67	0.096
BG1L-34 2	404	0.19	2.16	0.068
BG1L-34 3	312	0.11	2.73	0.057
BG2L-34 1	392	0.12	3.36	0.089
BG2L-34 2	310	0.11	2.83	0.066
BG2L-34 3	347	0.12	2.96	0.051

Table E-2.2 (Continued).

Sample I.D.	Peak Stress (psi)	Peak Strain (10^{-3})	Secant Modulus (10^6 psi)	Strain Energy at Fracture (10^6 psi)
BK1L-34 1	364	0.17	2.18	0.076
BK1L-34 2	340	0.17	1.99	0.107
BK1L-34 3	568	0.31	1.83	0.119
BK2L-34 1	419	0.20	2.06	0.065
BK2L-34 2	464	0.22	2.08	0.073
BK2L-34 3	491	0.22	2.21	0.170
BG1H-18 1	216	0.12	1.74	0.019
BG1H-18 2	320	0.20	1.63	0.059
BG1H-18 3	215	0.08	2.56	0.054
BG2H-18 1	465	0.22	2.14	0.122
BG2H-18 2	263	0.13	2.04	0.125
BG2H-18 3	310	0.16	1.99	0.048
BK1H-18 1	446	0.53	0.84	0.168
BK1H-18 2	393	0.58	0.68	0.174
BK1H-18 3	442	0.49	0.90	0.146
BK2H-18 1	322	0.67	0.48	0.205
BK2H-18 2	324	1.00	0.32	0.494
BK2H-18 3	378	0.75	0.51	0.231

Table E-2.2 (Continued).

Sample I.D.	Peak Stress (psi)	Peak Strain (10^{-3})	Secant Modulus (10^6 psi)	Strain Energy at Fracture (10^6 psi)
BG1L-18 1	611	0.26	2.34	0.199
BG1L-18 2	588	0.23	2.54	0.151
BG1L-18 3	483	0.19	2.58	0.089
BG2L-18 1	523	0.21	2.43	0.152
BG2L-18 2	436	0.19	2.33	0.096
BG2L-18 3	619	0.23	2.64	0.149
BK1L-18 1	274	0.27	1.01	0.051
BK1L-18 2	500	0.43	1.15	0.179
BK1L-18 3	447	0.64	0.70	0.248
BK2L-18 1	450	1.01	0.45	0.418
BK2L-18 2	460	0.99	0.46	0.432
BK2L-18 3	512	1.03	0.50	0.498
BG1H0 1	280	2.44	0.12	6.142
BG1H0 2	311	1.84	0.17	5.163
BG1H0 3	233	2.19	0.11	3.908
BG2H0 1	308	2.89	0.11	6.838
BG2H0 2	254	2.36	0.11	6.014
BG2H0 3	251	3.79	0.06	6.355

Table E-2.2 (Continued).

Sample I.D.	Peak Stress (psi)	Peak Strain (10^{-3})	Secant Modulus (10^6 psi)	Strain Energy at Fracture (10^6 psi)
BK1H0 1	185	3.38	0.05	1.964
BK1H0 2	145	2.29	0.06	1.177
BK1H0 3	154	3.94	0.04	3.154
BK2H0 1	69	3.71	0.02	2.030
BK2H0 2	107	3.75	0.02	4.347
BK2H0 3	74	2.85	0.03	2.943
BG1L0 1	293	1.54	0.19	5.817
BG1L0 2	252	1.13	0.23	4.953
BG1L0 3	421	2.49	0.17	14.165
BG2L0 1	249	3.46	0.07	7.716
BG2L0 2	200	2.80	0.07	4.102
BG2L0 3	236	3.46	0.06	9.553
BK1L0 1	187	6.04	0.03	17.725
BK1L0 2	179	5.33	0.03	13.555
BK1L0 3	222	6.06	0.04	22.481
BK2L0 1	88	2.33	0.04	1.331
BK2L0 2	113	3.63	0.03	2.162
BK2L0 3	105	4.45	0.02	2.629

APPENDIX E-3

DIRECT TENSILE CREEP TEST DATA
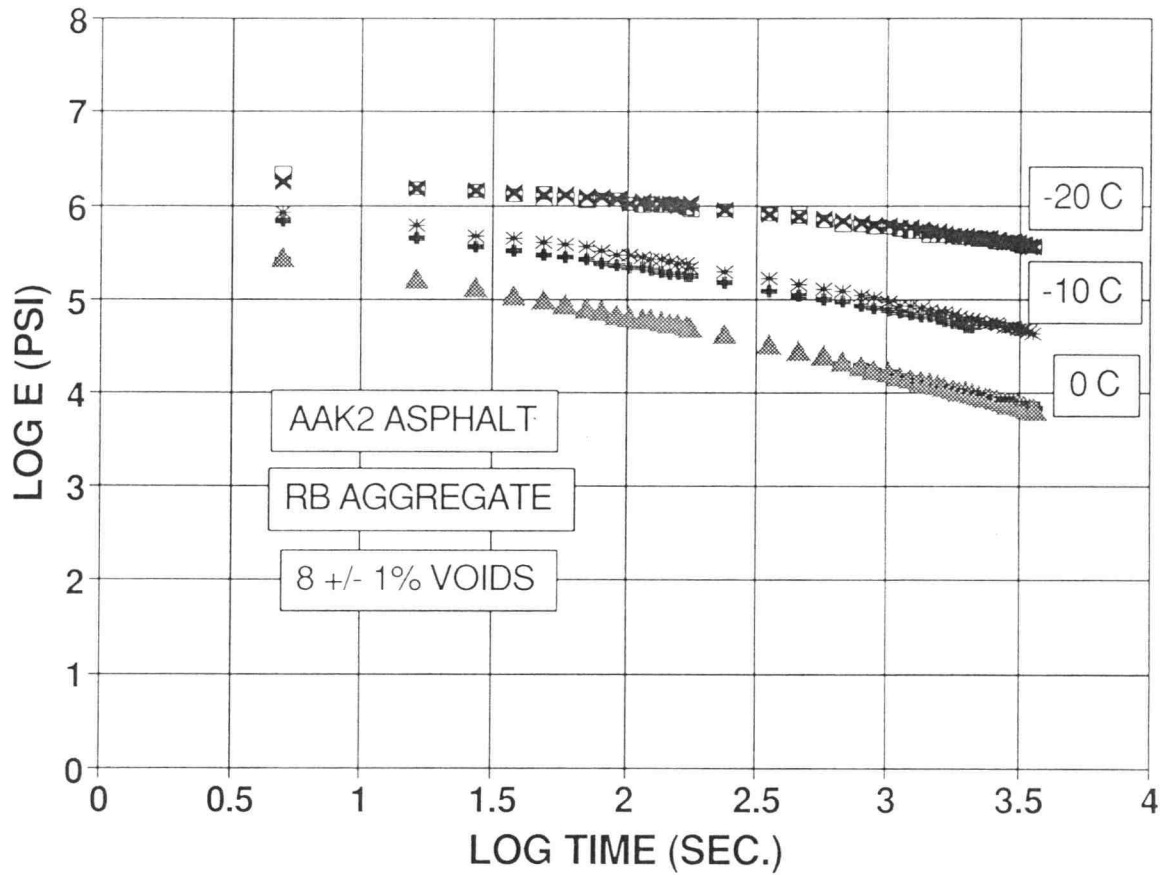
Figure E-3.1   Log$_{10}$-Log$_{10}$ Plot of Creep Modulus vs. Time For Replicate Asphalt Concrete Mixtures Containing AAK-2 Binder with RB Aggregate and 8 +/- 1% Voids at 0, -10 and -20 C.
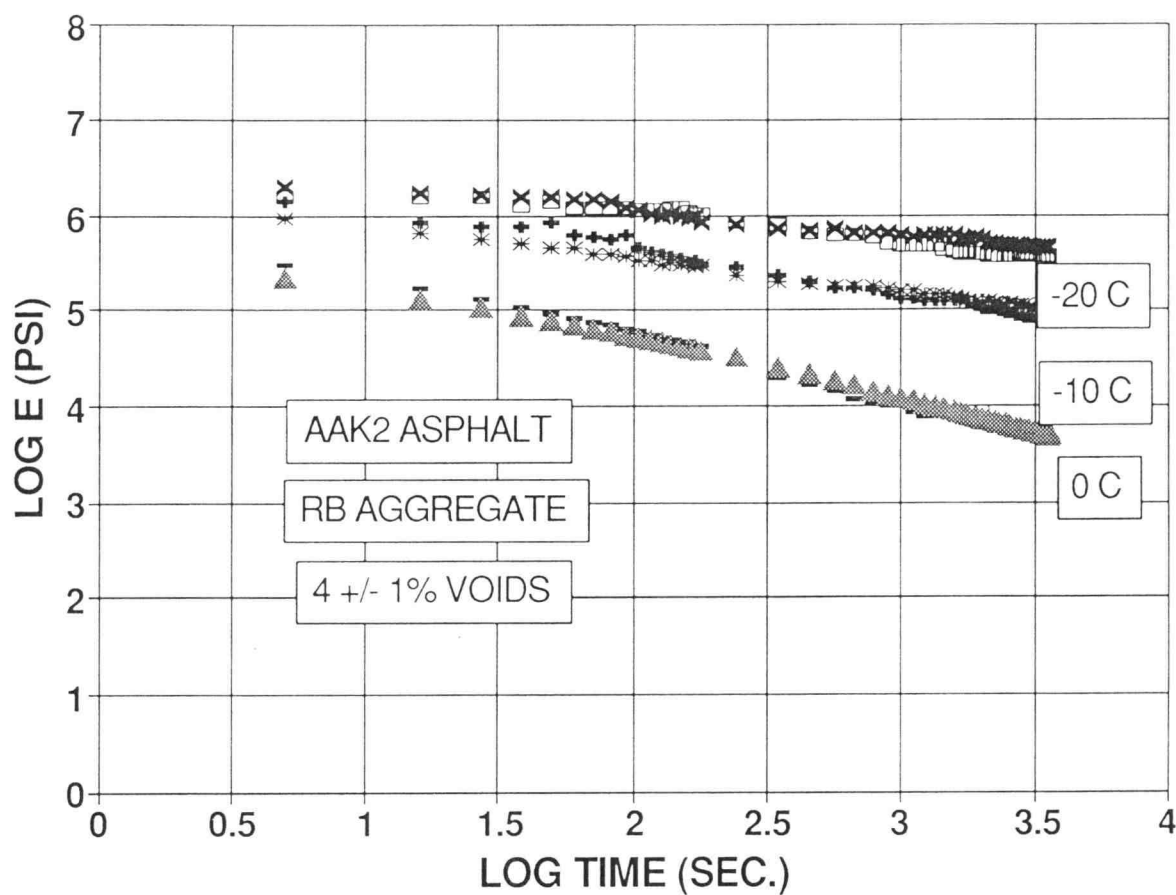
Figure E-3.2 Log_{10}-Log_{10} Plot of Creep Modulus vs. Time For Replicate Asphalt Concrete Mixtures Containing AAK-2 Binder with RB Aggregate and 4 +/- 1% Voids at 0, -10 and -20 C.
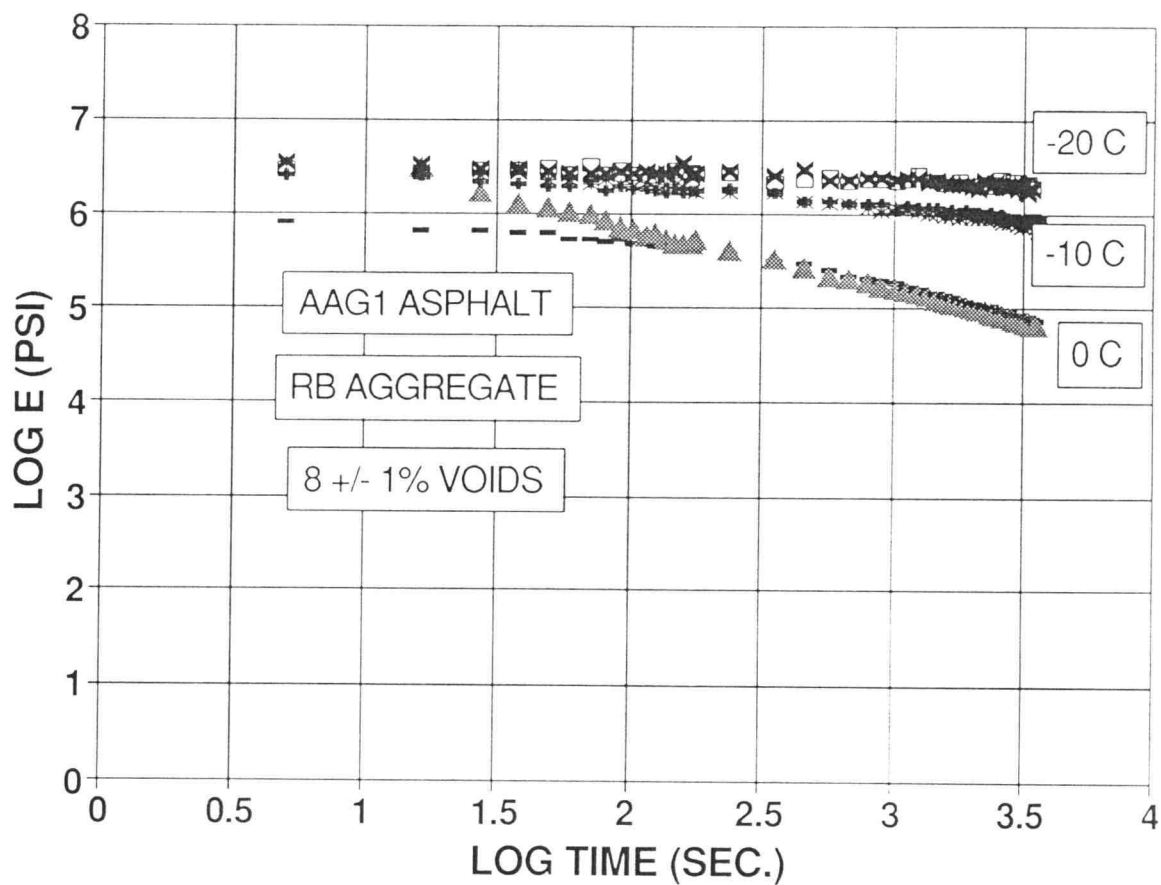
Figure E-3.3 Log_{10}-Log_{10} Plot of Creep Modulus vs. Time For
Replicate Asphalt Concrete Mixtures Containing
AAG-1 Binder with RB Aggregate and 8 +/- 1% Voids
at 0, -10 and -20 C.
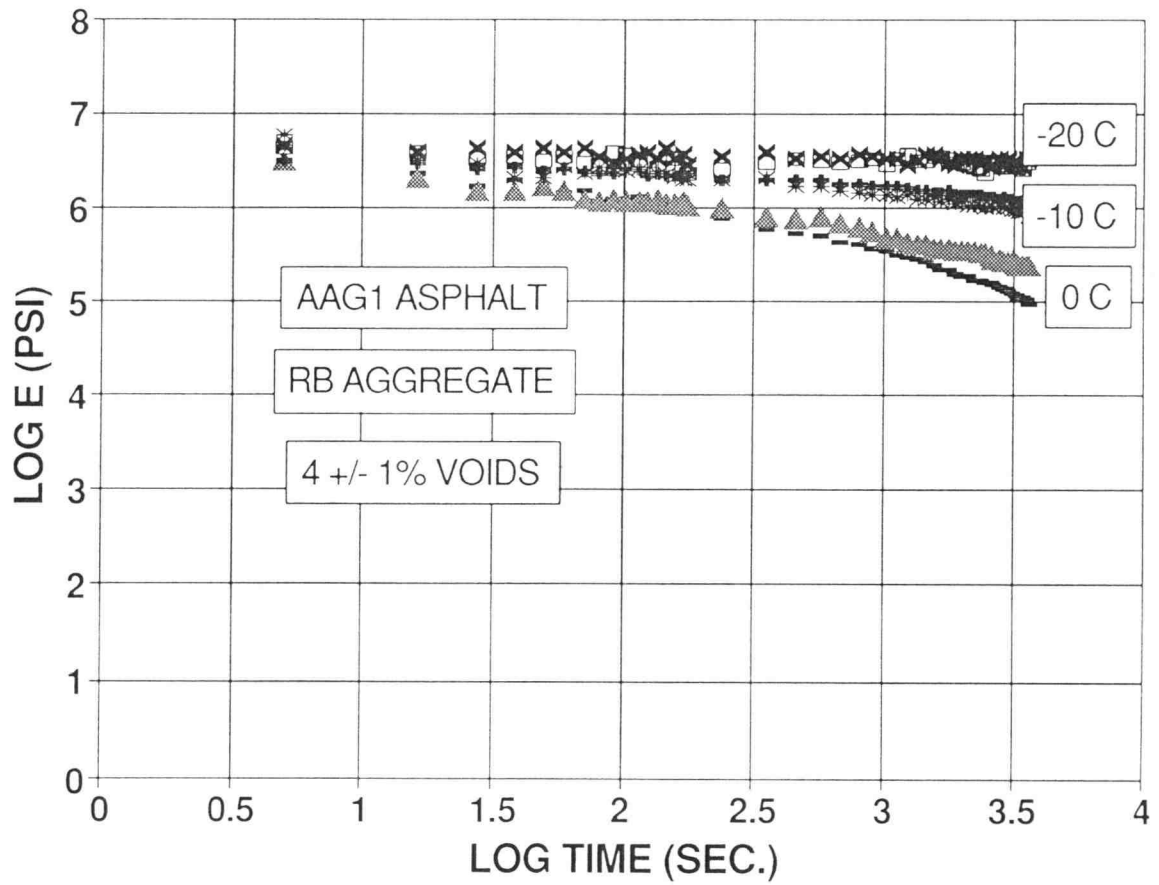
Figure E-3.4   Log$_{10}$-Log$_{10}$ Plot of Creep Modulus vs. Time For
Replicate Asphalt Concrete Mixtures Containing
AAG-1 Binder with RB Aggregate and 4 +/- 1% Voids
at 0, -10 and -20 C.

BK2H
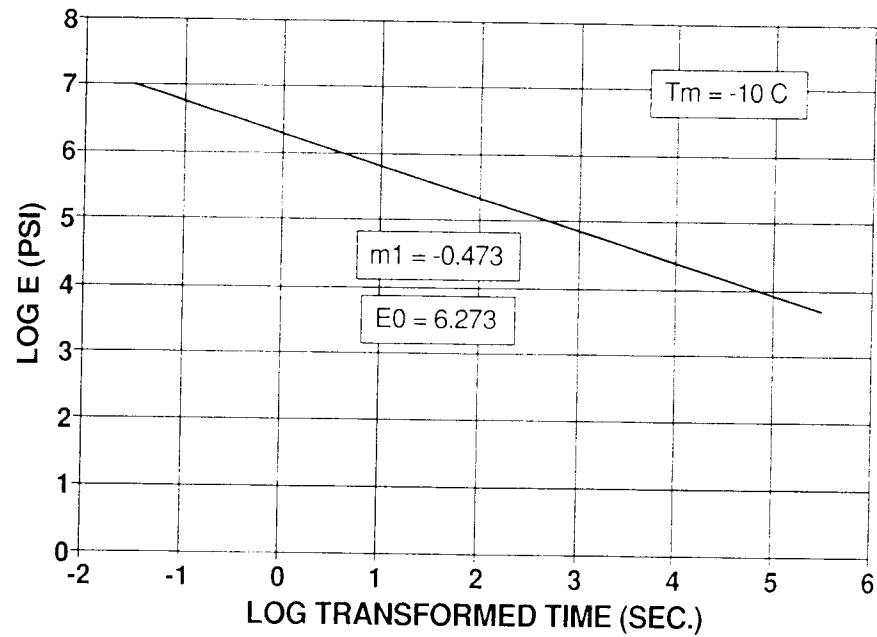
Figure E-3.5 (a)   Transformed Creep Modulus Curve at
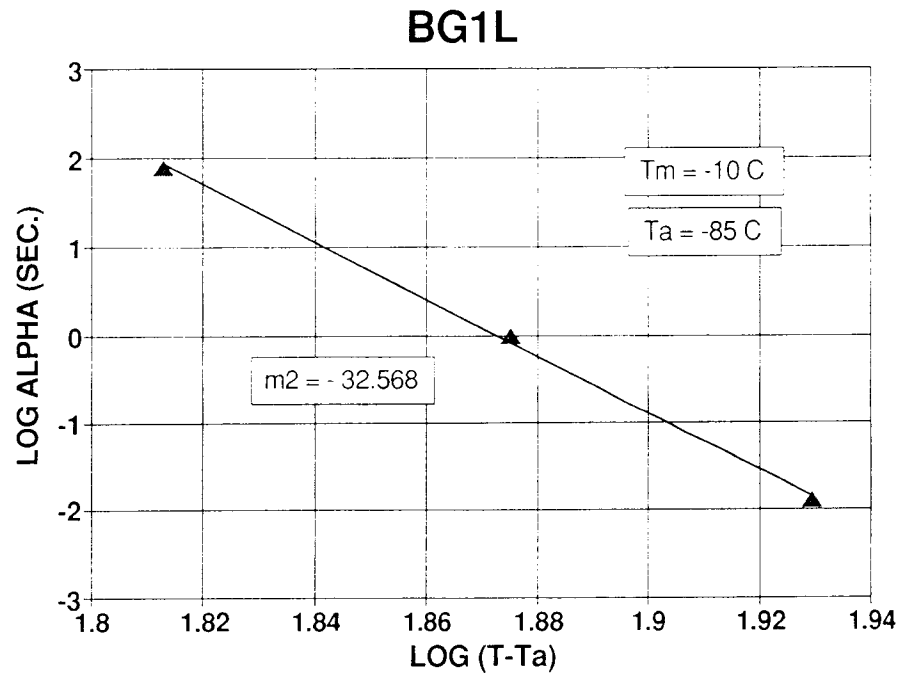Standard Temperature of -10 C.

BK2H
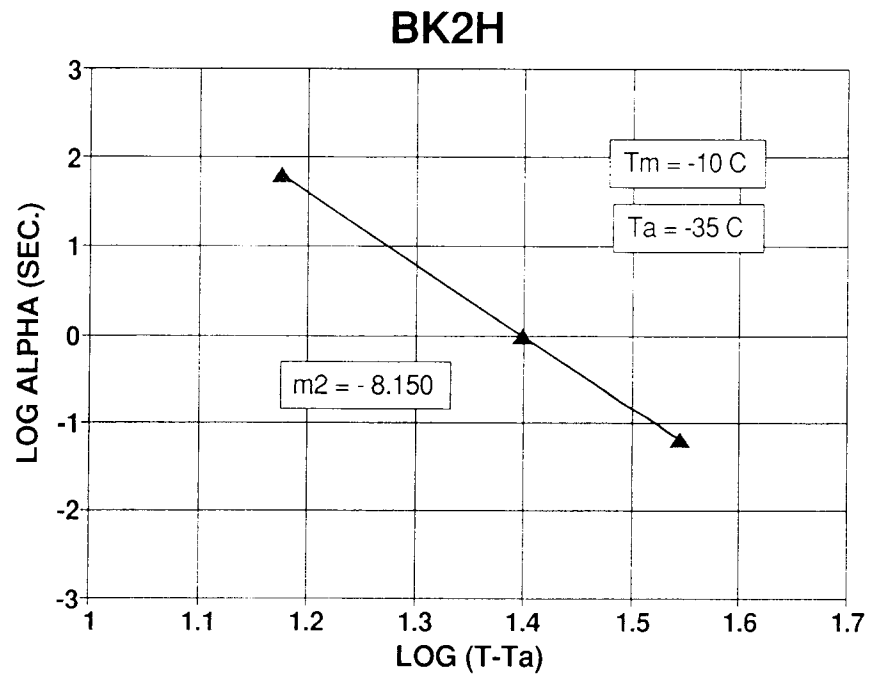
Figure E-3.5 (b) Log_{10} Time-Temperature Shift Factor
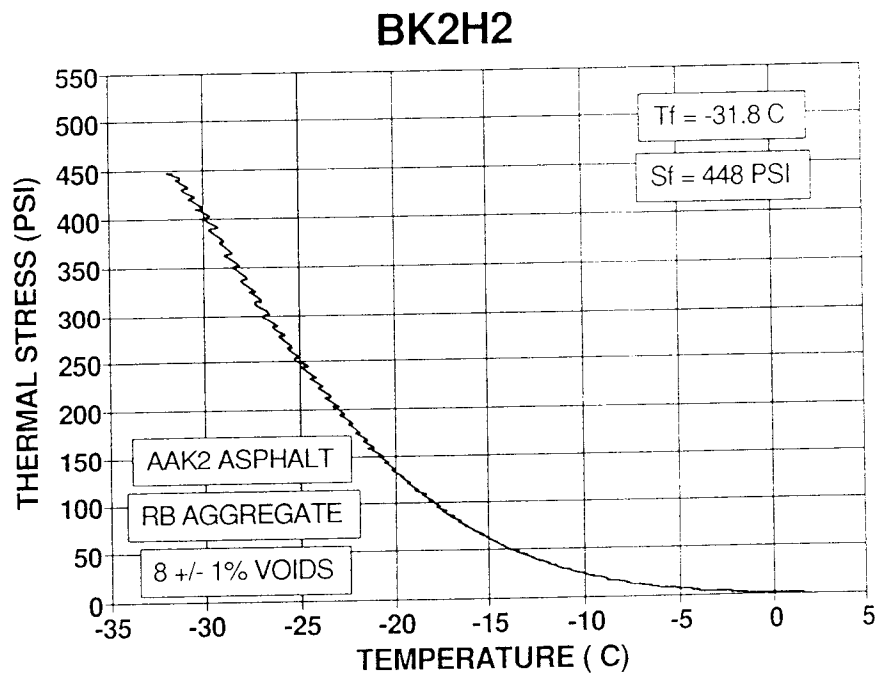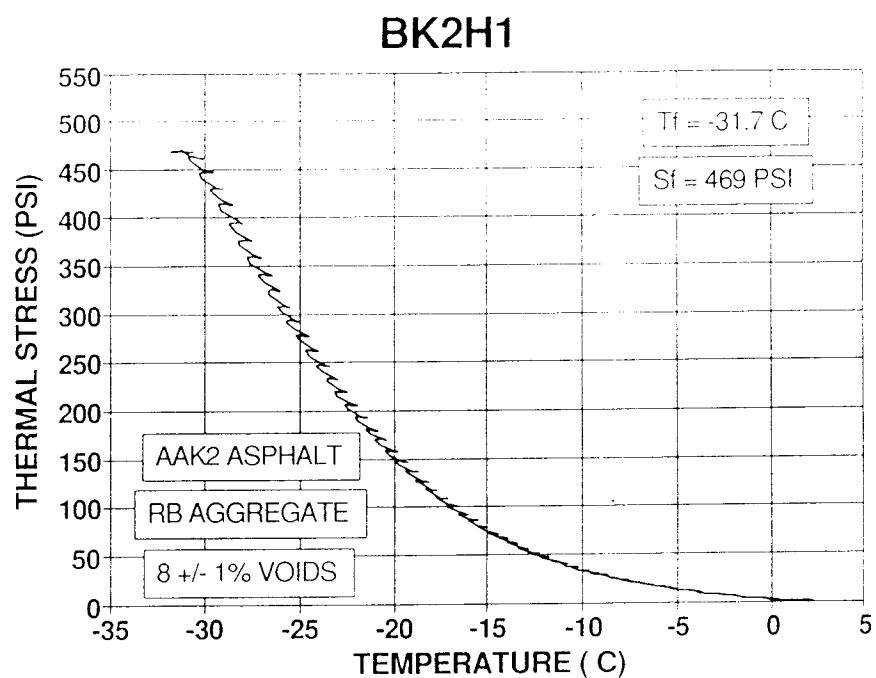(Alpha) vs. Log_{10} $(T-T_A)$ Curve.

Figure E-3.5   Plot of Transformed Creep Modulus Curve For Asphalt
Concrete Mixtures Containing AAK-2 Binder with RB
Aggregate and 8 +/- 1% Voids.

BK2L
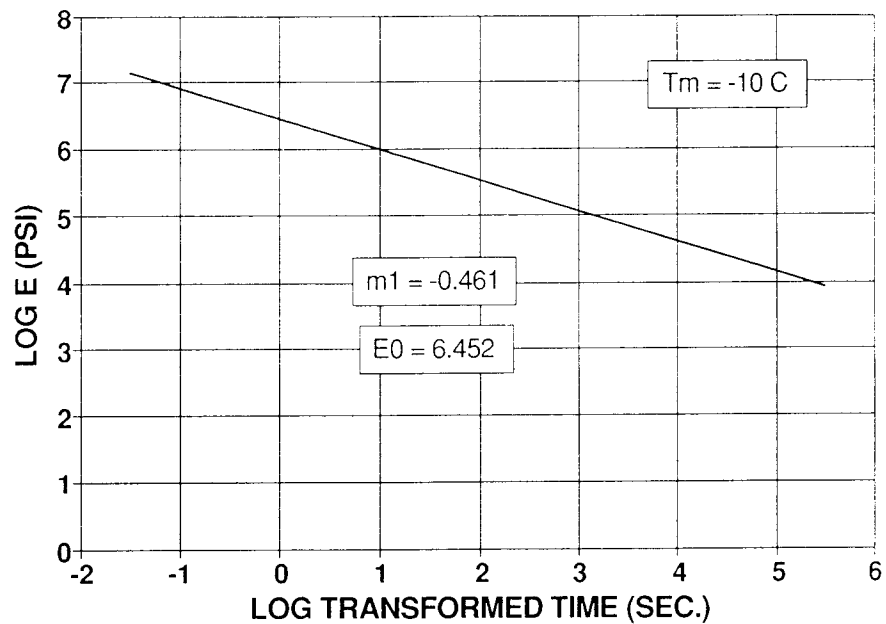
Figure E-3.6 (a)   Transformed Creep Modulus Curve at
                     Standard Temperature of -10 C.

BK2L
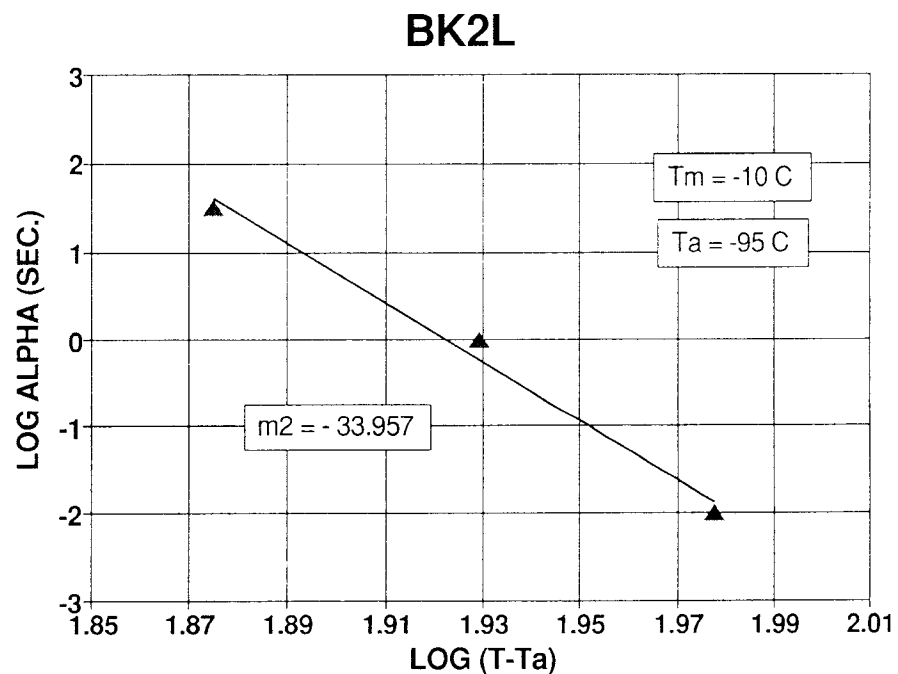
Figure E-3.6 (b) Log_{10} Time-Temperature Shift Factor
                     (Alpha) vs. Log_{10} $(T-T_A)$ Curve.
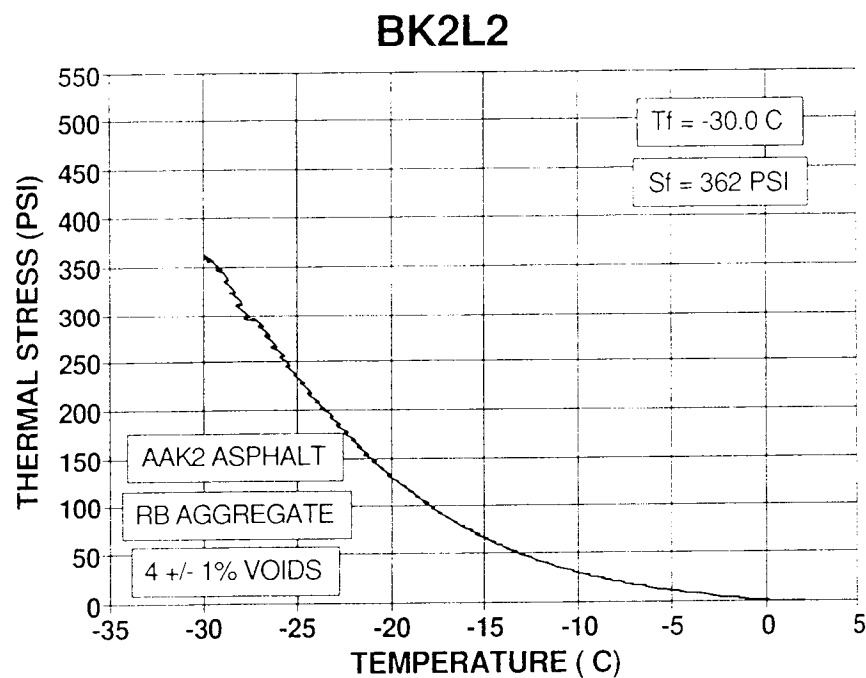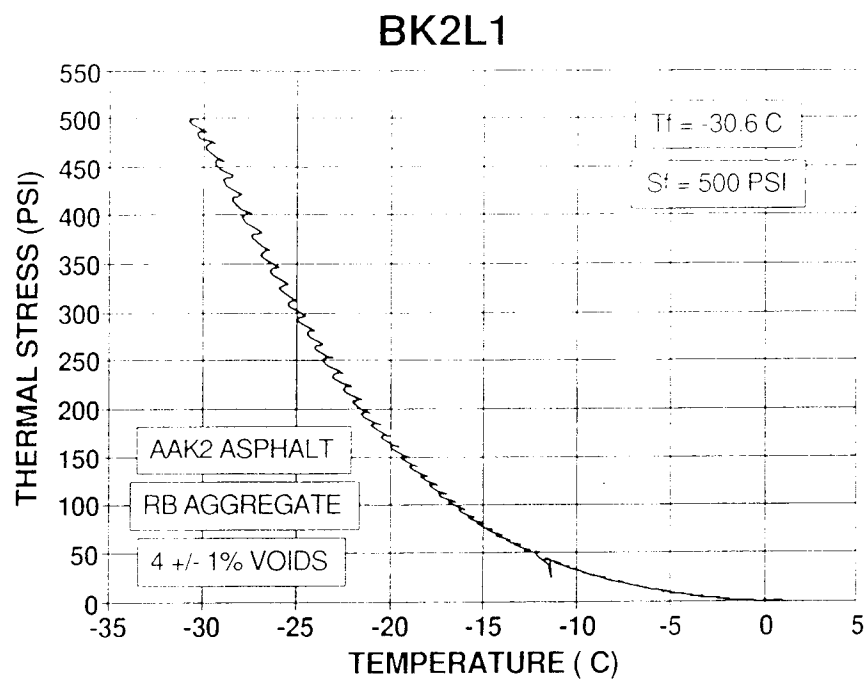
Figure E-3.6   Plot of Transformed Creep Modulus Curve For Asphalt
                     Concrete Mixtures Containing AAK-2 Binder with RB
                     Aggregate and 4 +/- 1% Voids.

BG1H
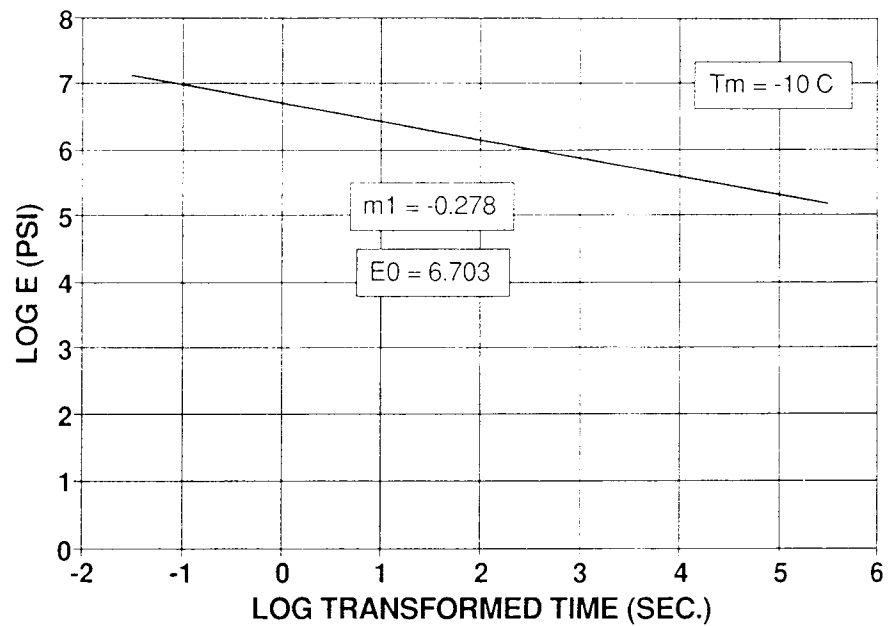
Figure E-3.7 (a) Transformed Creep Modulus Curve at Standard Temperature of -10 C.

BG1H
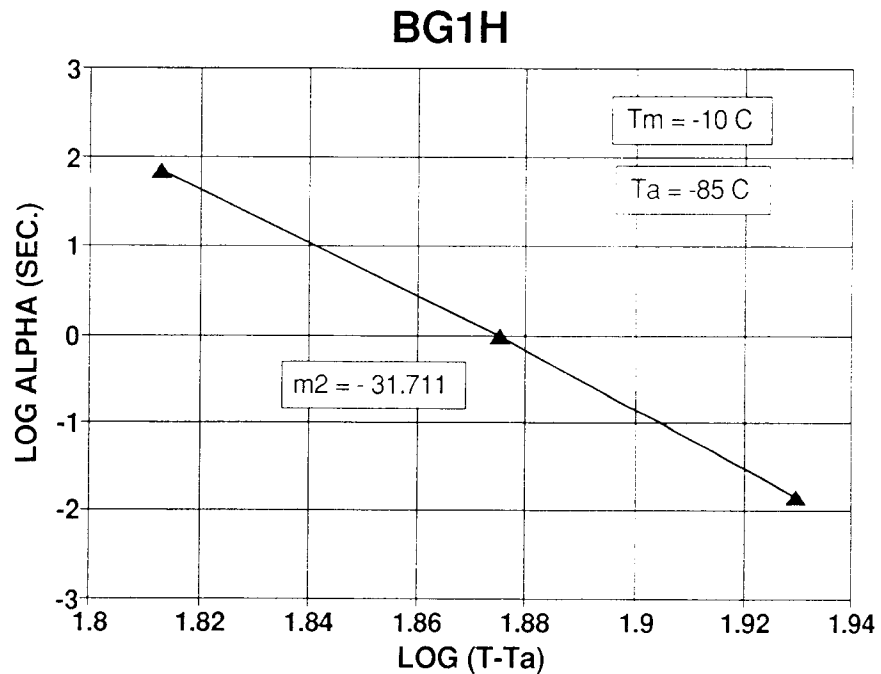
Figure E-3.7 (b) Log_{10} Time-Temperature Shift Factor (Alpha) vs. Log_{10} $(T-T_A)$ Curve.

Figure E-3.7 Plot of Transformed Creep Modulus Curve For Asphalt Concrete Mixtures Containing AAG-1 Binder with RB Aggregate and 8 +/- 1% Voids.
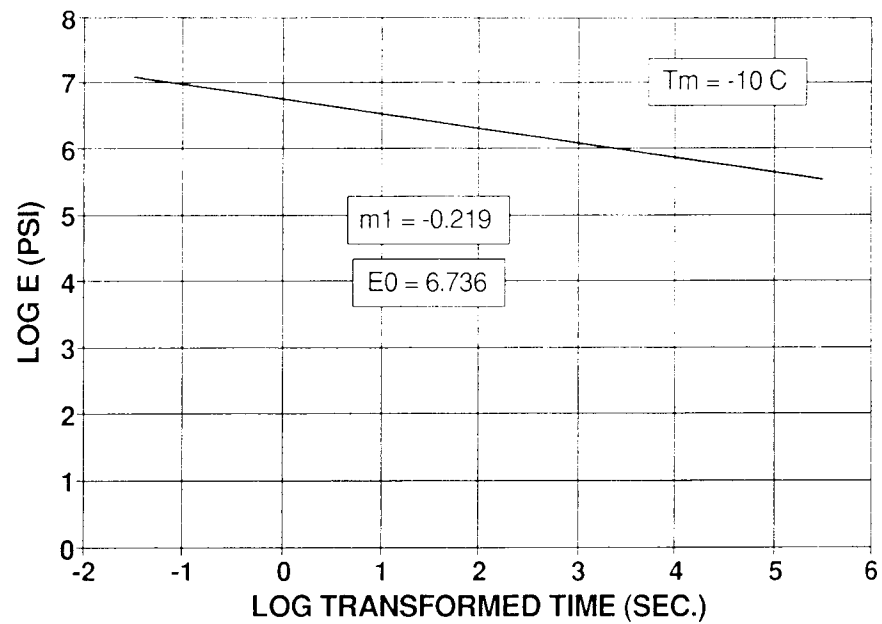
Figure E-3.8 (a)   Transformed Creep Modulus Curve at
                     Standard Temperature of -10 C.

Figure E-3.8 (b)   Log$_{10}$ Time-Temperature Shift Factor
                     (Alpha) vs. Log$_{10}$ (T-T$_A$) Curve.

Figure E-3.8   Plot of Transformed Creep Modulus Curve For Asphalt
                 Concrete Mixtures Containing AAG-1 Binder with RB
                 Aggregate and 4 +/- 1% Voids.

APPENDIX E-4

THERMAL STRESS RESTRAINED SPECIMEN TEST DATA

BK2H1

Thermal Stress (PSI) vs Temperature (C) plot. Labels: AAK2 ASPHALT, RB AGGREGATE, 8 +/- 1% VOIDS. Tf = -31.7 C, Sf = 469 PSI.

BK2H2

Thermal Stress (PSI) vs Temperature (C) plot. Labels: AAK2 ASPHALT, RB AGGREGATE, 8 +/- 1% VOIDS. Tf = -31.8 C, Sf = 448 PSI.
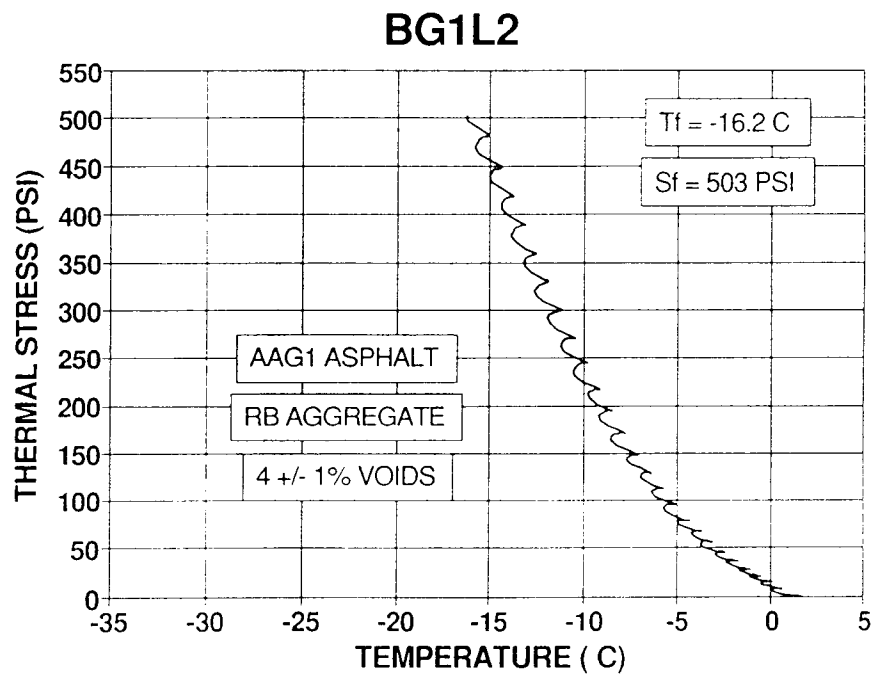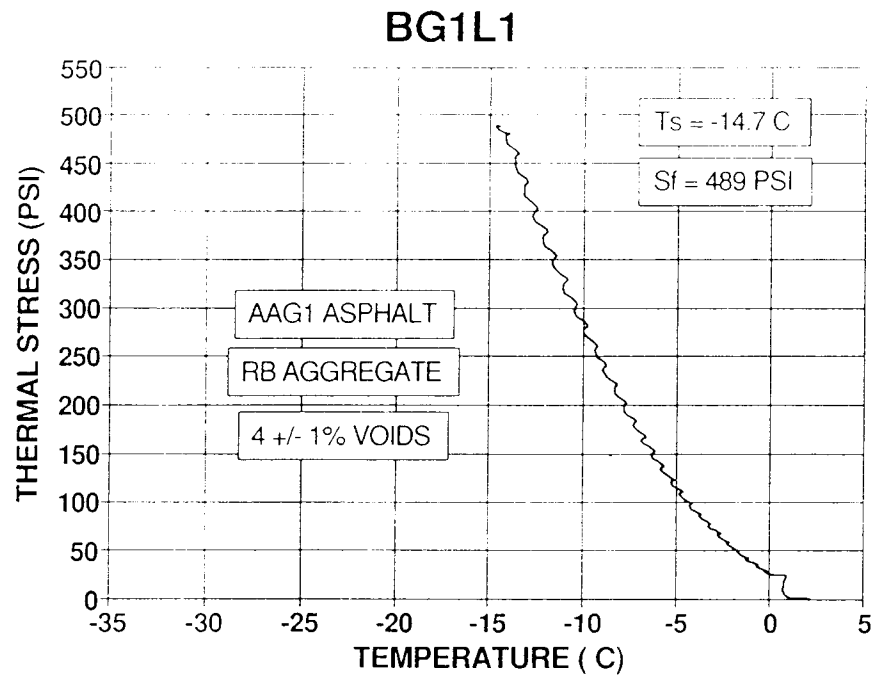
Figure E-4.1   Plot of Thermal Induced Stress vs. Temperature For Asphalt Concrete Mixtures Containing AAK-2 Binder with RB Aggregate and 8 +/- 1% Voids (dT/dt = 10 C/hr.).

BK2L1

# BK2L2

Figure E-4.2   Plot of Thermal Induced Stress vs. Temperature For
Asphalt Concrete Mixtures Containing AAK-2 Binder
with RB Aggregate and 4 +/- 1% Voids (dT/dt = 10 C/hr.).

BG1H1

BG1H2
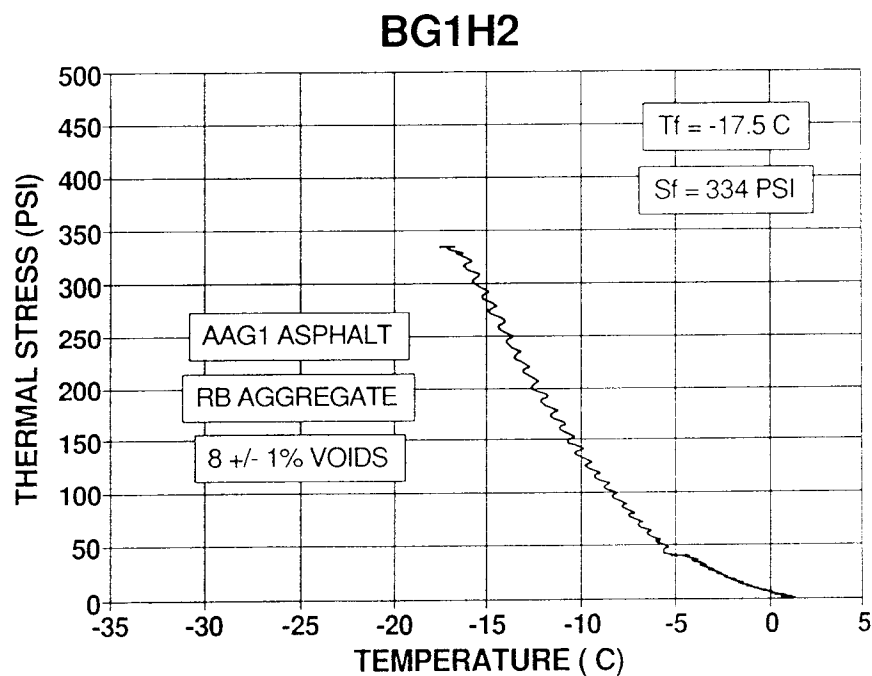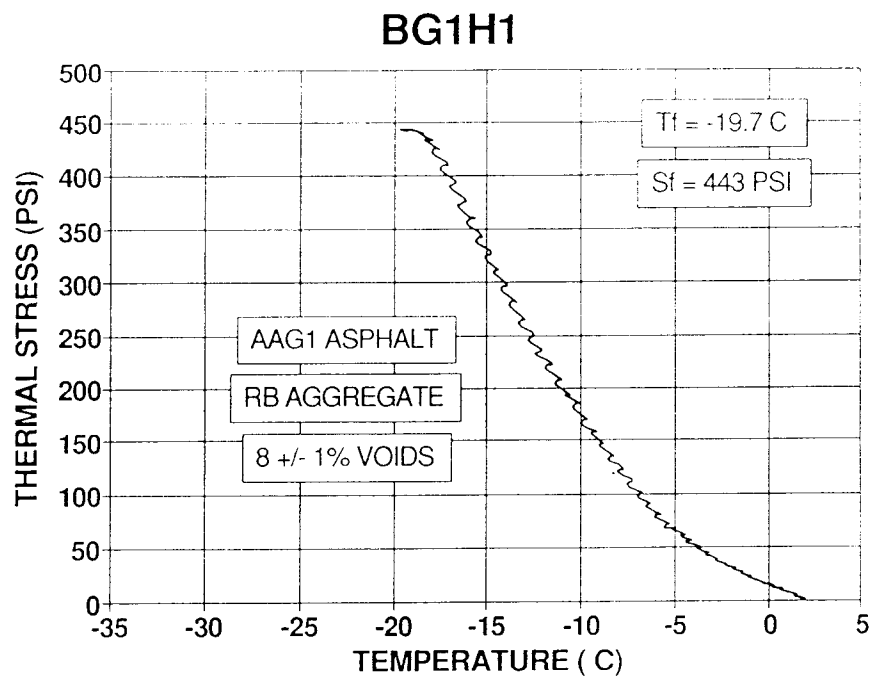
Figure E-4.3   Plot of Thermal Induced Stress vs. Temperature For
Asphalt Concrete Mixtures Containing AAG-1 Binder
with RB Aggregate and 8 +/- 1% Voids (dT/dt = 10 C/hr.).

BG1L1

BG1L2

Figure E-4.4   Plot of Thermal Induced Stress vs. Temperature For
Asphalt Concrete Mixtures Containing AAG-1 Binder
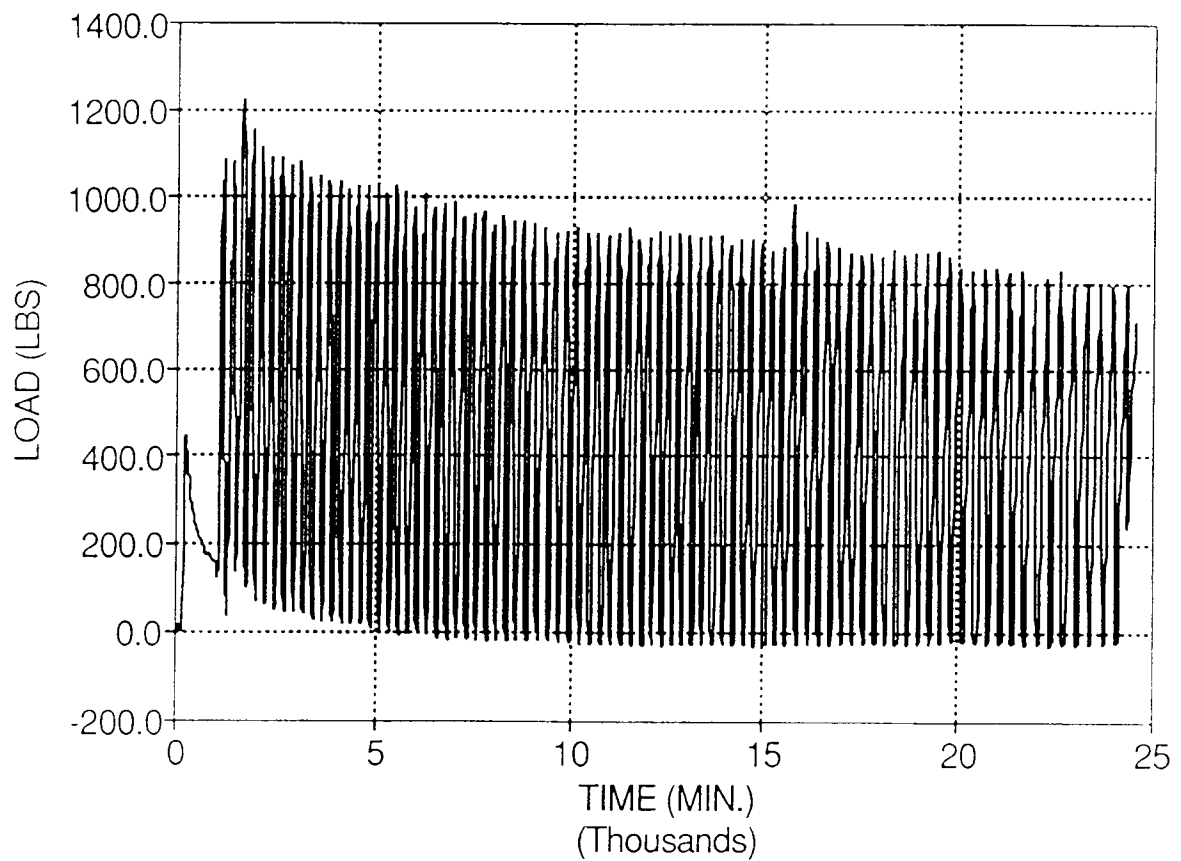with RB Aggregate and 4 +/- 1% Voids (dT/dt = 10 C/hr.).
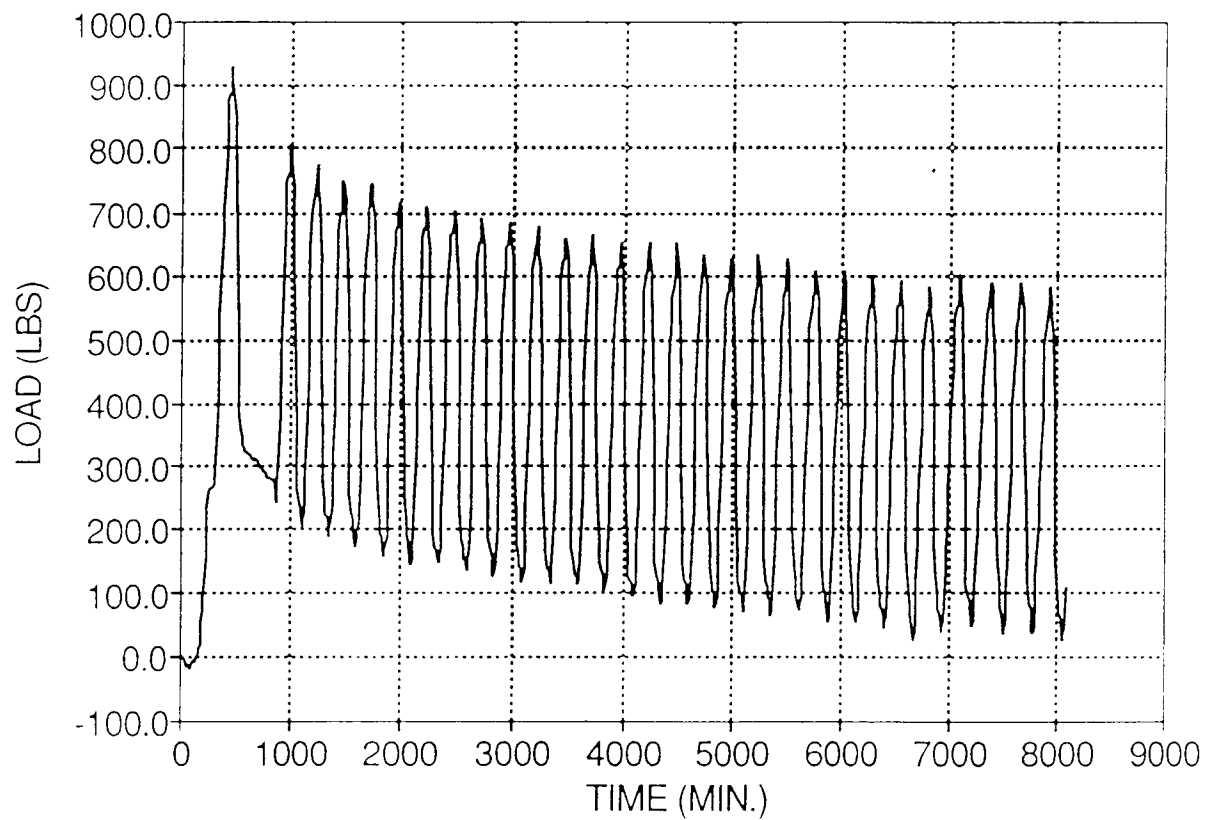
Figure E-4.5   Plot of Thermal Induced Load vs. Time For
an Asphalt Concrete Mixture Containing AAG-2
Binder with RB Aggregate and 4 +/- 1% Voids.

Figure E-4.6   Plot of Thermal Induced Load vs. Time For
an Asphalt Concrete Mixture Containing AAG-2
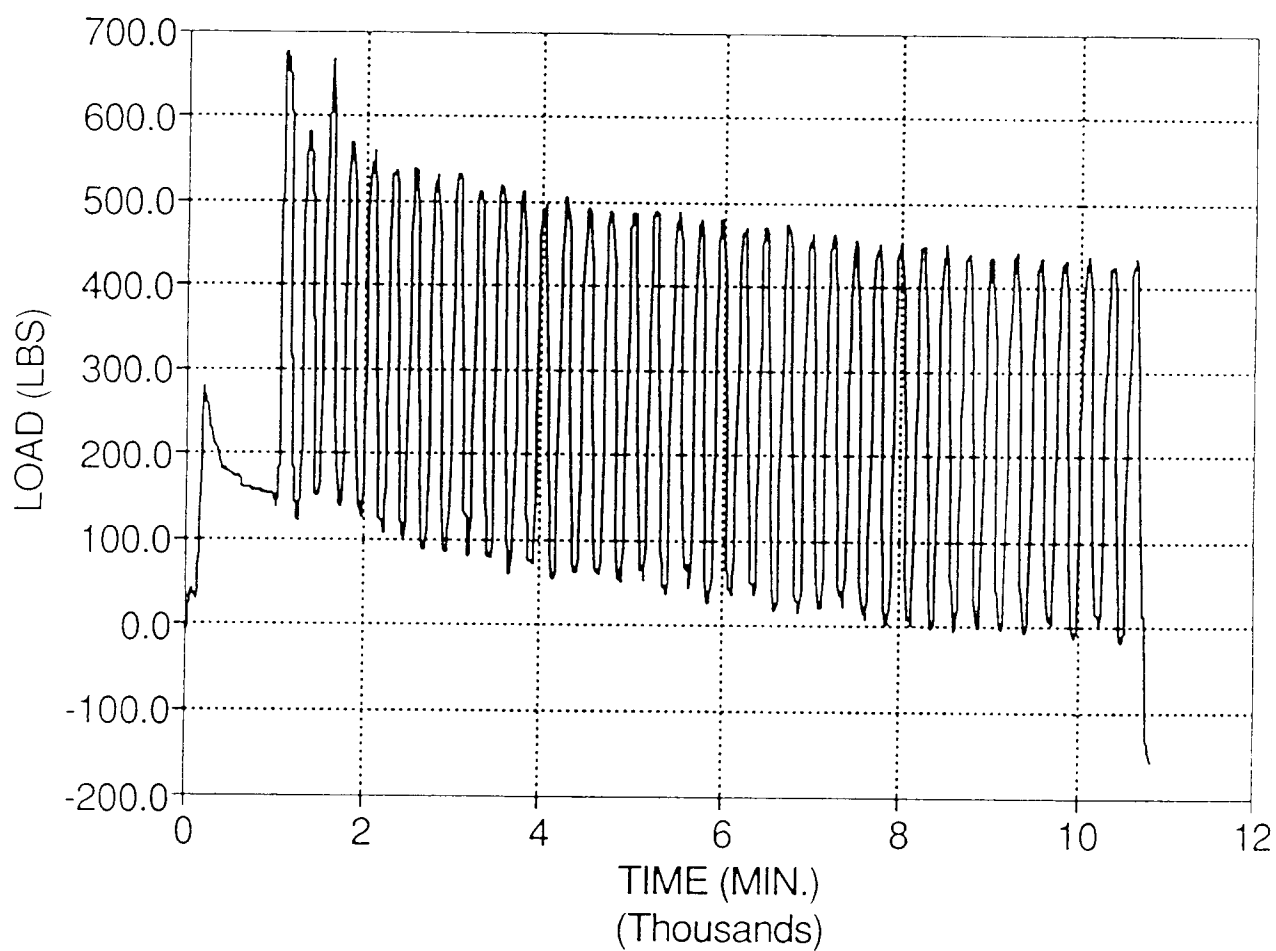Binder with RB Aggregate and 4 +/- 1% Voids.

Figure E-4.7   **Plot of Thermal Induced Load vs. Time For**
an Asphalt Concrete Mixture Containing AAK-1
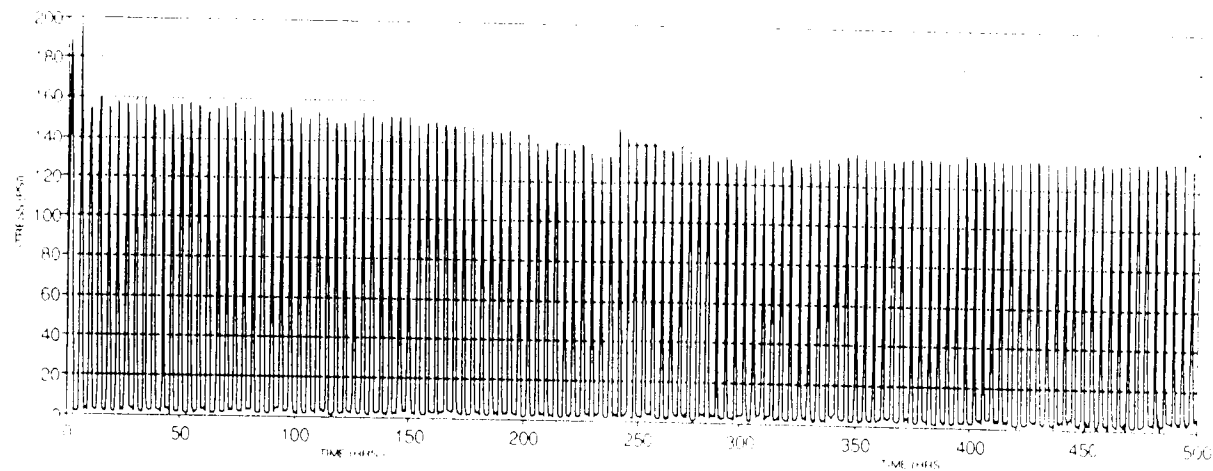**Binder with RB Aggregate and 8 +/- 1% Voids.**

Figure E-4.8   Plot of Thermal Induced Stress vs. Time For an Asphalt Concrete Mixture Containing AAG-1 Binder with RB Aggregate and 8 +/- 1% Voids.